Universität Potsdam

Institut für Physik und Astronomie

Characterization of biomolecules and their interactions using electrically controllable DNA nanolevers

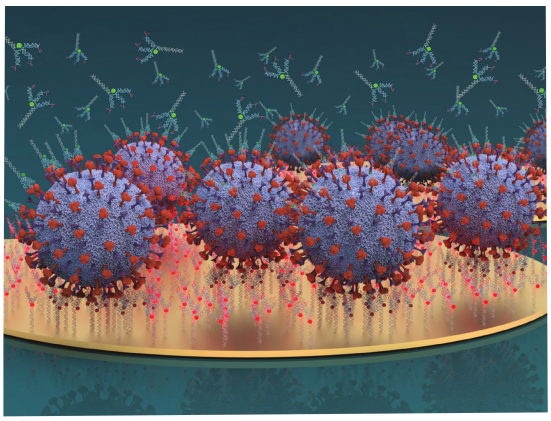

Dissertation zur Erlangung des akademischen Grades
"doctor rerum naturalium" (Dr. rer. nat)
in der Wissenschaftsdisziplin Biophysik

eingereicht an der
Mathematisch-Naturwissenschaftlichen Fakultät
der Universität Potsdam

Marlen Kruse

2022

Diese Arbeit wurde unter der Aufsicht von Prof. Dr. Carsten Beta am Fraunhofer IZI-BB (Institut für Zelltherapie und Immunologie, Institutsteil Bioanalytik und Bioprozesse), betreut von PD Dr. Ralph Hölzel in dessen Arbeitsgruppe (Biomolekulare Nanostrukturen und Messtechnik), durchgeführt.

Gutachter:

Prof. Dr. Carsten Beta
(A) Universität Potsdam
Institut für Physik und Astronomie
Institut für Biochemie und Biologie
Arbeitsgruppe: Biologische Physik

PD Dr. Ralph Hölzel
(B) Fraunhofer IZI-BB, Potsdam
Abteilung Biosystemintegration und Prozessautomation
Arbeitsgruppe: Biomolekulare Nanostrukturen und Messtechnik
(C) Freie Universität Berlin
Institut für Biologie

Prof. Dr. Wolfgang Fritzsche
(D) Friedrich-Schiller-Universität Jena
Institut für Physikalische Chemie
(E) Leibniz-IPHT, Jena
Abteilung Nanobiophotonik

Disputation: 18. Januar 2023

Published online on the
Publication Server of the University of Potsdam:
https://doi.org/10.25932/publishup-57738
https://nbn-resolving.org/urn:nbn:de:kobv:517-opus4-577384

Abstract

In this work, binding interactions between biomolecules were analyzed by a technique that is based on electrically controllable DNA nanolevers. The technique was applied to virus-receptor interactions for the first time. As receptors, primarily peptides on DNA nanostructures and antibodies were utilized. The DNA nanostructures were integrated into the measurement technique and enabled the presentation of the peptides in a controllable geometrical order. The number of peptides could be varied to be compatible to the binding sites of the viral surface proteins.

Influenza A virus served as a model system, on which the general measurability was demonstrated. Variations of the receptor peptide, the surface ligand density, the measurement temperature and the virus subtypes showed the sensitivity and applicability of the technology. Additionally, the immobilization of virus particles enabled the measurement of differences in oligovalent binding of DNA-peptide nanostructures to the viral proteins in their native environment.

When the coronavirus pandemic broke out in 2020, work on binding interactions of a peptide from the hACE2 receptor and the spike protein of the SARS-CoV-2 virus revealed that oligovalent binding can be quantified in the switchSENSE technology. It could also be shown that small changes in the amino acid sequence of the spike protein resulted in complete loss of binding. Interactions of the peptide and inactivated virus material as well as pseudo virus particles could be measured. Additionally, the switchSENSE technology was utilized to rank six antibodies for their binding affinity towards the nucleocapsid protein of SARS-CoV-2 for the development of a rapid antigen test device.

The technique was furthermore employed to show binding of a non-enveloped virus (adenovirus) and a virus-like particle (norovirus-like particle) to antibodies. Apart from binding interactions, the use of DNA origami levers with a length of around 50 nm enabled the switching of virus material. This proved that the technology is also able to size objects with a hydrodynamic diameter larger than 14 nm.

A theoretical work on diffusion and reaction-limited binding interactions revealed that the technique and the chosen parameters enable the determination of binding rate constants in the reaction-limited regime.

Overall, the applicability of the switchSENSE technique to virus-receptor binding interactions could be demonstrated on multiple examples. While there are challenges that remain, the setup enables the determination of affinities between viruses and receptors in their native environment. Especially the possibilities regarding the quantification of oligo- and multivalent binding interactions could be presented.

Zusammenfassung

In dieser Arbeit wurden Bindungsinteraktionen zwischen biologischen Molekülen mit Hilfe von elektrisch kontrollierbaren DNA-Nanohebeln untersucht. Die Technologie wurde zum ersten Mal auf Virus-Rezeptor Interaktionen angewendet. Als Rezeptoren wurden überwiegend Peptide und Antikörper untersucht. Die Peptide wurden auf vierarmigen DNA-Nanohebeln angeordnet. Ihre geometrische Anordnung entsprach der Anordnung der Rezeptorbindungsstellen der Proteine auf der Virusoberfläche.

An Influenza A Viren wurde die Machbarkeit der Bindungsmessung zuerst demonstriert. Dabei konnte die Anwendbarkeit und Sensitivität der Technologie durch Variation der Peptide, der Ligandendichte auf der Sensoroberfläche, der Messtemperatur und der Virussubtypen gezeigt werden. Weiterhin wurde Virusmaterial auf der Sensoroberfläche immobilisiert und anschließend wurden quantitative Bindungsmessungen mit den oligovalenten DNA-Peptid-Strukturen durchgeführt. Dieser Versuchsaufbau ermöglichte die Messung der Bindungsstärke in Abhängigkeit der Anzahl der pro DNA-Struktur gekoppelten Peptide.

Im Zuge des Ausbruchs der Coronavirus-Pandemie im Jahr 2020 wurden Bindungsinteraktionsmessungen zwischen einem Peptid aus dem hACE2-Rezeptor und SARS-CoV-2 Spike Proteinen durchgeführt. Auch hier konnten oligovalente Bindungseffekte quantifiziert werden. Außerdem wurde festgestellt, dass Veränderungen an der Aminosäuresequenz des SARS-CoV-2 Proteins starke Auswirkungen auf das Bindungsverhalten hatten. Auch Interaktionen zwischen dem Peptid und sowohl inaktiviertem Virusmaterial als auch Pseudoviruspartikeln wurden gemessen.

Für die Entwicklung eines Antigenschnelltests wurden die Affinitäten von sechs Antikörpern an das Nucleocapsidprotein des SARS-CoV-2 bestimmt.

Weiterhin konnte gezeigt werden, dass mit der Technologie auch die Bindung von unbehüllten Viren (am Beispiel von Adenoviren) und Virus-ähnlichen Partikeln (am Beispiel von Norovirus-ähnlichen Partikeln) an Antikörper vermessen werden kann.

Neben Bindungsinteraktionen, wurden auch Größenbestimmungen mit Hilfe von DNA Origamis durchgeführt. Die Hebellänge von ca. 50 nm ermöglichte die elektrische Bewegung ("switching") von Virusmaterial. Es konnte so gezeigt werden, dass die Technologie es ermöglicht, Objekte mit einem hydrodynamischen Durchmesser von mehr als 14 nm zu bewegen.

In einer theoretischen Betrachtung der Experimente konnte gezeigt werden, dass der Sensoraufbau und die verwendeten Parameter die Messung von Bindungsratenkonstanten in einem Reaktions-limitierten Bereich ermöglichen.

Insgesamt konnte die Arbeit an vielen Beispielen zeigen, dass die switchSENSE Technologie für die Messung von Virus-Rezeptor Interaktionen geeignet ist. Während es weiterhin Herausforderungen gibt, so ermöglicht der Aufbau doch die Bestimmung von Affinitäten zwischen Viren und Rezeptoren. Insbesondere die Möglichkeiten zur Quantifizierung von oligo- und multivalenten Bindungsinteraktionen konnten aufgezeigt werden.

Contents

Part I
Introduction

Binding interactions of biological molecules are fundamental processes in nature. They are necessary for both the function of an organism e.g. a human being, and the interaction with the outside world for example during the transport of signals, for enzymatic activity etc. [1]. Binding interactions are also involved in diseases caused by pathogens like viruses [2].

When investigating molecular interactions of biomolecules, one inevitably arrives at processes that do not only involve biology, but also chemistry and physics. Descriptions and investigations of binding processes of biological molecules need all three basic natural sciences. The chemical aspects form a basis as they involve for example covalent bindings of atoms that make up larger molecules. [3]. From the biological side, there is the study of proteins and their structure, the interdependence of structure and function, the organization principle of structures like lipid bilayers, etc. [1, 4]. The physical side comprises for example the description of forces between atoms or molecules like electrostatic interactions or quantum mechanical descriptions of atomic orbitals, etc. [5]. It continues with the construction and understanding of measurement techniques, which are often based on optical or electrical signal collection [6]. This involves fluid dynamics, mechanical and thermal aspects and the theoretical description and evaluation of results [7]. To understand or at least to increase the understanding of interactions between biological molecules, all three main natural sciences are needed.

One kind of interaction that this thesis focuses on, is the one between virus particles and proteins. Viruses infect all living organisms [2] and can cause catastrophic pandemics. This has been seen recently in 2020, when a new coronavirus called severe acute respiratory syndrome coronavirus 2 (SARS-CoV-2) emerged and spread quickly around the world with disasterous consequences [8]. And this is only the most recent example of a viral pandemic. Influenza is another virus that has been causing epidemics and pandemics of varying severity throughout human history [9]. Yearly, it strains the health systems and the economy [10].

Viruses have to infect their host organisms in order to reproduce and many viruses including influenza and coronaviruses rely on multivalent interactions between the proteins on both the viral and the cell surface for virus attachment [2, 11]. By utilizing multiple binding sites for the binding process, the individually weak interaction strength is increased. The measurement of these multivalent interactions is intrinsically complex, making a quantitative analysis challenging regarding experimental procedures (e.g. [12]) and theoretical models (e.g. [13–15]). The attachment is a fundamental step in the infection process and a deeper understanding might enable in the amelioration of diagnostics and therapy.

In this thesis, an existing technology called switchSENSE was utilized to

measure multivalent interactions between viruses and proteins. This had never been done before. The technology is based on electrically controllable DNA nanolevers and an optical detection system [16]. In this work, it was combined with specifically developed DNA nanostructures [17–19], which can be functionalized to carry a variable number of peptides. The geometrically controllable oligovalent DNA nanostructures were immobilized on the sensor surface and binding of viral material was measured under various conditions.

The thesis begins with a description of the theoretical background including a short introduction to binding theory, experimental techniques and the model systems used (part I). The second part is dedicated to the materials and methods that were utilized during this thesis (part II). The third part shows the results (part III), including the main section on virus-receptor interaction (section 7). It begins with results of the work with influenza A virus material (subsection 7.1). Subsequently, the results of the experiments performed with SARS-CoV-2 proteins and virus material are presented in subsections 7.2 and 7.3. Other virus types were also investigated including a non-enveloped virus and virus-like particles as can be seen in subsection 7.4. Additional experiments were performed on sizing of viruses (section 8) and protein-protein interactions (section 9). Finally, a theoretical analysis of mass transport limited or reaction limited interaction measurements (section 10) is given.

1 Binding interactions of biological molecules

Binding interactions play a fundamental role in nature and in science (e.g. in drug discovery [20]), while the understanding of common interactions remains incomplete. The following chapter includes the theoretical background necessary for this thesis and the presentation of the current state of research. A proficient reader might skip directly to the material and methods (part II) or results section of the work (part III).

Binding of biological molecules is described in the first subsection, followed by subsections on multivalent binding and measurement techniques. The last subsection describes the biological materials that were utilized in this thesis, which includes DNA, peptides, antibodies and viruses.

1.1 Covalent and non-covalent interactions

Binding interactions of molecules can be covalent or non-covalent. Covalent interactions describe chemical reactions between functional groups of molecules or atoms by sharing or exchanging of electrons. Functional groups, as the name suggests, can influence a biomolecule's properties and reactivity. Carboxyl (-COOH) or amino groups (-NH_2) are examples of functional groups that enable amino acids to form proteins [1].

However, there are also non-covalent interactions between (bio-) molecules and atoms. These are entirely electrostatic. They are based on interactions of charges and do not result in chemical bonds [1].

The ionic interaction between sodium and chloride ions is an example of a non-covalent electrostatic interaction. After ionization of the two molecules, sodium is positively charged, while chloride is negatively charged [1, 21]. The interaction between the two ions can be described by Coulombs law

$$F = \frac{1}{4\pi\epsilon_0\epsilon_r} \cdot \frac{Q_1 Q_2}{r^2} \tag{1}$$

where F is the force between the two point charges Q_1 and Q_2, r is the distance between the point charges, ϵ_0 is the electric field constant $\epsilon_0 = 8.85 \cdot 10^{-12} \frac{\mathrm{As}}{\mathrm{Vm}}$, and ϵ_r is the dielectric constant of the dielectric medium [22]. Ionic interactions can be of similar strength as covalent bonds [1].

Not only ions can interact based on electrostatics, but also dipoles. There are permanent and non-permanent or induced dipoles. Permanent dipoles are made up of binding partners with different levels of electronegativity, resulting in a polar atomic bond. Water (H_2O) is an example of a polar molecule [1]. Shielding effects by water due to its polarity influence the strength of the interactions considerably [5]. Non-permanent dipoles can be induced dipoles. The presence of an electric field, for example generated by an ion in close proximity, can influence the dispersion of the electron distribution around a molecule. The dispersion of electrons can fluctuate and can induce the formation of a temporary dipole. The force between induced dipoles is called van-der-Waals force. Furthermore, ions, permanent and induced dipoles can interact [1].

Hydrogen bond formation is a special form of non-covalent interactions. As described above for permanent dipoles, a more electronegative atom induces a partial charge of a hydrogen atom. This partial charge can then interact with a hydrogen bond acceptor. The hydrogen bonds are especially important for proteins and the formation of their structure [1].

Non-covalent interactions are of great importance for biological processes that require flexible and dynamic process, like for example enzymatic activity, or protein-protein interactions [3].

Proteins usually have specific tasks in an organism and often, part of the task involves recognition of and binding to other proteins or molecules. A binding event can induce a conformational change or a secondary reaction. Often, proteins are highly specific for a particular binding partner. The amino acid sequence and length as well as a the three-dimensional structure of a protein determine the binding strength of a protein. The interactions between proteins are generally non-covalent and weak as compared to covalent interactions [1].

1.2 Molecular binding interaction theory

In this work, non-covalent interactions between biological molecules are investigated. The terminology for molecular interactions might need some clarification. Binding partners of proteins are generally called "ligands". They can be other proteins, but also nucleotides, lipids etc. In biochemistry, "receptors" or "receptor proteins" are proteins that interact with another protein and this interaction triggers a subsequent reaction (e.g. a conformational change that leads to a signal transmission) [1].

The technology for measuring binding interactions that is used here, relies on the immobilization of one binding partner, while the second one is free in solution (see subsection 1.4.1). For the immobilized binding partner the terms ligand or receptor are used. For the binding partner that is free in solution, the term "analyte" is applied (as in e.g. [23]). An analyte can be anything like protein, a virus, a small molecule, an aptamer, ...

The theoretical model of an interaction begins with the simplest one: a bi-molecular binding reaction:

$$\mathrm{A} + \mathrm{B} \underset{k_{\mathrm{off}}}{\overset{k_{\mathrm{on}}}{\rightleftharpoons}} \mathrm{AB} \tag{2}$$

where A and B stand for the two interacting molecules and AB is considered the complex. k_{on} and k_{off} are the rate constants [24]. There are various terminologies for the rate constants, like "forward and reverse rate constant", "association and dissociation rate constants", "k_1 and k_{-1}" instead of "k_{on} and k_{off}" and even more. These terms all describe the rate constants that govern either the complex formation or the complex separation. In this thesis the terminology of a common measurement technique is adopted, which is: association and dissociation rate constants and the notation of k_{on} and k_{off}. The association rate constant has the unit $\mathrm{M}^{-1}\mathrm{s}^{-1}$, while the dissociation rate constant has the

unit s^{-1}. The rate constants describe the changes in concentrations of reactants and product over time as the reaction equilibrates [24].

In order to describe a bi-molecular reaction quantitatively, one assumes that the net concentrations of A, B and AB stay constant in equilibrium condition. The equilibrium is not static though. It only means that as many new complexes are formed, as dissociate [24]. The dissociation constant K_D is the quotient of k_{off} and k_{on} and is given in the unit $\frac{mol}{L} = M$:

$$K_D = \frac{k_{off}}{k_{on}} \tag{3}$$

The dissociation constant can also be related to the concentrations of the molecules and the complex [24]:

$$K_D = \frac{[A][B]}{[AB]} \tag{4}$$

where the square brackets indicate a molar concentration. K_D can also be understood as the concentration of free molecule B, at which half of the molecules A are bound in the complex. For a surface sensor based description, the K_D is the value of the concentration of the molecule in solution, at which half of the receptor molecules on the sensor surface are occupied in equilibrium.

Dissociation constants can be measured without the determination of rate constants. In this case, the concentrations of the bound complex are measured, while the concentration of the molecule A is held constant. Molecule B is titrated, and a measurement of $[AB]/[A]_{Total}$ or the amount of AB follows. From plotting the data points of the titration, K_D can be determined. This classical measurement technique of the dissociation constant cannot determine rate constants [24].

The binding strength of an analyte towards a ligand is called affinity. The dissociation constant is low for binders that have a high affinity and vice versa [24]. K_D values for interactions of biological molecules often range between millimolar and nanomolar [1]. Although stronger binders exist. One of the highest affinities known is the one between the molecules biotin and avidin with a dissociation constant on the order of $K_D \simeq 10^{-15}$ M [3].

The rate constants are considered relevant for example in drug discovery [25, 26].

1.3 Multivalent binding

Multivalent binding can be found in nature. An example from the macroscopic world would be the burdock (Arctium), which gave the idea for the development of velcro. In the microscopic world of biological molecules, the attachment of some viruses to a host cell surface involves multivalent interaction [2]. The definition of multivalency is not trivial and requires differentiation from a similarly important but different effect, namely allosteric cooperativity. Multivalency is the term for binding interactions of systems that involve “one (or more) intramolecular interaction” as defined by Juriaan Huskens in the book “Models

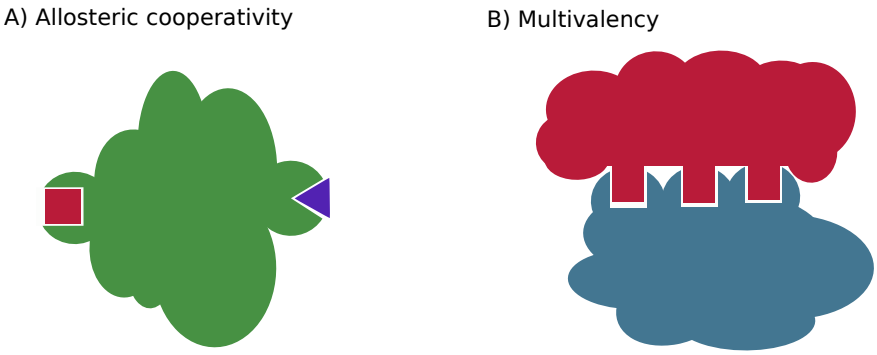

Figure 1: Cooperativity and multivalency: A) For cooperativity at least one binding partner is multitopic (has multiple interaction sites). B) Multivalency requires both binding partners to be multitopic and at least one interaction to be intramolecular.

and Methods in Multivalent Systems" [27]. Both binding partners have to have more than one interaction site that is involved in the binding process (see Figure 1 B)).

The definition can be clarified by comparing multivalency to cooperativity (which is also called "allosterism" or "allosteric cooperativity"). In this case at least one of the binding partners has multiple binding sites and binding interactions at one binding site influence the binding interaction at another (see Figure 1 A)) [27]. A popular example is the binding of oxygen molecules to the protein hemoglobin. Hemoglobin has the ability to bind four oxygen molecules. The binding of one oxygen molecule positively enhances the binding ability of the second binding site and so on [1].

The effect of allosteric cooperativity can be positive or negative. When the binding of one ligand facilitates the binding of a second ligand, the effect is called positive cooperativity. Negative cooperativity would describe the opposite, namely, the binding of the first ligand hinders the binding of a second ligand [1].

The distinction of multivalency from cooperativity is not easy, as multivalency can include cooperativity, but can also be non-cooperative [27]. Oligovalency describes a subgroup of multivalent interaction with only a few interaction sites involved.

Multivalent binding interactions are for example utilized for the construction of therapeutics with a desired binding behavior in drug design [28, 29]. The complexity of the problem however challenges both experimental and theoretical analysis. Theoretical models discuss the influence of linkers including their lengths and flexibility on the multivalent binding affinity [14, 30, 31], the prediction of thermodynamic quantities like the free energy [32] or effects that enhance multivalent binding interactions like rebinding [33]. Theoretical models are not only used for predicting optimal design of multivalent binding molecules, they

are also helpful in the interpretation of data from experiments on multivalent binding [34, 35].

Regarding experimental approaches to study multivalent binding interactions, there have been lots of reports on the design of scaffolds from chemical [36] or biological structures [17, 37], which were developed in order to enhance binding affinity or in order to study multivalent binding [38]. While the design of a controllable system is the first step, secondly the experimental technology for actually measuring the binding interactions must be chosen. There is a variety of technologies available, some of which are described in the following section.

1.4 Experimental techniques

There are many technologies available for the measurement of binding interactions of biological molecules. Some determine qualitative results, which in this case describe observations of whether binding is happening (Yes/No answer). Other techniques deliver quantitative results, meaning a numerical value is determined for the binding process or the rates at which it happens. Depending on what question is supposed to be answered during an experiment, it can be advantageous to choose either a qualitative or a quantitative approach. Qualitative experiments can also form a basis, from which quantitative experiments are designed [24].

With regard to quantitative methods, there are those that are able to determine dissociation constants (K_D) only and those techniques that can measure both association and dissociation rate constants (k_{on} and k_{off}).

In the following subsections, some techniques are described in more detail. This includes the switchSENSE technique and enzyme linked immunosorbent assays, two techniques that were used in this thesis. Surface plasmon resonance is widely used for molecular binding interactions and can be compared to switchSENSE regarding its possibilities and challenges. Finally, single molecule interaction measurement techniques are shortly presented, as they are successfully applied to the measurement of multivalent binding interactions.

The following list of technologies to measure binding interactions is incomplete. There are many more techniques available [20, 24].

1.4.1 SwitchSENSE technology

The main work of this thesis has been performed on a device called DRX^2, which uses a technology named “switchSENSE”. Originally, the technique was developed based on research on electrical manipulation of DNA strands [39, 40].

In this technology, DNA strands are immobilized on a gold electrode that is connected to a voltage source. Since DNA is negatively charged [1], it reacts to the applied potential of the surface electrode [41]. While the DNA is tethered to the gold surface at one end (see Figure 2), it is free to move about above the surface.

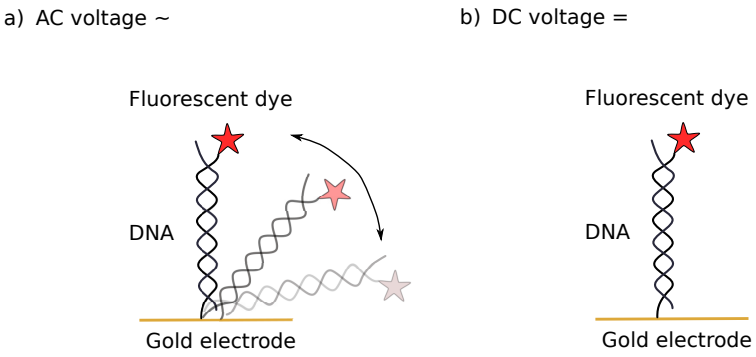

Figure 2: Electrical manipulation of DNA: an end-tethered DNA strand is manipulated by a voltage that is applied to a gold electrode. a) An applied alternating voltage induces an oscillatory behavior. b) When a direct voltage is applied, the DNA assumes a static and upright position as it is repelled from the surface.

There are two measurement modes available. One measurement mode is called switching mode and gives the technology its name. It is based on an oscillatory behavior of the DNA lever, that is induced by an applied alternating voltage (see Figure 2 a)). When the electrode is negatively charged, the DNA is repulsed and assumes an upright standing position. When the electrode surface carries a positive charge, the DNA is attracted to the surface and lies down horizontally. An applied alternating voltage therefore results in an oscillatory behavior of the DNA according to the charge on the surface [39].

The research by Rant et al. [42] showed that double-stranded DNA behaves differently than single-stranded DNA. While single-stranded DNA oscillates close to the surface, double-stranded DNA behaves more like a rigid rod. The height of the distal end of the DNA strand is observed by a fluorescence molecule. When the charge of the surface is switched to positive and the DNA starts to lie down, dragging the fluorophore with it towards the surface, a gradual quenching effect can be seen as a reduction of light intensity on the sensor [41]. When the double-stranded DNA is in an upright position, the maximal amount of light reaches the photodetector. The fluorescence (F) scales with the distance (z) of the fluorescent dye above the metal surface to the third power [39]:

$$F \sim z^3$$

Therefore, the measured intensity can be associated with the position of the distal end of the double-stranded DNA. The oscillatory movement of the DNA can be measured in relation to the electrical signal of the alternating voltage [39, 40].

When the DNA moves through the liquid of the microchannel, in which it is located, hydrodynamic friction occurs. The speed of the motion of the DNA lever depends on the ionic strength of the liquid, the length of the DNA

nanolever and the size, shape and charge of any attached molecule [43]. Therefore, the resulting movement of the lever, as it is traced during the switching behavior, is varied by a binding event. A pure DNA strand behaves differently than a DNA strand that carries a ligand molecule. Another change is visible, once an analyte molecule attaches on top of the ligand molecule [16, 44]. The parameters, which are measured, rely on the fluorescence signal, but they can be analyzed in different ways. The graph of the downward or upward moving fluorescence intensity over time can be integrated (over various time intervals). The maximal fluorescence in the upward position or the minimal fluorescence in the horizontal position can be used as signal [23].

The switching of the DNA, the ligand and the analyte is one possibility of applying the technology. However, there is a second measurement mode, which is widely used in this thesis and is called static mode (see Figure 2 b)). In this case, the electrode is negatively charged and the DNA stays in an upright position during the entire measurement process. The signal of a binding event is determined by the close chemical proximity of the binding partners to the fluorophore. This can lead to a decrease or an increase in fluorescence intensity upon binding. The underlying principle in this case is fluorescence quenching [23]. Both measurement modes are extremely sensitive.

1.4.2 Enzyme-linked immunosorbent assays

An example for a technique that is often used qualitatively is the enzyme-linked immunosorbent assay (ELISA). Rate constants cannot be determined in ELISAs. Generally, ELISAs are easy to handle as they do not require expensive or specialized instruments, but can be performed using standard lab equipment like pipettes and micro-titer plates and rather standard chemicals. They are also very common and are performed widely. While the assay development can be difficult and its execution requires great deliberation, a functioning assay can be considered very reliable. The scientist controls the individual steps of the experiment and negative and positive controls can support a dependable result. [45]

There are various ways of performing ELISAs. In the following, the protocol for the ELISAs is presented that was used to find the results that are presented in this thesis. A receptor is immobilized on a surface (e.g. a micro titer plate). The antigen, which is in solution, is added to the wells at various concentrations. After washing steps, which are performed to remove all unbound sample, an antibody solution is added to the wells. The antibody binds a different epitope (binding site) or a specific tag on the antigen. Typically after another washing step, a secondary antibody, which carries an enzyme, is added and it binds to the first antibody. An enzymatic substance is then added, which induces a visible color change. The resulting amount of antigen on the surface is determined by absorption spectroscopy. If the original binding between the ligand and the antigen had not taken place, none of the following binding interactions can happen either and no color change is visible at the final step [45, 46].

In this thesis, some chapters include results from ELISAs, which often formed

a basis of the quantitative experiments performed with the DRX^2. ELISAs in this thesis were used to answer qualitative questions regarding "yes or no" binding. A binding, which was unambiguously proven by ELISA, generally was expected to show up in the switchSENSE experiments as well. Cooperation partners performed all the ELISA experiments that are presented in this work. This is additionally mentioned in all relevant chapters.

1.4.3 Surface plasmon resonance

A very common and widely used technology to determine binding rate constants is based on the principle of surface plasmon resonance (SPR). It utilizes collective electron oscillations at an interface (typically metal-dielectric) that are induced by light excitation. The so-called resonance frequency is sensitive to the refractive index of the thin layer at the interface. If all other parameters that influence the resonance frequency are held constant (e.g. incidence angle, wavelength of light), a binding event at the surface can be seen as a shift of the resonance minimum of reflected light [47].

Surface plasmon resonance is widely used as a biosensor for molecular interactions. The technique has some advantages and some drawbacks. Some of these features are comparable to the switchSENSE technique.

The two techniques are both able to determine binding rate constants in real time. Additionally, the two techniques are both extremely sensitive and have a low sample consumption [47].

One disadvantage lies in the complexity of the techniques. Both SPR and switchSENSE require trained scientists, who operate the devices, set up the assays and interpret the data correctly. Miss- or over interpretation of data is a common problem [12].

The two techniques both require immobilization of one of the binding partners on the sensor surface. In the case of SPR, there are various surface chemistries available, which enable on-chip hybridization (e.g. carboxymethylated dextran matrix) [47]. Generally, the immobilization of ligand molecules can be problematic. The immobilization has to be stable and the molecule has to remain active. It is furthermore possible that an immobilized biological molecule behaves differently than a molecule that is free in solution. Therefore, the immobilization can influence the interaction [48]. This is a factor for both SPR and switchSENSE, although immobilization techniques differ. There are of course ways to determine the influence of this effect (e.g. assay reversal). Furthermore, other techniques can be used in comparison that do not require immobilization of one of the binding partners (e.g. microscale thermophoresis).

While the immobilization is a drawback that the two techniques share, they both do not require labeling of the binding partners and are therefore considered "label-free". In the case of SPR, the refractive index change of the surface is measured, while switchSENSE uses the fluorescence molecule on the immobilized DNA in close proximity to the ligand molecule for detection. Labeling of one of the binding partners can be as problematic as immobilization (i.e., the label can influence the binding behavior of the molecules).

An advantage of switchSENSE as compared to SPR lies in the controllability of ligand density on the sensor surface. The immobilized single-stranded DNA, to which the functionalized complementary strand hybridizes, allows immobilization at a controlled density, and even enables the immobilization of different ligands on one surface. The immobilization of DNA (for example aptamers) is especially uncomplicated in the switchSENSE technique.

Another advantage of switchSENSE as compared to SPR is the ability to not only measure binding interactions, but also conformational changes and hydrodynamic radii [49], which is not possible with SPR.

Furthermore, it is challenging to quantify multivalent interactions with SPR. The technological specifics of switchSENSE can be advantageous in this respect, as is shown in this thesis.

Generally though, it must be mentioned, that the comparison of measurement techniques of molecular binding interactions is difficult. The technique influences the results. Therefore, differences in results for the same interactions from different techniques are omnipresent and might be difficult to overcome [50].

1.4.4 Single-molecule interactions

The techniques described above rely on averaged signals of many interactions. However, there are also techniques that target individual interactions. These can be very helpful in the understanding of multivalent binding behavior.

There is the possibility of using single molecule force-spectroscopy as described by Cuellar-Camacho et al. [51]. In this technology, the tip of a scanning force microscope (SFM) was used to acquire information about the binding strength of individual interactions, in this case between viral surface proteins and a ligand. By varying the speed, at which the ligand coated tip was removed from the viruses that are immobilized on a surface, the individual binding strengths were investigated for individual virus particles. This technique allowed for the investigation of single bonds ($n = 1$) or multiple bonds ($n > 1$).

Another interesting approach is total internal reflection microscopy as described by Müller et al. [52]. There has been work performed on influenza A viruses binding to sialic acid using this technique, which was able to gain information on the oligovalent binding behavior of individual viruses binding to a surface. The viruses were fluorescently labled and the use of total internal reflection microscopy allowed for the observation of virus particles that were firmly bound to the surface. The group observed residence times of virus particles on a ligand coated surface. While taking into account the mobility of the particles, the group was able to differentiate between dissociation rate constants for different valencies. Furthermore, they described an effect they associated with the involvement of neuraminidase in the binding process.

1.5 Model system

The switchSENSE technology was applied to virus-receptor interactions. The ligands chosen in this thesis were peptides, antibodies and proteins. As analytes, proteins and virus particles were used.

1.5.1 DNA

Nucleotides make up nucleic acids, which store information in a cell. They form long biopolymers. The type of nucleic acid used in this thesis is deoxyribonucleic acid (DNA). It is made up of four different nucleotides: Adenine (A), Guanine (G), Cytosine (C) and Thymine (T). Nucleotides are made up of three components, namely monosaccharides, phosphate residues and bases. The phosphodiester binding between two nucleotides carries a negative charge, which forms the so called negatively charged DNA phosphate backbone [1].

The 5' end of a DNA strand carries a phosphate group, while the 3' end is made up by a hydroxyl group. In order to describe a sequence of DNA, it is common to name the bases from the 5' end to the 3' end, while using the first letter of each base. A double strand is formed via hydrogen bonds between complementary bases (G – C and A – T) of two single strands of DNA. This process is called Watson-Crick-base pairing. It is possible to generate DNA sequences in vitro, which has made them extremely important for science (e.g. forensics) [1].

The Watson-Crick base pairing with partially complementary DNA strands allows for the design of structures that can be extremely elaborate (e.g. [53]), which has opened an entire field of research called DNA origami.

In this thesis, DNA is used as a mechanical lever, to which ligand molecules are tethered in order to investigate their binding behavior. Generally, double-stranded DNA with a length of 48 base pairs is immobilized on the sensors in the DRX^2 [23].

For two experimental projects described here, geometrically arranged DNA nanostructures were used that enable the investigation of oligovalent binding behavior. A DNA-peptide nanostructure developed by Dr. David M. Smith et al. [18, 19] was optimized for the use in the switchSENSE technology. It is made up of four arms of partially complementary DNA, where three arms can be functionalized to carry peptides and one single-stranded arm is used for immobilization on the sensor surface (see Figure 3).

The design of the DNA nanostructure enables the presentation of zero, one, two or three ligands at a controllable distance. This formation is geometrically compatible to the binding sites of the analyte protein. Generally, this approach has proven to enhance binding affinity of peptides compared to monovalent interactions [17, 54]. Theoretically, it is possible to vary the distance between the ligands by extending the number of base pairs or to increase the flexibility of the DNA structure by introducing single-stranded bases at junctions.

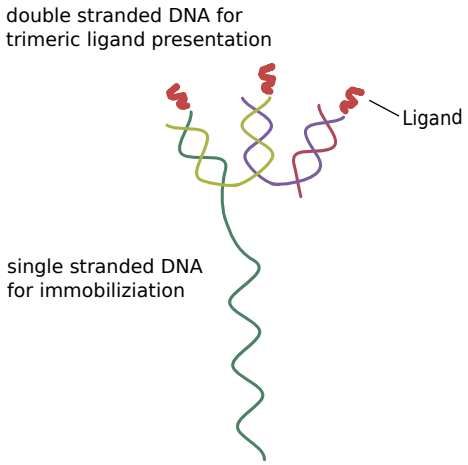

Figure 3: Four-arm DNA nanostructure: The single-stranded overhang of the DNA is used to immobilize the structure on the gold surface of the DRX^2. The trimeric structure on the top can be functionalized with a ligand. The DNA strands are partially complementary as is indicated by the different colors. This schematic representation is not drawn to scale.

1.5.2 Peptides

Peptides, like all proteins, are made up of amine-coupled amino acids. What differentiates this subgroup is the limited number of amino acids. The individual amino acids of the sequence can influence the charateristics of a peptide strongly. Peptides can interact non-covalently with other molecules via electrical interactions (e.g. van-der-Waals interactions, hydrophobic effects, hydrogen bonds) [4].

Peptides are found in nature as for example hormones or toxins. Additionally, they play a major role in the immune system. There have been reports on peptides used in therapeutics (e.g. for the treatment of diabetes related fluid loss [4]) or in biosensors [55].

Peptides can be immobilized on sensor surfaces and specifically bind analytes. There are various strategies for immobilizing peptides on sensor surfaces, including adsorption, or covalent chemical coupling via functional groups. Coupling and immobilization can interfere with the binding ability of a peptide.

Peptides can be produced automatically and easily by solid phase peptide synthesis. The production is fast and inexpensive compared to other biomolecules as for example antibodies [56].

However, peptides can show unspecific binding and generally have lower binding strength towards their target than antibodies. The lower specificity and sensitivity of peptides are challenges that remain [57]. The low binding strength can be addressed by using multivalency [58, 59]. This can be done for example by attaching the peptides to various scaffolds to reach multivalent

presentation. These can be polyglycerol structures [15] or nucleotides [17].

When arranging the peptides in a well-defined order, which matches the geometrical structure of epitopes on the analyte structure, a significant increase of binding strength can be observed (e.g. [17] and most recently [54]).

1.5.3 Antibodies

Antibodies are proteins and part of the immune system. Emil von Behring, who was awarded the Nobel Prize for Medicine in 1901, frist described the antitoxin against diphtheria toxin. When the human immune system is brought into contact with an infectious substance (e.g. a virus or bacterium), the immune system reacts - among other things - with the production of antibodies, which can bind to the antigen and enable phagocytosis. There are different classes of antibodies. The one used here is the most common in humans and is called: immune globulin G (IgG). It has a molecular weight of around 150 000 Da and is made up of two heavy chains and two light chains, which are connected by disulfide bridges. The lower part of the Y-like structure is called the "fragment crystallizable" (FC), while the upper part above the joint region is called the "fragment of antibody binding" (Fab) [60].

The Fab-fragments contain the antigen-binding region, the so-called complementary determining regions (CDRs), which vary for different antibodies. This region binds to the target structure on the antigen [60]. For binding interaction studies, it is possible to use entire antibodies, fragments like the Fab fragment or even smaller subparts of the functional region (e.g. a peptide derived from the CDR [61]). The binding can be similar for fragments as compared to the entire structure. However, the surrounding amino acids of the CDR, which are not directly involved in the binding process, can be of essential importance regarding stabilization of the geometrical structure and variations can influence the overall binding strength [4].

IgG antibodies use two Fab fragments, which can carry up to 12 paratope regions [60], making the antibody a good example of a naturally occurring oligovalent binder.

1.5.4 Viruses

Viruses are widely present in nature. They are infectious biological entities that rely on host organisms for replication. One definition found in "Principles of virology" describes viruses as "obligate intracellular parasites" [2]. Viruses were originally discovered as pathogenic agents that could not be retained by bacteria proof filters in the late 19^{th} century and the beginning of the 20^{th} century. The sizes of viruses span from around 16 nm (circovirus) to almost 1 µm (so called giant viruses like the Mimivirus ($\sim$ 0.75 µm in diameter)). Viruses contain a viral genome, which is made up of DNA or RNA and which includes the codes for viral components. In order to replicate, viruses use the cells of a host organism and self-assemble from newly synthesized components. In order to infect host

cells, the virions (infectious virus particles) bind to a host cell, are internalized and reproduce inside the cell [2].

Viruses can have various shapes and structures. One differentiates (among other characteristics) between viruses that are enveloped, which means they are surrounded by a lipid bilayer (e.g. influenza virus or coronavirus), and viruses without an envelope (e.g. adenovirus) [2].

The understanding of virology remains incomplete. New viruses are discovered, including highly pathogenic ones like the novel SARS-CoV-2. However, viruses have also been found to be beneficial and might even have necessary effects in organisms. Additionally, viruses are nowadays used as therapeutics for example as so-called "vectors" (i.e. transport entities) in vaccinations or in viral oncotherapy [2, 62].

As viruses depend on the host organism for replication, the first step of the viral life cycle generally lies in the attachment to a host cell. This is often performed by proteins, which for enveloped virus particles are anchored in the lipid bilayer and attach to a receptor structure on the target cells [2].

The negative effects of pathogenic viruses have been present especially during the last two years when the severe acute respiratory syndrome coronavirus 2 (SARS-CoV-2) spread globally. The effect has been catastrophic, including over 6 million reported deaths by August 2022 [63], while this number is most likely an underestimation [8]. The economic costs for Germany alone are on the order of billions of Euros [64].

Similarly to SARS-CoV-2, influenza viruses have caused epidemics and pandemics, including the so-called Spanish flu in 1918, with millions of deaths [9]. Annual epidemics of varying severity put a strain on health infrastructure and damage the economy as workers fall sick [10].

For the case of influenza, the attachment and subsequent viral fusion with the host cell is well studied [2, 65]. Influenza viruses carry three membrane proteins, of which hemagglutinin is the one that is involved in the attachment process. It is a glycoprotein and can bind to sialic acid containing receptor cells [65].

Hemagglutinin makes up around 80 % of all surface proteins of influenza [66]. It has a homotrimeric structure with an average distance of around 4 nm between binding sites and a distance of around 10 nm between two hemagglutinin proteins on the viral membrane [67]. The individual binding strength of hemagglutinin to sialic acid is weak, at a value in the millimolar range [65]. The multivalent presentation of the protein enhances this affinity. The overall affinity of influenza viruses to the receptor surface is high [65]. After attachment to the host cell, the virus is endocytosed, which is induced by an acidification of the interior of the endosome by an influx of protons (H+ ions). Subsequently, the hemagglutinin undergoes a conformational change, which brings the two membranes close together. This enables a fusion of the virus membrane with the cell membrane of the endosome and subsequent release of viral genetic material into the cell [2, 66]. The process of influenza virus particles binding to a receptor cell is exemplary for the multivalent binding strategy of viruses. Therefore, influenza was chosen as a model object for the study of multivalent binding

behavior.

Part II
Material and methods

This part describes all experimental work in detail. The devices that were utilized are presentented as well as all procedures and material. In section 2, the switchSENSE measurement principle is explained in detail, including sample preparation, binding interaction measurements and hydrodynamic radii determination. The devices that were primarily used for the experimental work are described in section 3. Section 4 specifies the exact parameters chosen for the actual experiments to ensure reproducibility. A list of the utilized material is given in section 5 and a short overview of the data analysis can be found in section 6.

2 switchSENSE

The switchSENSE technology is based on the electrical manipulation of DNA strands and optical detection of fluorescence signals. While the technology can be used for various experiments (e.g. DNA melting or enzymatic activity), in this thesis it was applied to binding interaction measurements and measurements of hydrodynamic radii. These measurement principles are explained in the following.

2.1 Sample preparation

To enable characterization measurements of biological molecules and their interactions using the DRX^2, the sensor surface is functionalized with double-stranded DNA, to which a ligand molecule of interest is attached. The coupling of the ligand to the complementary single-stranded DNA can be performed prior to the experiment by covalent coupling or a tag can be utilized in the so-called capture coupling method. Either way, the ligand molecule of interest has to be attached to the DNA.

The analyte molecule, which is injected into the channel for binding kinetics measurements, remains unchanged. High sample purity and exact determination of concentrations are prerequisits for quantitative analysis. The analyte sample should be dissolved in the same buffer as the running buffer, if possible.

2.1.1 Ligand - DNA coupling

Two coupling strategies are available, namely covalent coupling or immbilization via a capture molecule.

For covalent coupling, the ligand molecule of interest is chemically coupled to the single-stranded DNA prior to immobilization and outside of the DRX^2. Various coupling chemistries are available in pre-organized and standardized coupling kits. The amine coupling kit for molecules with a molecular weight of

more than 5 kDa by Dynamic Biosensors was used regularly [68]. The chemistry is NHS-EDC based [69]. It is recommended to utilize 100 µg of analyte protein for one coupling reaction. After the coupling protocol is performed, the sample is purified by either ion-exchange chromatography or centrifugation. Subsequently, the buffer is exchanged and the concentrations are determined by spectral photometry [68].

For capture coupling, the complementary DNA strand carries a capture molecule like tris-NTA, biotin or protein G [70]. The actual ligand of interest is then immobilized by a "capture assay". After hybridization of the DNA-capture molecule complex, the ligand is injected and binds to the capture molecule. The immobilization can be observed in real time. No further preparation of the ligand sample is needed. Subsequently, the analyte binding to the captured ligand is measured [23].

Both strategies have advantages and disadvantages. The amount of ligand needed for one capture immobilization (V = 40 µL, c = 500 nM) is lower than for performing one covalent coupling protocol (100 µg). However, the yield of the covalent coupling is normally high enough for multiple immobilizations.

The risk of losing sample, when a mistake is made during the chemical coupling procedure, remains higher for the covalent coupling than for the capture immobilization.

It has to be taken into consideration that the binding strength of the capture reaction has to be higher than the one between the ligand and the analyte. Otherwise, the signals of the two interactions can overlap and lead to false results.

2.1.2 On-chip hybridization

A monolayer of around one million DNA strands is immobilized on each of the six gold electrodes of one channel on the measurment chips [71]. Prior to any hybridization, the surface is regenerated by a solution of high pH (pH 13, most likely NaOH, provided by Dynamic Biosensors) to denature the double strands. Afterwards, in order to functionalize the surface again, the complementary DNA strand is flushed into the microchannel over a hybridization time of 350 s, while an alternating voltage is applied to the electrodes.

The hybridization can be observed in real time, which is exemplarily shown for cNLB48 in Figure 4. In the beginning ($0\,\mathrm{s} \leq t \leq 20\,\mathrm{s}$), the single-stranded DNA oscillates close to the gold surface, which results in a low fluorescence signal due to energy transfer from the fluorophore to the gold electrode. Once the complementary strand becomes available, double strands start to form on the sensor surface ($20\,\mathrm{s} < t \leq 200\,\mathrm{s}$ in Figure 4). The double-stranded DNA has a longer persistence length [4] and therefore the fluorophore will be moved further away from the gold surface during repulsion phases. This increases the fluorescence signal. When all available DNA strands are hybridized, a saturation of the fluorescence signal is reached ($t \geq 200\,\mathrm{s}$ in Figure 4).

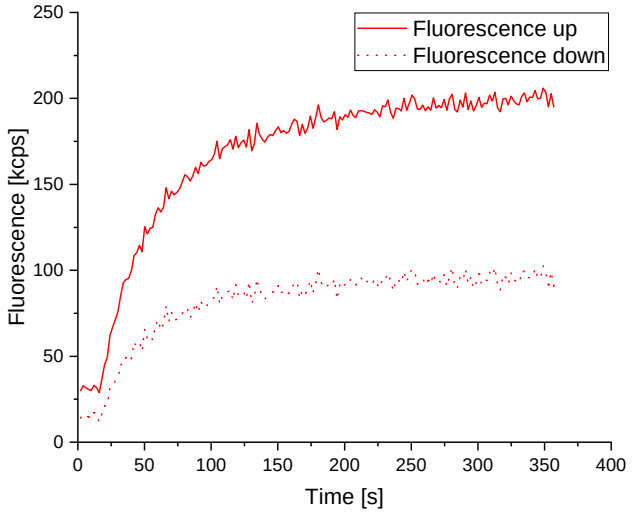

Figure 4: Hybridization of DNA. The injection of complementary DNA leads to an increase of the “fluorescence up’(solid red line) and “fluorescence down" (dotted red line) signal. The graph shows the immobilization of pure complementary DNA.

The on-chip hybridization curve can indicate a successful coupling. First, an observable increase of fluorescence amplitude during hybridization indicates that complementary DNA is available in the sample. Secondly, the hybridization curve is influenced by size and charge of the DNA and its covalently coupled molecule. A successful coupling therefore generally results in a hybridization curve that can be distinguished from pure complementary DNA. This might not be the case for small and uncharged molecules though.

2.2 Binding interaction measurements

The binding of an analyte molecule to an immobilized ligand results in a change in the observed fluorescence signal. Two measurement modes are available.

2.2.1 Dynamic mode

In the dynamic mode, an alternating (AC) voltage is applied to the gold electrodes. The negatively charged DNA is influenced by the charge of the gold surface. A negatively charged electrode leads to a repulsion of the DNA, while a positive charge leads to an attraction of the DNA lever. Since the DNA is anchored to the surface at one end, the AC voltage results in an oscillatory movement of the lever [23].

An electrically triggered time correlated single photon counter measures the light that is emitted by the fluorescence molecule at the distal ends of the levers. The light intensity varies according to the position of the DNA above the electrode surface due to quenching effects. The fluorescent light intensity oscillates periodically and can be observed in real time and correlated to the AC voltage signal [39].

Upon a binding event, the speed of the nanolever through the buffer solution is slowed down as the hydrodynamic friction increases. This reduction in speed can be detected in real time [16].

2.2.2 Static mode

In static mode, a negative direct voltage is applied to the gold electrodes. This results in a constant upright standing position of the DNA levers. Upon a binding event in close chemical proximity to the fluorophore, the light emission intensity varies. It can increase or decrease depending on the type of interaction. This measurement mode does not depend on the size of the analyte. It cannot be used to determine hydrodynamic radii [23].

2.2.3 Comparison

In general, both measurement modes are highly sensitive and well suited to measure binding interactions.

In the course of this work it was observed that the dynamic mode strains the chip surface more than the static mode. When only buffer is injected as analyte (also called "blank measurement"), a stronger signal decrease can be observed in the case of the dynamic mode than in the static mode. This is most likely due to mechanical stress on the DNA levers. It can lead to a detachment of entire levers from the surface, which can be problematic for reproducibility of the results.

Still, the dynamic mode can be necessary in specific cases as for example for measuring conformational changes upon binding. In that case, it can be difficult to differentiate between binding signal and conformational change signal.

Additionally, the rapid switching speed ($f \sim$ kHz) of the dynamic mode can be beneficial when considering diffusion limitations of binding interactions.

Furthermore, the measurements in the dynamic mode return various data subsets: "Dynamic Response" for three time intervals, "Dynamic Response Down" for two time intervals, "Fluorescence", "Fluorescence Down" and "Fluorescence Amplitude". Depending on the interaction, one of the data subsets can be optimal for analysis. In static mode, only "Fluorescence" is measured. This corresponds to the fluorescence intensity.

2.3 Determination of hydrodynamic radii

Additionally to measuring binding interactions, the DRX^2 was also used for the determination of hydrodynamic radii. This is done by applying an alternating

voltage and measuring the switching speed of the lever. Depending on the size and charge of the DNA lever, eventually carrying a ligand and/or an analyte molecule, the hydrodynamic friction changes. The signal of the motion is then compared to the one of pure double-stranded DNA (48 base pairs) [23].

Determination of hydrodynamic radii or "sizing measurements" have to be carried out in specific buffers (XE40 buffers [23]). The theoretical model, from which hydrodynamic radii are calculated and which is called the "lollipop-model", was developed with the characteristics of these buffers (e.g. ionic strength) [49]. When an alternative buffer is used, absolute values of hydrodynamic radii cannot be determined. However, those results can be used for qualitative comparisons and are then called "molecular dynamics" measurements rather than sizing measurements.

It is possible to perform sizing measurements during kinetic measurements. In this case, the DNA nanolever oscillates prior to the association, while carrying only the ligand molecule, and after the association prior to the dissociation, when the analyte should have bound. The results of the kinetic measurement and of the sizing measurement should complement each other. The binding of an analyte to a ligand should lead to a change in the switching motion during the sizing measurement after the association.

Normally, the sizing or molecular dynamics measurements are performed on several electrodes consecutively. Every additional electrode increases the measurement time but also the statistical validity. Generally, two or three electrodes were chosen.

2.4 Assay setup and software

To perform an experiment with the DRX^2, three softwares are necessary: switchBUILD for assay setup, switchCONTROL for device control and assay execution, and switchANALYSIS for data analysis and visualization.

2.4.1 Assay setup

The switchBUILD program versions 1.10.0.32 and 1.12.0.21 were used for assay setup. A passivation assay was performed at the start of each day to prevent unspecific binding to the sensor surface by injection of a thiol-containing passivation solution. Subsequently, the type of measurement that should be performed was selected from predefined options. Generally, kinetic or sizing measurements were performed. The experiments were always terminated by a standby routine to reset the chip surface to pure double-stranded DNA for storage at the end of a measurement day [23].

2.4.2 Assay execution

The switchCONTROL software operates the DRX^2. It is used for direct communication between the computer and the instrument. All running parameters are presented and can be controlled here. Measurements can be observed in

switchCONTROL in real time. The workflows that were previously compiled in switchBUILD are loaded into switchCONTROL and are then executed. It is possible to change specific parameters of the predefined setup of the switchBUILD assay elements (e.g. hybridization time or frequency of the AC voltage). After an experiment is completed, the resulting data is stored in a .zip file and can be evaluated using the switchANALYSIS software. Furthermore, any technical issue regarding the instrument is recorded in switchCONTROL [23].

2.4.3 Analysis

The switchANALYSIS software is used to analyze data from the DRX^2. Fluorescence data can be visualized in plots of signal intensity over time.

For kinetic data, it is possible to calculate association and dissociation rate constants and dissociation constants. This can be done by global or individual fit functions, for mono- or bivalent interactions.

From sizing data the software can calculate hydrodynamic radii in the range between 2 nm to 14 nm [23].

It is possible to export data in various formats and analyze them further. As the underlying functions, which the software uses for the calculation of binding rates, were unclear at the time and the controllability of the analysis is limited, the data was exported to OriginPro for analysis (see section 6). switchANALYSIS was primarily used to visualize the data, for qualitative comparisons and for the evaluation of sizing measurements.

3 Devices

The device that was primarily used for the production of data was the DRX^2 by Dynamic Biosensors. All binding interaction measurements were performed on the device as well as sizing measurements. The device and its components are described in detail in this section. Additional devices used in this thesis are shortly mentioned.

3.1 DRX^2

The DRX^2 by Dynamic Biosensors GmbH (Martinsried, Germany) was used for binding interaction and sizing measurements.

3.1.1 Setup

The DRX^2 is a tabletop device. The instrument contains a fluidic system with two pumps, namely a 5 mL syringe pump and a peristaltic pump (Watson-Marlow). The fluidic system enables the device to transport sample solutions from vials in the autosampler rack as well as solutions from buffer reservoirs through the channel of a measurement chip and across the sensor surface [71].

The optical detection system is made up of a microscope, filters, lenses, detectors and LED light sources. Through the light microscope the position above

the electrodes can be observed prior to and after fluorescence measurements. The microscope is used to automatically determine the correct focal plane for the fluorescence detection measurements. Light from LED light sources excites the fluorophores on the electrode surface and a system of filters ensures emitted light is detected and excitation light is suppressed. The light emitted by the fluorescence molecules is then detected in real time by an electrically triggered time correlated single photon counter [16]. The DRX^2 is equipped with two detectors for two separate wavelength ranges. The device can measure fluorescence emitted in the green wavelength range and in the red wavelength range simultaneously [23].

A voltage source is connected to each gold electrode in the microfluidic channel. The electrodes in each channel can be individually addressed. Alternating voltages (AC) and direct voltages (DC) can be applied. The voltage ranges between -1 V and 1 V and the frequency can be varied. It is recommended to use a frequency between 0.1 Hz and 4 Hz for low frequency switching and between 1 kHz and 1 MHz for switching at high frequencies [71].

The autosampler vial rack and the measurement chip are temperature controlled. The chip temperature can be varied between 10 °C and 50 °C. The standard measurement temperature of the chip is 25 °C, while the vial rack is kept at 20 °C [71].

3.1.2 Measurement chips

All measurement chips, which are also called "biochips" by Dynamic Biosensors GmbH, are made up of a glass substrate carrying four microfluidic channels. A 60 µm thick foil separates the glass from the indium tin oxide coating that serves as counter electrode. The channels have a width of 1 mm. Over a distance of 3.34 mm, six gold electrodes with a diameter of 120 µm are located in each channel (see Figure 5) [71].

On the gold electrodes, single-stranded DNA nanolevers are covalently coupled to the surface by a gold-thiol bond. During the production process of the chip, the DNA levers form a self-assembled monolayer and subsequently the density is adjusted by electrical desorption [72].

The DNA strands are coupled to the gold surface at the 5' end. The 3' end carries a fluorescent molecule.

Chip types The standard chip that was used for most experiments carries the following notation: MPC-48-1-R1-S. MPC stands for multipurpose chip, 48 is the number of nucleotides of the DNA lever on the chip, 1 is the number of DNA sequences on the chip, R1 is the "name" of the fluorophore, where R stands for red and S stands for standard.

Another chip type used is MPC2-48-2-G1R1-S. The 2 after MPC indicates that there are two DNA sequences on the electrodes, which is also indicated in the 2 after 48. G1 in this case stands for "green 1", the color of the emitted light from the second fluorophore.

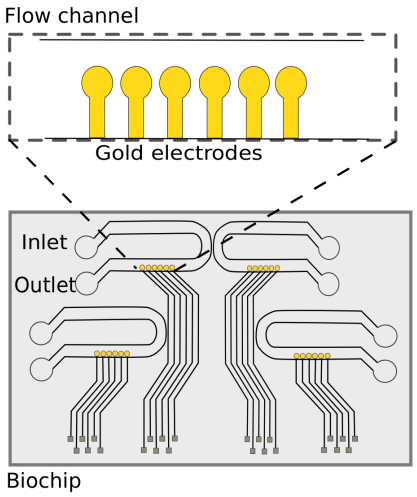

Figure 5: Measurement chip design: One chip consists of four microfluidic channels. They contain six electrodes each, which can be individually adressed by a voltage source. The schematic is not drawn to scale.

The DNA strands have names. The name of the immobilized strand is made up of the abbreviation of "nano lever" (NL), the name of the DNA sequence (e.g. B) and the number of base pairs (e.g. 48). On the standard chips, the immobilized strand is therefore called NL-B48. The complementary strand can be identified by a lowercase "c" before the name (e.g. cNL-B48). The sequences of the used DNA nanolevers can be found in Table 1.

Most experiments were performed with standard MPC-48-1-R1-S biochips. The behavior of the various chips can differ based on the utilized analytes, ligands, ligand densities and fluorophores.

For switching measurements of virus samples, an adapter chip was utilized (see subsection 4.5 and section 8).

Chip handling The chips were handled according to the manufacturer's instructions: they were kept in desiccation bags at 4 °C in the dark for storage. Chips in unopened bags are usable for up to six months according to the manufacturer. Prior to insertion of the measurement chips into the device, they were taken out of the fridge to reach room temperature and to avoid condensation. On each day prior to the first measurement, a passivation of the chip surfaces and a fluorescence status test were performed. The passivation reduces unspecific binding, while the chip status test reveals, which electrodes are best suited for experiments. As a rule of thumb, electrodes that showed a fluorescence intensity signal of less than 50 kcps during the chip status test were no longer used. The measurement chips were normally left in the DRX^2 during the week, when experiments were performed daily. When the experiments for the week were done, the chips were regenerated and complementary DNA was hybridized

Name	Sequence 5' → 3'
NL-A48	TAG TGC TGT AGG AGA ATA TAC GGG CTG CTC GTG TTG ACA AGT ACT GAT
cNL-A48	ATC AGT ACT TGT CAA CAC GAG CAG CCC GTA TAT TCT CCT ACA GCA CTA
NL-B48	TAG TCG TAA GCT GAT ATG GCT GAT TAG TCG GAA GCA TCG AAC GCT GAT
cNL-B48	ATC AGC GTT CGA TGC TTC CGA CTA ATC AGC CAT ATC AGC TTA CGA CTA

Table 1: DNA sequences of the standard measurement chips. NL-A48 and NL-B48 are coupled to the gold electrode at the 5' end. They carry a fluorescent molecule at the 3' end. cNL-A48 and cNLB-48 are usually functionalized with a ligand molecule at the 5' end and are complementary to NL-A48 and NL-B48.

(standby routine). Prior to ejection, the channels of the measurment chips were vented first in the DRX^2 and after ejection again manually using N_2. Once opened, chips were normally not used for more than four weeks, depending on the experiments and the strain they posed on the chip surface.

3.2 Anion exchange chromatography

After the chemical binding of complementary DNA to a ligand molecule, it is necessary to separate the conjugate from free DNA and free ligand. This was done by anion exchange chromatography with a device called ÄKTA Start by GE Healthcare Bio-Sciences (Uppsala, Sweden). The recommended buffers (Buffer A, 150 mM NaCl, and Buffer B, 1 M NaCl, see section 5.2 for exact recipe) were used to create a salt gradient. After cleaning and priming procedures (100% Buffer A), the DNA-conjugate sample is manually injected and the purification run starts with a step to 20% Buffer B (flow rate: 1 mL min^{-1} for a time $t = 1$ min), followed by a linear increase to 100% Buffer B using a flow rate of 1 mL min^{-1} for $t = 10$ minutes. The salt concentration is increased gradually leading to a separation of the components of the sample according to their surface charge from the chromatographic column. A UV-detector is used to determine the absorption of DNA and protein of the washed-out solution. The fractions are collected in standard Eppendorf tubes. The resulting chromatogram can then be compared to existing chromatograms to determine, which fractions correspond to the free DNA, the free protein and the conjugate.

3.3 Spectral photometry

Spectral photometry was used to determine protein concentrations. A Nano Drop ND 1000 Spectrophotometer was used for determining protein concentrations. The method is based on absorption of light of proteins at a wavelength

of 260 nm. The Nano Drop was first blanked by buffer solution and all concentration measurements were repeated three times.

3.4 Fluorimeter

The fluorimeter Perkin Elmer LS55 Luminescence Spectrometer was used to determine absorption and emission spectra of four fluorophores attached to cNLB48 during the beta testing phase of the adapter chip. The solutions containing the fluorescently labelled DNA were injected into a cuvette and the standard measurement protocol was performed to acquire emission and absorption spectra.

3.5 Dynamic light scattering

The Zetasizer Nano ZS by Malvern Instruments Ltd was used to determine hydrodynamic radii of protein and virus samples. The method is based on light scattering on particles and their Brownian motion. The auto correlation is used to determine hydrodynamic radii. The device was primarily used for quality control and comparative measurements.

4 Experimental assays

In this subchapter the specific parameters are presented, that were used for the individual measurements. The determination of the correct assay setup is an essential part of the experimental effort. The protocols are arranged corresponding to the order of relevance and extent of the experiments. The order is identical to the one of the presentation of the results in part III. If not otherwise stated, all measurements were performed on standard multipurpose biochips, at a system temperature of 25 °C, with PE40 as auxiliary buffer and PE140 as running buffer. Conjugate hybridizations were done at the recommended concentration of 500 nM and volume (40 µL) for a hybridization time of 350 s, if not specifically stated otherwise.

4.1 Peptide-influenza A viruses

The results of the peptide - influenza A virus experiments have been published in the article “Measuring Influenza A Virus and Peptide Interaction Using Electrically Controllable DNA Nanolevers” by Kruse et al. in the Journal Advanced Materials Technologies in October 2021 [73].

4.1.1 DNA-peptide nanostructure

The DNA nanostructures were developed and assembled by Dr. Christin Möser and the group of Dr. David M. Smith at Fraunhofer IZI, Leipzig, Germany. The conjugation of peptides PeB to the DNA was done with copper-free click chemistry [17, 74].

In short, the oligonucleotides that carry amino groups were incubated with DBCO-NHS ester. They were then coupled to peptides, which carry an azide group. Purification and incubation steps ensured correct coupling interactions. The structures were heated in a thermocycler to ensure correct folding. This was furthermore verified by native polyacrylamide gel electrophoresis [17, 74].

The protocol allowed varying the number of peptides between zero, one, two, and three peptides per construct. The DNA nanostructures were then named ss0PeB, ss1PeB, ss2PeB and ss3PeB, where 'ss' stands for single strand referring to the cNL-B48 overhang, the figure indicates the number of coupled peptides and PeB is the name of the peptide. When all or a subset of the four nanostructures is described in the text, they are referred to as ss0/1/2/3PeB.

For the experiments, all possible variations were employed. The DNA nanostructure without peptides served as negative control.

4.1.2 Binding assay

The static measurement mode was selected for all experiments.

Since the experiments strained the chip surface, generally no more than four measurement cycles were performed per channel. It was ensured that the fluorescence amplitude of the measurement electrode in the chip status tests was higher than 50 kcps.

The virus samples were dissolved in running buffer PE140 and the concentration was adjusted to lie between 10 µg mL^{-1} to 160 µg mL^{-1}. The parameters for the association and dissociation measurements were varied and optimized. The main results presented here were acquired with an association flow rate of 1 µL min^{-1} and an analyte volume of 50 µL resulting in an association time of 50 min. The experimental parameters of the dissociation were varied.

The system temperature was kept at 25 °C, with an exception for the temperature variation measurements.

4.1.3 Sandwich assay

For the sandwich assay experiments, the four-arm DNA nanostructures were fluorescently labelled. This was done by hybridizing NL-W48-B48-G1 to the cNL-B48 section of the nanostructure of ss0/1/2/3PeB. NL-W48-B48-G1 is a 96 nucleotides long single-stranded DNA that is tagged with a green fluorophore (G1). It was mixed with ss0/1/2/3PeB at a 1:1 ration (v/v) (20 µL of $c = 1\,\mu M$ each) in a glass vial and incubated at room temperature for one hour in the dark.

A capture assay was selected in switchBUILD. ss2PeB was hybridized on the sensor surface as the capture molecule and X31 virus material served as ligand in this setup. The concentration of the virus solution was chosen at 40 µg mL^{-1} and the association volume of 50 µL was injected at a flow rate of 1 µL min^{-1}. Subsequently, the fluorescently labelled DNA-nanostructure was injected as analyte and the binding interaction was measured using a flow rate of 3 µL min^{-1} for a sample volume of 40 µL. The dissociation was observed for 20

min, while a flow rate of 500 µL min^{-1} was generated by the peristaltic pump. Here as well, all measurements were performed in the static measurement mode.

4.2 Peptide - SARS- CoV-2

Kruse et al. have published a manuscript that includes the following experimental methods under the title "Characterization of binding interactions of SARS-CoV-2 spike protein and DNA-peptide nanostructures" in the journal Scientific Reports [75].

4.2.1 DNA-peptide nanostructure

The DNA-peptide conjugates were synthesized according to the method described in subsection 4.1.1. The synthesis was performed by Basma Altattan from the group of Dr. David M. Smith at Fraunhofer IZI, Leipzig. In this case however, the DNA structure carried the SBP1 peptides. The monovalent presentation of the SBP1 peptide was accomplished by coupling the peptide to an amine-modified cNL-B48 DNA strand by copper-free click chemistry [75].

4.2.2 Binding assay

The surface was regenerated with fresh DNA-peptide structures prior to each measurement.

For measurements with spike protein fragments, concentrations generally ranged between 25 nM and 500 nM. Higher concentrations were chosen for individual fragments (e.g. RBD). An analyte volume of 300 µL and a flow rate of 50 µL min^{-1} were chosen for the association. This resulted in an association measurement time of six minutes. The dissociation was observed for 20 min, while the peristaltic pump supplied buffer at a flow rate of 1 mL min^{-1}.

For the experiments with inactivated virus material and pseudo viruses, the association volume was reduced to 100 µL and the flow rate was decreased to 5 µL min^{-1}. The dissociation was measured for 10 min at a flow rate of 1 mL min^{-1} (peristaltic pump).

4.3 Antibody - SARS CoV-2

4.3.1 Coupling

All six antibodies were covalently coupled via EDC-NHS chemistry to single-stranded DNA cNL-B48-01 with components and instructions of the "Amine-Coupling Kit 1 for proteins > 5 kDa" by Dynamic Biosensors GmbH [68]. For each conjugation 100 µg of antibody was employed. After the antibody was added to the freshly prepared cNL-B48-crosslinker solution, the mixture was incubated for one hour at room temperature and then kept at 4 °C in the dark over night. Afterwards an ion exchange chromatography using the ÄKTA Start was performed to separate the conjugate from free antibody and free DNA. Subsequently, the DNA-antibody conjugate was concentrated and buffer was

exchanged to PE140 using the provided centrifugal filter units (3 kDa MWCO). The concentration was determined by spectral photometry (Nano Drop ND 1000 Spectrophotometer). The conjugate was kept at 4 °C until further use.

4.3.2 Binding assay

Conjugate hybridization was chosen as immobilization method and cNL-B48-antibody conjugates were injected at a concentration of 200 nM for a hybridization time of 350 s. The reduced concentration was chosen because of the low initial concentrations of cNL-B48-antibody conjugates after the coupling reaction. By reducing the concentration during hybridization, less amount of conjugate sample was needed. Although the hybridization time is automatically increased for concentrations of less than 500 nM by the switchBUILD software, it was observed that 350 s were sufficient to reach a saturated fluorescence signal. Longer hybridization times led to a reduction of the fluorescence amplitude, presumably due to a loss of DNA strands or fluorophores. Therefore, the hybridization time was decreased manually to 350 s in switchCONTROL prior to each measurement. All measurements were carried out in static mode.

For determining binding rate constants of SARS CoV-2 nucleocapsid proteins (from E.coli bacteria and HEK293 cells) to the antibodies, analyte concentrations ranging between 25 nM to 100 nM were used. During the association measurement, an analyte volume of 80 µL was injected at a flow rate of 20 µL min^{-1} for four minutes. The dissociation was observed for 10 min or 20 min, while injecting 20 mL or 40 mL of running buffer PE140 at a flow rate of 2 mL min^{-1} using the peristaltic pump.

For the final quantitative determination of the binding rate constants of nucleocapsid protein from *E.coli* cells binding to the six antibodies, all measurements were performed on the same measurement chip, on the same channel and on the same electrode in order to minimize chip specific influences.

For the binding affinity measurements of antibody G230AH2 and the nucleocapsid protein from human embryonic kidney 293 cells, the same parameters of the binding assay were chosen, but the measurements were performed on another biochip.

For the interaction measurements between the antibody G230HC9 and inactivated virus solution, the association volume was chosen at 100 µL and the flow rate was set to 5 µL min^{-1}. For the dissociation, 40 mL buffer solution was injected at a flow rate of 2 mL min-1 for 20 min. As a negative control growth medium (RPMI 1640 + 10 % FCS) was injected after immobilization of cNL-B48-HC9.

4.4 Antibody - adenovirus

4.4.1 Coupling

The coupling was performed analogous to the protocol in subsection 4.3.1. 100 µg antibody was employed for the reaction (50 µL at a concentration of 2 mg

mL^{-1}). Ion exchange chromatography was used for purification of the conjugate. As had generally been observed for coupling antibodies to cNL-B48, the chromatogram showed two separate peaks where the conjugate is expected. It can be assumed, that the peaks correspond to a varying number of cNL-B48 strands per antibody [76]. The first peak most likely corresponds to a 1:1 ratio of cNL-B48 and antibody, while the second peak corresponds to two cNL-B48 strands coupled to one antibody. Therefore, the fractions of the first peak were collected, a buffer exchange was performed (to PE140) and the resulting sample was utilized for binding interaction experiments.

The yield for antibody-cNL-B48 coupling by using the amine-coupling kit from Dynamic Biosensors is low (estimated at ~ 10 %). A site specific coupling as well as an improvement of reaction yield would be of interest. For the purpose of the binding kinetics experiments in this thesis however, the yield was sufficient.

4.4.2 Binding assay

A concentration of 200 nM was chosen for an on-chip hybridization time of 660 seconds.

The analyte concentration of the adenovirus solution was varied between 105 pM and 250 pM. The association parameters included a flow rate of 1 µL min^{-1} for 50 min for an association volume of 50 µL. The parameters for the dissociation were varied.

4.5 Sizing of influenza A viruses

During a beta testing phase of newly developed adapter chips, experiments on oscillation of virus particles were performed. These required the use of the adapter chips, DNA-origami levers and a variation of the assay setup.

4.5.1 Adapter chips

The adapter chips were used according to the beta testing instructions. The experimental assays were still designed in switchBUILD and carried out in switchCONTROL software. switchBUILD has no predefined assay that is suitable, but the manufacturer provided a so-called “sequential hybridization” protocol. This was incorporated into the assay in the task flow of switchCONTROL.

4.5.2 Functionalization of origamis

The origamis (50 nm nanolevers, see subsection 8.3) were functionalized with the cNL-B48-ligand conjugate prior to hybridization in the DRX^2. 35 µL of origami solution ($c = 1$ nM) were mixed with 5 µL of ss3PeB at a concentration of 100 nM. The mixture was incubated in the dark at room temperature for at least 1 h. No further purification steps were performed.

The switchCONTROL task flow had to be adjusted. Hybridization time was extended to 600 s, the AC voltage range was set to $V_r = +0.1$ V and $V_a = +0.25$ V and the duty cycle was set to 0.5.

For stopped flow measurements, the "auto potentials" were inactivated. Furthermore, the AC voltage range was set to $V_r = -0.1$ V and $V_a = +0.5$ V and the duty cycle was set to 0.5. The switching frequency was set to 1 kHz or 0.05 kHz, depending on the experiment.

5 Material

5.1 SARS-CoV-2 proteins

All samples were used according to manufacturer's instructions. No further purification steps were taken.

Name	AA/MW	Modifications	Expression System	Producer
RBD	AA 319-519, ∼ 30 kDa	His Tag, Avi Tag	Human	Genscript USA, Inc.
RBD	AA 329-538, ∼ 30 kDa	His Tag	Drosophila S2	Fraunhofer IZI, Leipzig, Germany
S1	AA 16-685, ∼ 79 kDa	His Tag	Human	Genscript USA, Inc.
S1	AA 15-682, ∼ 100 kDa	His Tag	Drosophila S2	Fraunhofer IZI, Leipzig, Germany
SARS-CoV-2 Spike protein (ECD)	AA 16-1213, ∼ 135 kDa	His Tag, Flag Tag	Sf9 insect	Genscript USA, Inc.
SARS-CoV-2 S Protein	AA 16-1213, ∼ 135 kDa	His Tag	HEK293	Acro Biosystems
SARS-CoV-2 Spike (S) Protein	AA 14-1213, ∼ 137 kDa	His Tag, Mutated polybasic/furin cleavage site to alanine & K986P/V987P	HEK293	Invivo BioTech Services GmbH
Active Trimer	AA 16-1213, ∼ 138 kDa	His Tag, Trimer motif (26 AA linker) at C-terminus	HEK293	Acro Biosystems
Super Stable Trimer	AA16-1213, ∼ 138 kDa	F817P, A892P, A899P, A942P, K986P, V987P & alanine substitutions R683A/R685A (furin cleavage site)	HEK293	Acro Biosystems

Table 2: SARS-CoV-2 Spike protein fragments and full length proteins and their characteristics.

Nucleocapsidprotein from *E.coli* cells Recombinant nucleocapsid protein of SARS-CoV-2 from *E.coli* cells was provided by HybroTech GmbH. They had originally received the sample from the Charité Berlin in PBS buffer.

Nucleocapsidprotein from HEK 293 cells Recombinant nucleocapsid protein of SARS-CoV-2 from HEK 293 cells was purchased from GenScript Biotech (Netherlands) B.V.. The manufacturer was RayBiotech, USA. It consisted of amino acids Met1-Ala419 and carried a C-terminal his-tag. It was delivered in PBS buffer.

5.2 Buffers

Buffers PE140 and PE40 were either purchased from Dynamic Biosensors or self-made. Self-made buffers were prepared with ultrapure water. The pH was adjusted by adding diluted NaOH- or HCl-solutions. Self-made buffers were sterile filtered prior to the preparation of aliquots.

Name	Components	pH	Supplier
PE140	10 mM Na_2HPO_4/NaH_2PO_4, 140 mM NaCl, 0.05 % Tween20, 50 µM EDTA, 50 µM EGTA	7.4	Dynamic Biosensors, self made
PE40	10 mM Na_2HPO_4/NaH_2PO_4, 40 mM NaCl, 0.05% Tween20, 50 µM EDTA, 50 µM EGTA	7.4	Dynamic Biosensors, self made
Buffer A	50 mM Na_2HPO_4/NaH_2PO_4, 150 mM NaCl	7.2	Dynamic Biosensors
Buffer B	50 mM Na_2HPO_4/NaH_2PO_4, 1 M NaCl	7.2	Dynamic Biosensors

Table 3: Buffers and their components.

5.3 Virus material

Only inactivated virus material was used in this work. The ß-propio-lactone (BPL) inactivation method was chosen, as it should leave the structure of the virus particles intact [77, 78] (although the influence of BPL on viral activity is still a subject of research [79]). All samples were stored at -80 °C until use, if not otherwise stated. Unfrozen samples were kept at 4 °C. A loss of activity was observed for unfrozen influenza A samples and resulted in the necessity to perform experiments timely after unfreezing.

Influenza A virus Influenza A virus material was provided by the Robert Koch Institute (RKI), Berlin, Germany. The samples were ß-propio-lactone inactivated and purified by density gradient centrifugation. The samples were delivered in PBS buffer. Dilutions for experiments were prepared using PE140 buffer.

Protein concentrations had been determined by the RKI by BCA test: X31 or A/Aichi/2/1968 (H3N2) had an original concentration of 1.4 g L^{-1}, A/California/7/2009 (H1N1) had a concentration of 1 g L^{-1} and A/Panama/2007/1999 had an original concentration of 1.15 g L^{-1}.

The virus samples were shortly vortexed prior to dilution in PE140 buffer.

Hemagglutinin Recombinant hemagglutinin was purchased from the distributor Biozol Diagnostica Vertrieb GmbH, München. It had been produced by Sino Biological Inc. under the name "Influenza A H3N2 (A/Aichi/2/1968) Hemagglutinin/HA Protein (His Tag)". It was expressed in baculovirus-insect cells and was delivered lyophilized. According to the SDS-PAGE image on the data sheet the molecular weight was 66.2 kDa. The lyophilized protein was diluted in PE140 and stored in aliquots at -20 °C until further use.

SARS-CoV-2 Inactivated SARS-CoV-2 samples were used in two experimental setups.

For the binding experiments, in which DNA-peptide nanostructures served as ligands, Dr. Alexandra Rockstroh from Fraunhofer IZI, Leipzig, provided ß-propio-lactone inactivated SARS-CoV-2. The sample had an original concentration of $\sim 1.5 \cdot 10^6$ PFU mL^{-1} prior to inactivation. They were delivered in MES buffer.

For the experiments, in which the antibodies against the nucleocapsid protein were utilized as ligands, the Charité Berlin, Germany, provided inactivated SARS-CoV-2. The virus particles were UV-inactivated and suspended in cell culture medium.

SARS-CoV-2 pseudo-viruses SARS-CoV-2 pseudo-viruses were purchased from preclinics GmbH, Potsdam, Germany. They are lentivirus-based and carry the spike protein of the SARS-CoV-2 on the viral membrane. They were inactivated by ß-propio-lactone. The sample was purified by centrifugation and filtration. Protein concentrations were determined by spectral photometry. A detailed description of the production process can be found in the paper by Kruse et al. [75].

Adenovirus ß-propio-lactone inactivated adenovirus, type 6, strain tonsil 99 was purchased from HyTest Ltd, Turku, Finland. The virus was produced in HeLa cells and purified by centrifugation. Protein concentration was given as 1 mg mL^{-1}.

5.4 Ligands

PeB peptide The peptide called PeB was developed by Henry Memczak and stems from the complementary determining region of an antibody against hemagglutinin on the surface of influenza A virus X31 [57]. It is described in Memczak et al. [61] and is made up of the following sequence: ARDFYDYDVFYYAMD.

The N-terminal of the peptide was modified with azidobutyric acid to enable coupling via copper-free click chemistry. It has a molecular weight of 1995 Da. The modified peptide was purchased from Peptide Specialty Laboratories GmbH, Heidelberg, Germany.

SBP1 peptide The SBP1 peptide is made up of 23 amino acids (IEEQAKTFLDKFNHEAEDLFYQS) and the sequence is taken from the work of Zhang et al. [80]. They developed the peptide based on the α1-helix region of the human angiotensin-converting enzyme 2 (hACE2). The peptide was purchased from Peptide Specialty Laboratories GmbH, Heidelberg, Germany and was modified with azido butyric acid and 16 PEG-linkers at the N-terminal. SBP1 has a molecular weight of 3202 Da.

SARS-CoV-2 nucleocapsid protein binding antibodies Jörg Schenk and Frank Sellrie of HybroTech GmbH, Potsdam, Germany, produced the six antibodies: G229FA10, G230JC3, G230Ah2, G230DE6, G230GG4 and G230HC9. The antibodies were produced in mice and were delivered in PBS buffer.

Anti-adenovirus antibody The 8C4 monoclonal IgG antibody against adenovirus, type 6, strain tonsil 99 was purchased from HyTest Ltd., Turku, Finland. The antibody was delivered in PBS and was kept at 4 °C until use.

6 Data analysis

The data from the DRX^2 measurements were primarily visualized and analyzed using the switchANALYSIS software by Dynamic Biosensors. For all quantitative evaluations, the raw data was exported to OriginPro (OriginLab Corporation, Northampton, MA, USA). The following formulae are adjusted from the book "Binding and Kinetics for Molecular Biologists" by Goodrich and Kugel [24].

For fitting the graphs of associations, a monoexponential curve was utilized:

$$I(t) = I_\mathrm{i} + (I_\mathrm{f} - I_\mathrm{i})(e^{-k_\mathrm{obs}\cdot t})$$

where I is the fluorescence intensity signal, t is the time, I_i is the initial fluorescence signal at $t = 0$, I_f is the final fluorescence intensity signal after saturation and k_obs is the observed rate constant.

The dissociation graphs were fitted with the following formula:

$$I(t) = I_\mathrm{i} + (I_\mathrm{f} - I_\mathrm{i})(1 - e^{-k_\mathrm{off}\cdot t})$$

where k_off is the dissociation rate constant.

From k_obs and k_off we could calculate k_on using the concentration of the virus solution c:

$$k_\mathrm{obs}(c) = k_\mathrm{on} \cdot c + k_\mathrm{off}$$

Finally the dissociation constant K_D was determined by calculating the quotient of k_{off} and k_{on}.

Part III
Results

In this part, the results of the experimental research work are presented. The main section consists of the results for virus-receptor interactions (section 7). This includes different viruses like influenza A, corona- and adenoviruses as analytes and peptides, antibodies and proteins as ligands. In the following section 8, the virus material was immobilized on DNA levers that enabled the observation of an oscillation. The interaction of antibodies and the immobilized fluorescent dye was investigated as well as an antibody binding to a small molecule. The results are presented in section 9. The final section 10 includes a theoretical evaluation of reaction- and mass transport-limited binding kinetics with regard to the utilized system specifics.

7 Virus - receptor binding interaction

This is the first study, in which the switchSENSE technology was applied to virus-receptor interactions. The chapter is structured according to the various projects on viruses and their binding interactions. It begins with the first and most intesively studied virus: influenza A virus and its binding to a peptide (subsection 7.1). This was the first proof of concept and layed the groundwork for all following experiments. Afterwards, the binding of severe acute respiratory syndrome coronavirus 2 (SARS-CoV-2) to a peptide was studied (subsection 7.2), followed by subsection 7.3 on SARS-CoV-2 binding to various antibodies. Finally, the work on unenveloped viruses namely the adenovirus and norovirus-like particles is presented in subsection 7.4. A general discussion of the chapter gives an overview of the challenges and advantages of using electrically controllable DNA-nanolevers for the measurement of virus-receptor interactions (subsection 7.5).

7.1 Influenza A - peptide interaction

Parts of the work were published under the title of “Measuring Influenza A Virus and Peptide Interaction Using Electrically Controllable DNA Nanolevers” by Kruse et al. in the journal “Advanced Materials Technologies” in 2021 [73].

Viruses can cause dangerous diseases in humans [2]. Influenza is a pathogenic virus that causes disease, death and economic costs every year [2]. The so-called Spanish Flu from 1918, an influenza A virus (IAV) pandemic, led to millions of deaths around the world [9]. A recent yet milder example of an outbreak of an influenza virus was the swine flu in 2009 [81]. Yearly outbreaks of varying severity have to be managed by societies [9]. Therefore, influenza has been researched intensively and remains a relevant object of science [81]. While effective vaccinations have been developed, the rapid mutations and variations of the virus require yearly adjustments of vaccines [82, 83].

Influenza A is an enveloped virus, i.e. surrounded by a lipid bilayer and it belongs to the family of Orthomyxoviridae [2]. Three protein types can be found on the lipid membrane, namely hemagglutinin (HA or H), neuraminidase (NA or N) and the M2 proton channel [2, 84].

During virus attachment to a host cell, hemagglutinin binds to sialic acid (SA) containing receptors [65]. Hemagglutinin has a homotrimeric structure and has three receptor binding sites on its globular head domain [65]. Furthermore, it is abundantly available on the viral surface [2]. Therefore, multivalent binding can happen between the cell surface receptors and the three binding sites on one hemagglutinin protein, but also with multiple hemagglutinin proteins on the surface of one virus particle [2]. The two processes can happen simultaneously and are linguistically differentiated by the terms intra- and inter-hemagglutinin binding.

The individual binding strength of one binding site of hemagglutinin to sialic acid is relatively weak ($K_D \sim \mu M$), but the multivalent binding increases the overall binding strength [2, 65].

The switchSENSE technology was to be employed for the investigation of multivalent binding of hemagglutinin to a receptor. The first step however was to examine, whether virus-receptor interactions were measureable at all with the DRX^2, as this had never been tried before. Up to that point in time, the technology had been used primarily for protein-protein and DNA-protein interactions [16]. Larger objects, like the influenza A virus, had not been utilized as analytes, yet.

The peptide PeB and a variation of it called PeB^{GF} were used as receptors. They were derived from a monoclonal anti-hemagglutinin antibody and had displayed a micro-molar affinity towards hemagglutinin of the virus strain A/Aichi/2/1968 (H3N2, also called X31) [61].

The first step was to measure the binding of hemagglutinin to an immobilized peptide (see subsection 7.1.1). Then, the results of X31 virus material binding to DNA-peptide nanostructures are presented in subsection 7.1.2. In subsection 7.1.3, the receptor density was reduced in order to visualize dissociation of the virus material. The results for a variation of virus subtypes is presented in subsection 13. Furthermore, the temperature dependence of the binding signal was tested (see subsection 7.1.5). In subsection 7.1.6, the peptide was exchanged to PeB^{GF}. In the last subsection 7.1.7, the dual color detection of fluorescence signal was used in a sandwich assay to determine binding rate constants.

7.1.1 Hemagglutinin binding to PeB^{GF}

The first challenge of the project was the preparation of the DNA-ligand conjugate. Originally, the peptide PeB^{GF} was coupled to cNL-B48 by EDC-NHS coupling chemistry using the dynamic biosensors coupling kit for proteins smaller than 5 kDa. While the coupling process was generally possible, purification posed the first challenge. Since the short peptide carries little charge, the anion exchange chromatography was not suitable for purification of the conjugate. High pressure liquid chromatogrphy (HPLC) was necessary. Luckily, the HPLC

had been used for purification of the peptide PeB already, so a protocol existed. With the generous help of Christian Warmt, the peaks of uncoupled DNA and uncoupled peptide were individually determined in test runs. Then it was possible to find the peak that corresponded to the conjugate (cNL-B48-PeB^{GF}). The final result of the successful HPLC purification process of one conjugation can be seen in Figure 6.

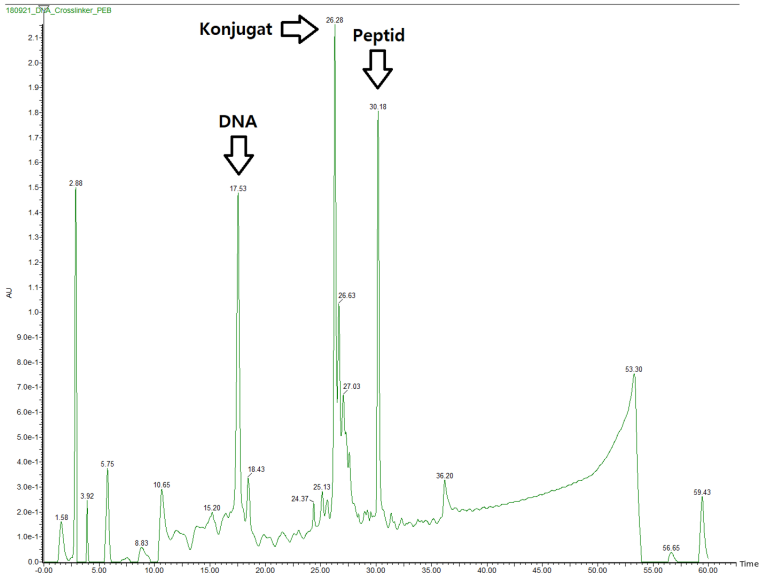

Figure 6: HPLC chromatogram and peak attribution for DNA, peptide and conjugate. The DNA and the peptide had been individually analyzed for their appearance in the chromatogram. The additional peak was then attributed to the conjugate. The corresponding fractions were collected.

The resulting chromatogram shows the peaks of the uncoupled DNA, of uncoupled peptide and of the conjugate. Additional smaller peaks around the conjugate can be attributed to impurities of the samples. The sensitivity of the HPLC was able to separate the conjugate from the uncoupled DNA and the free peptide. The resulting fraction was collected and the buffer was exchanged to PE40 for immobilization in the DRX^2.

The hybridization of the collected conjugate showed an increase in the flurescence amplitude, indicating the presence of complementary DNA. Furthermore, sizing experiments of the conjugate sample revealed differences between pure DNA (cNL-B48) and cNL-B48-PeB^{GF}.

The conjugate was immobilized and binding to recombinant hemagglutinin as analyte was measured (see Figure 7). The association showed an exponential decrease of the fluorescence signal for two injections of hemagglutinin. The signal change is stronger for the lower concentration of 1.2 µM. This can be

explained by the assay setup.

In between the two concentrations, the surface was not regenerated with fresh DNA-PeB^{GF}. The first injection of hemagglutinin at a concentration of 1.2 µM led to a signal decrease during the association, indicating a binding to the receptors on the sensor surface. The subsequent dissociation showed only a slight increase of the fluorescence signal. This indicates an incomplete dissociation, meaning some of the receptors remained occupied. When hemagglutinin at a concentration of 2.4 µM was then injected, the number of available receptors was reduced compared to the first injection, which resulted in a weaker signal change compared to the injection of hemagglutinin at a concentration of 1.2 µM.

It would be advisable to change the assay setup of the experiment to include regenerations in between each concentration, a longer dissociation time and a higher flow rate, as well as more concentrations (at least three). Generally though, these results already show that the cNL-B48-PeB^{GF}-conjugate can bind to recombinant hemagglutinin. Furthermore, the concentration range is compatible with the expected dissociation constant for the interaction between the peptide and the protein ($K_D \sim \mu M$ [61])

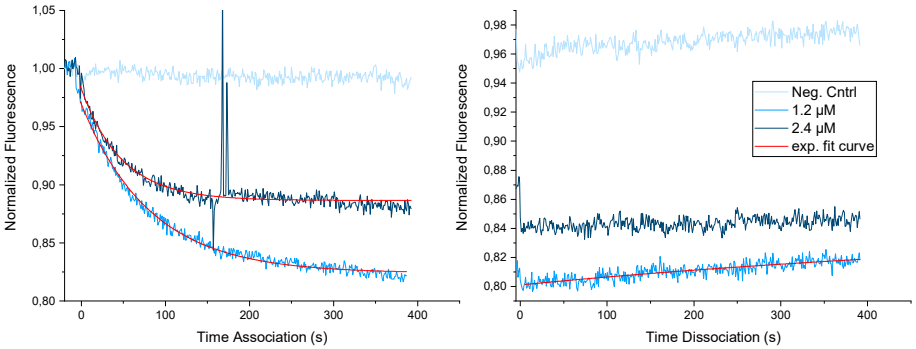

Figure 7: Binding interaction of hemagglutinin to cNL-B48-PeB^{GF}. An exponential signal decrease is observable during the association, while the dissociation shows almost no signal change.

For the negative control, pure cNL-B48 was immobilized on the sensor surface and hemagglutinin at a concentration of $c = 2.4\,\mu M$ was injected. This did not lead to a signal change, which proves that the hemagglutinin does in fact bind the PeB^{GF} and not the DNA, the fluorophore or the sensor surface.

7.1.2 X31 binding to DNA-peptide nanostructures

After the successful binding interaction experiments with recombinant hemagglutinin and PeB^{GF}, the next step was to utilize virus material as analyte. The Robert Koch Institute (RKI) in Berlin provided various charges of inactivated influenza A virus samples.

The first charge had an original protein concentration of around 140 µg mL^{-1}, as determined by BCA test by the RKI. When this sample was inserted as analyte after immobilization of cNLB-PeB^{GF}, no binding was observable at the utilized concentrations.

It had never been shown before that virus-receptor interactions were measureable with switchSENSE technology and there were two possible explanations for the lack of signal.

The first explanation was that the coupling chemistry was suboptimal. It might have influenced the binding ability of the peptide. Although the conjugate did bind to hemagglutinin (see Figure 7), this had been a recombinant protein and in a monomeric form. Therefore, it might have behaved differently than the hemagglutinin on the virus particles.

The second explanation was that the concentration of the virus sample was too low to induce a signal change. The limit of detection for virus-receptor interactions was unknown.

Fortunately, the group of Dr. David Smith was also working with PeB and its binding to X31. Their work had included chemical coupling of peptides to DNA nanostructures to increase binding affinity by multivalent presentation [17]. The switchSENSE technology provided the opportunity to measure binding interactions and to quantify the effect of the oligovalency.

Dr. Christin Möser from the group of David Smith adjusted their DNA structures so they could be integrated into the switchSENSE technology. She developed a four-arm structure, in which three arms can be modified to carry a peptide each and the fourth arm consisted partly of cNL-B48. This fourth arm allowed direct and easy immobilization by conjugate hybridization on the gold electrode surface of the DRX^2. The DNA nanostructures carried PeB instead of PeB^{GF}, which also binds X31 [57].

To characterize the DNA-peptide structures, they were immobilized on the sensor surface (see Figure 8 a) and b)).

For ss3PeB, the signal of the fluorescence amplitude increased faster and the amplitude was larger than for pure cNL-B48 (see Figure 8 b)). The DNA-peptide nanostructures have a larger hydrodynamic radius than the pure cNL-B48 DNA and diffusion would be expected to be slower for ss3PeB. However, the ss3PeB structures carry more negative charges than cNL-B48, which influences the fluorescence amplitude and the interaction with the charged surface.

Furthermore, the interval, over which the alternating voltage was varied, might have been favorable for the DNA-peptide structure. It was observed multiple times that the optimal range for the voltage interval could not be determined during the status test, when inflection points for the fluorescence signal depending on the applied voltage for the individual electrodes were not found. When this happened, the DRX^2 used a default voltage interval. This was generally not optimal. The functionalization graph shown in Figure 8 for the pure DNA (red graph) was most likely one of those cases, in which a suboptimal voltage interval was chose due to the lack of inflection points. The voltage range was more suitable for the DNA-peptide structures.

After the immobiliation of the DNA-peptide structure, the virus solution

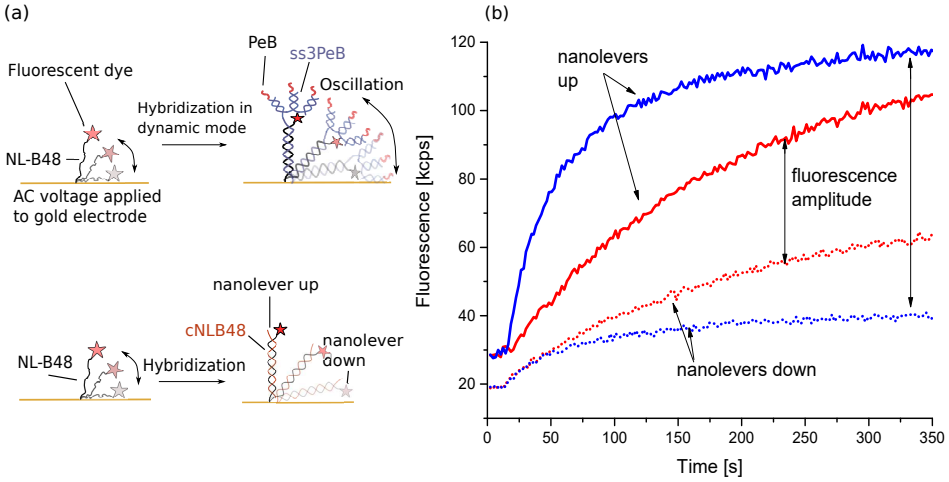

Figure 8: Hybridization of DNA-peptide structures A) drawn schematically (not to scale). B) Graph of the resulting fluorescence signal over time during injection of complementary DNA. The red graph corresponds to the functionalization of pure complementary cNLB48, while the blue graph shows the functionalization of ss3PeB.

was injected into the channel. A schematic representation of the process can be seen in Figure 9. The size of the virus compared to the size of the DNA nanostructures and the distance between DNA nanolevers are drawn to scale.

The size of the viruses as well as the distance between DNA structures on the surface are averages.

Virus diameters for influenza A viruses have been reported to lie between 120 nm to 300 nm [84]. Additionally, it is known that influenza A viruses have a heterogeneous size distribution. There are spherical as well as filamentous geometries [84]. Furthermore, the virus particles are not rigid but rather flexible [2].

The DNA strands on the electrode surface are arranged statistically [40] and the reported average distance between them is around 50 nm [71]. These facts combined suggest that one virus particle can bind to more than one DNA-peptide nanostructure on the sensor surface.

The experiments with immobilized DNA-peptide nanostructures and X31 as analyte were successful. The second charge from the RKI had a protein concentration of 1.4 mg mL^{-1} and showed a strong binding signal. The surface was regenerated with fresh DNA-peptide structures after each measurement. An exemplary binding curve for ss2PeB as ligand and X31 as analyte can be seen in Figure 10.

The association signal shows a strong concentration dependent signal decrease upon injection of virus material.

The dissociation curves show no signal change over the measurement time

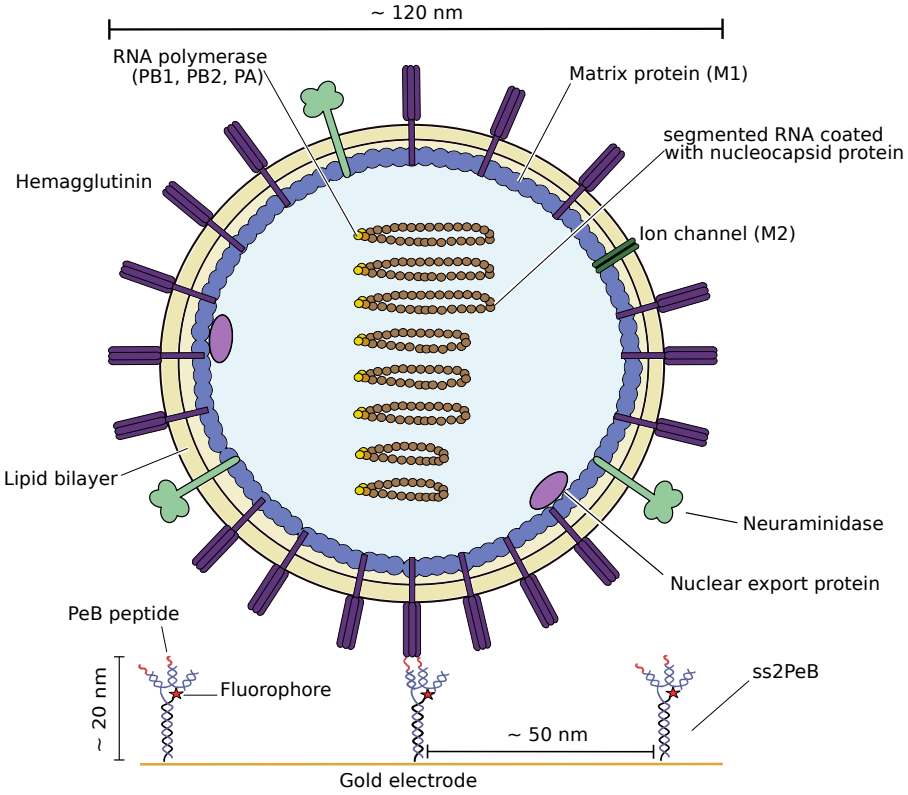

Figure 9: Schematic overview of the binding process of X31 virus material binding to ss2PeB. The DNA nanostructure is immobilized on the gold electrode surface and virus-containing solution is injected into the microchannel. The average size of the virus particles and the distribution of the DNA-peptide nanostructures permit multivalent binding interactions (intra- as well as inter-hemagglutinin binding).

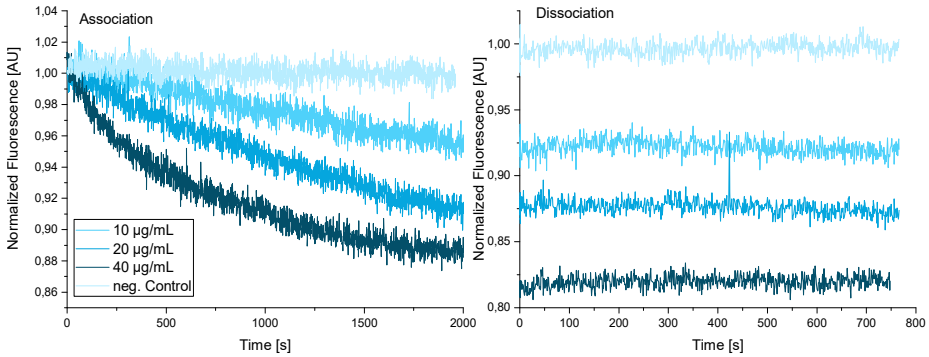

Figure 10: Binding of X31 to ss2PeB measured in static mode. The association shows a strong signal change upon virus injection, while the dissociation signal stays almost constant during the measurement time.

of 750 s. It is suspected that the virus particles remained bound to the sensor surface and did not dissociate over time. This can be explained by the aforementioned multivalent binding. There is the intra-hemagglutinin binding of the two peptides per construct binding to the homotrimeric protein HA on the viral surface and the inter-hemagglutinin binding of multiple proteins binding to multiple DNA-peptide structures on the sensor surface. The two effects combined stabilize the virus capture on the surface drastically. For one virus particle to unbind, all binding interactions would have to detach simultaneously. Otherwise, also rebinding effects can occur due to the high local concentration of the binding partners [28].

Regarding the general binding behavior, also the influence of electrostatic forces have to be taken into account. In literature, it is reported that H3N2 viruses (like X31) have positively charged hemagglutinin on their virus membrane to attach to the negatively charged cell surfaces [85]. The negatively charged DNA-peptide structures and the negatively charged gold electrode surface might facilitate association and impede dissociation.

The negative control was carried out with immobilized ss0PeB. DNA nanostructures without any peptides were used as ligands on the sensor surface and X31 solution was injected as analyte at various concentrations. The curve presented here corresponds to the highest virus concentration used (40 µg mL^{-1}). The control experiment confirmed that the virus material does not bind unspecifically to the pure DNA structure or the sensor surface.

As can be seen in Figure 10, the resulting signal was not fit. Two main problems prevented fitting of the graphs. One reason was the absence of a measureable dissociation rate. This is the first step for the determination of K_D [24]. Without a reliable k_{off}, it is not possibile to calculate K_D.

The second reason is that the association curves could not be fit satisfactorily by a mono-exponential fit curve. Originally, a mono-exponential fit was to be used in order compare resulting binding rates of ss1/2/3PeB to X31. The idea

was to simplify the complicated binding process of the ss1/2/3PeB ligands to the virus. The three ligands were supposed to be treated as "pseudo monovalent" binders with varying individual binding strengths towards the virus protein. Unfortunately, the mono-exponential function did not fit the signal curves, which showed a rather linear behavior. This has also been described in literature for multivalent binding of viruses to a surface [52]. Linear, bi- or tri-exponential functions would have described the graphs. The process of the virus particles binding to oligovalent DNA-peptide structures is complicated and that could be used as a theoretical justification of a bi-or trivalent exponential curve. However, the informative value of the numerical results for the binding interaction parameters would be limited [12].

Additionally, the experiments were repeated multiple times for the individual DNA-peptide nanostructures and it was found that the calculated rate constants varied considerably. The influence of the material has to be taken into consideration. This includes the measurement chips that degenerate with the number of experiments as well as the biological samples. Especially the virus material showed a loss of activity over time in specific storage conditions (see also subsection 7.5).

7.1.3 Variation of surface density of ligands

As was shown in the previous subsection (see Figure 10), the virus material remained bound to the DNA-peptide nanostructures during the measurement time of the dissociation. This was most likely due to the strong multivalent interaction. The lack of clear dissociation signals impeded the quantification of binding rate constants and encouraged the development of an assay that enabled the measurement of a dissociation. There were various ways to address this problem. A possible solution would have been a competition assay: the injection of a second analyte with a higher binding affinity to the immobilized ligands than the virus. Another strategy was to decrease the density of ligands on the sensor surface to reduce the multivalent binding of one virus particle to numerous DNA-peptide structures (inter-hemagglutinin binding). Additionally, longer dissociation times and the use of the monovalent peptide presentation (ss1PeB) to exclude intra-hemagglutinin binding could enable the measureability of a dissociation. The strategies were combined and the results are presented in the following subchapter.

In order to decrease the density of ligands on the sensor surface the number of available DNA-peptide nanostructures on the sensor surface was reduced. This was done by mixing the ligand structure with DNA that carried a fluorescence-quenching molecule called QRF (short for "quencher of red fluorophore") at the 5' end. The ratio of the mixture would then determine the number of available DNA-peptide nanostructures.

In a functionalization test run, the ratio of cNL-B48-QRF to cNL-B48 was varied in order to determine the optimal ratio. This meant to decrease the ligand density to a minimum, while the signal strength remained high enough to be measureable. The result of the test functionalization experiment can be

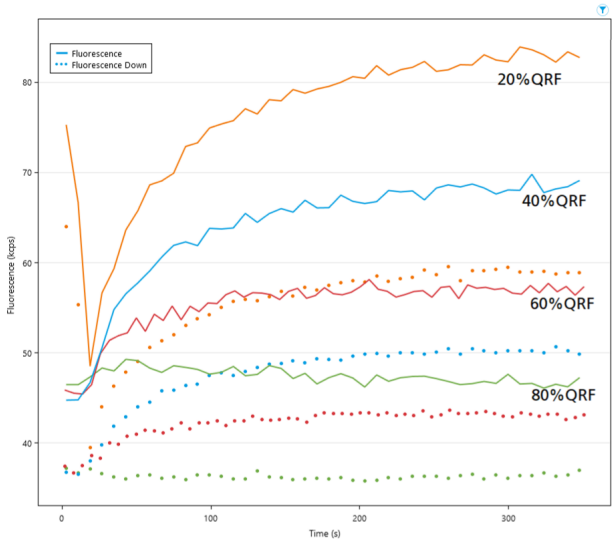

Figure 11: Test-functionalization at various ratios of cNL-B48-QRF and cNL-B48. An increased amount of cNL-B48-QRF led to a lower fluorescence amplitude upon hybridization. At a ratio of 80% cNL-B48-QRF, there was practically no more signal change visible upon injection of the DNA.

seen in Figure 11.

The results showed that the amount of cNL-B48-QRF influenced the signal strength of functionalization as expected: the higher the amount of cNL-B48-QRF in the mixture, the lower the signal strength. The use of 80% cNL-B48-QRF led to a complete loss of signal increase during functionalization. This signal strength would not be sufficiently large enough for binding interaction experiments. The signal for 40% and 20% cNL-B48-QRF showed a signal increase that appeared high enough for binding interaction mesurements. As the signals were already low, though, it was decided to continue with a 20% cNL-B48-QRF.

cNL-B48-QRF was mixed with ss1PeB at a ratio of 20/80 and then immobilized on the measurement chip. Afterwards, X31 at a concentration of 40 µg mL^{-1} was injected. The association was performed with the same measurement parameters as in the previous subchapter, but the parameters of the dissociation were varied. The measurement time was increased to over four hours and the flow rate was increased to 500 µL min^{-1}. The idea was that these settings in addition to the low density of ligands and the monomeric peptide presentation of the ss1PeB would enable the visualization of the virus dissociation. This was indeed the case as can be seen in Figure 12.

In this setup, it was possible to fit the resulting graph with a mono-exponential fit curve and to determine a dissociation constant. It lies in the pico-molar range.

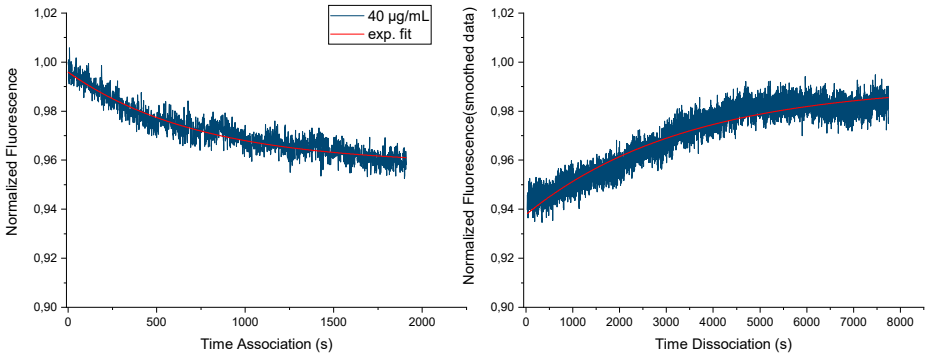

Figure 12: Binding interaction signal of X31 and ss1PeB, after functionalization with 20% cNL-B48-QRF. The reduced number of ligands in addition to the monovalent peptide presentation and the long dissociation time led to a visible dissociation of the virus material.

This value should be treated carefully, as the influence of binding to multiple DNA-structures is unclear, and the concentration of the virus material is also not certain. Takemoto et al. describe a dissociation constants on the order of nM [86] for the interaction of X31 and sialic acid mesured with SPR. There are various explanantions for this discrepacy. First, Takemoto et al. utlized a different technique and a different ligand. During the experiment with the DRX^2, the effect of the electrical interaction of the positively charged viral surface and the negatively charged DNA and sensor surface might also have influenced the dissociation constant. Furthermore, the addition of 20% of cNL-B48-QRF might not have been sufficient to exclude multivalent binding altogether. Additionally, the fluorescence signal increased during the dissociation, but started to decrease again towards the end of the measurement. This indicates, that there might be additional effects like bleaching of the fluorophores or a loss of DNA structures from the surface. Generally, it could be shown that the reduction of receptor density and increase of measurement time and flow rate led to a measureable dissociation.

Interestingly though, no dissociation was measureable during experiments with ss2PeB and ss3PeB mixed with 20% cNL-B48-QRF also for long measurement times of over four hours. This shows that the oligovalent presentation of the peptides did in fact increase the binding strength considerably.

To discuss the results from a pessimistic viewpoint of the results, it would also be possible, that the results were influenced by the cNL-B48-QRF. It is thinkable, that the long measurement time and illumination might degrade the "QRF", a quenching molecule that is not specified by the company. The degradation of the quenching molecule over such a long measurement time could have led to the signal increase. This could have been misinterpreted as the dissociation of the virus particles. The fact that there was no signal increase visible during dissociation for binding interactions of X31 to ss2PeB and ss3PeB mixed

with 20% QRF however, might point towards actual dissociation of virus particle in the case of immobilized ss1PeB (with 20% QRF). An additional test for this hypothesis could be the same experiment without the injection of virus particles. It would enable the investigation of the behavior of the quenching molecule over long measurement times.

Generally though, the possibility of reversible receptor density variation on the sensor surface is an advantage of switchSENSE technology. The controllability of surface density is easily achieved using the DNA-QRF strands. Especially for cases, in which multivalency might affect the results, it is advantageous to reduce the receptor density. Furthermore, general binding theory recommends low receptor density to reduce effects of mass transport limitations [87].

It would be favorable to find a quantitative relation between the fluorescence signal of the functionalization and the number of available DNA-ligand strands on the sensor surface. The manufacturer estimates the number of DNA-strands per electrode to be around one million [71]. However, this value decreases with the amount of experiments done on one electrode. This can be observed during functionalization as the signal saturates at lower fluorescence intensities over time. This indicates a loss of fluorophores, their activity or a loss of DNA strands on the electrode surface. It is for now unclear, with how many DNA strands per electrode an experiment begins. Therefore, the addition of a certain percentage of QRF to the DNA-ligand solution can result in different surface densities, depending on the original starting value of available DNA strands. A reliable quantification of these available DNA strands on the surface would be very desirable.

7.1.4 Virus subtype variation

The peptide PeB coupled to the four-arm DNA nanostructure was furthermore used in binding experiments with two additional subtypes of influenza A viruses. Henry Memczak had shown that the peptide also binds other subtypes [57] and these experiments were repeated with the switchSENSE technology. The two subtypes were influenza A/California/7/2009 (H1N1) and influenza A/Panama/2007/99 (H3N2). The measurements were performed similarly to the ones presented in subchapter 7.1.1. The results of the variation of the subtype can be seen in Figure 13.

The binding curves showed distinct signal changes for the injections of the subtypes during the association. The H3N2 subtype (Panama) showed a signal increase during association and a small signal decrease during dissociation. The H1N1 subtype (California) on the other hand showed a slight signal decrease during the association and no signal change during the dissociation. Compared to the signal change of X31 though, the two subtypes showed weak signals. It has to be mentioned though that the experiments for X31 were performed on a different biochip and it has been observed, that this can influence the resulting signal strength.

In general, the results are compatible with the expectations. The H3N2 subtype (Panama) showed a strong signal change. X31 is a H3N2 virus as well.

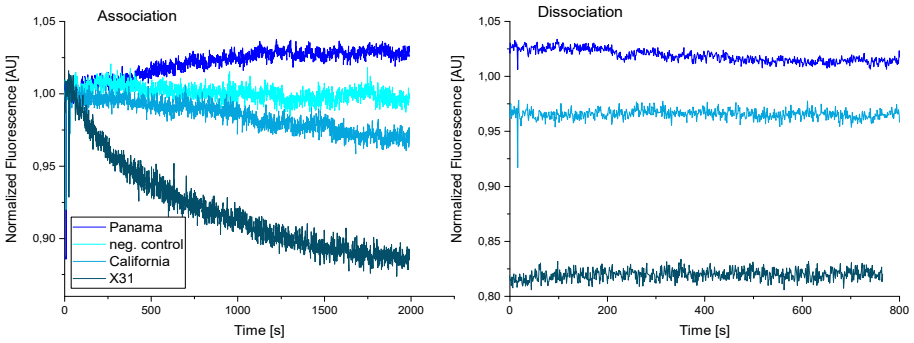

Figure 13: Variation of subtypes of influenza A virus.

H1N1 on the other hand is reported to have a less developed local positive charge distribution in the hemagglutinin on the viral membrane than the H3N2 [85]. Furthermore, the differences in protein structure of the hemagglutinin proteins for H3N2 and H1N1 will be a reason for the weaker binding affinity.

Generally, the results prove that the peptide binds various subtypes of influenza A viruses. Henry Memczak et al. had shown that a broad specificity might be beneficial for a therapeutic application to inhibit virus infections [61].

7.1.5 Temperature variation

The measurement temperature can influence binding interactions based on the thermodynamic properties of the binding partners [24]. This has also been observed for the interaction between X31 and PeB [57]. In SPR experiments, higher temperatures led to stronger signals. This was supposed to be tested in the DRX^2 as well and it was suspected that the same effect would be visible.

Therefore, ss3PeB was immobilized on the sensor surface and X31 at a concentration of 40 µg mL^{-1} was injected at varying measurement temperatures. The range lay between 20 °C and 40 °C. The standard measurement temperature of 25 °C was also included in the presentation of the results that can be found in Figure 14.

The results of the experiments showed that the signal strength increased with rising temperatures. For the temperatures of 30 °C and 40 °C, the absolute signal change was similar, but the binding happened faster for the higher temperature. In the time interval $0\,\mathrm{s} < t < 1000\,\mathrm{s}$, the measurement signal decreased fastest for 40 °C and slowest for 20 °C. The curve for 40 °C also showed a kind of equilibration behavior during the association that was not seen to this extent in the other cases. Furthermore, the dissociation showed a signal increase for the case of 40 °C that was not seen for any other temperature. This behavior could be studied in more detail.

Macroscopically, the viruses infect humans that have a body temperature of around 37 °C [88]. It is a reasonable assumption that this temperature is most favorable for the infection process, which includes the attachment to the host

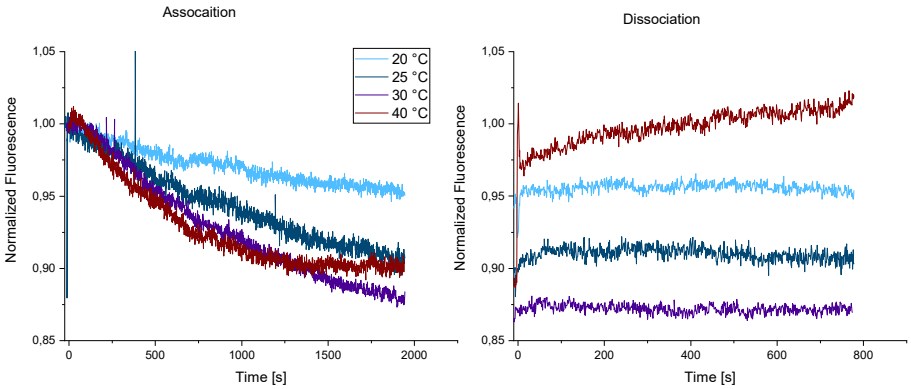

Figure 14: Temperature variation during binding interaction measurements. ss3PeB was immobilized on the sensor surface and X31 was injected into the channel at a fixed concentration (40 µg mL^{-1}). The temperature range was chosen between 20 °C and 40 °C with a step size increase of 10 °C. Additionally the result for the default temperature of 25 °C is shown in the graph.

cell. Microscopically, the explanation could be that the binding of PeB to X31 viruses relies strongly on van-der-Waals forces [57].

It would therefore be advisable to investigate the temperature dependence in more detail and to decrease the step size between different temperatures (e.g. temperature range between 30 °C and 40 °C and a step size of 1 °C or 2 °C). In general, it could be shown that the temperature dependence of the virus-receptor binding process can be observed in the DRX^2.

7.1.6 Peptide variation

It was furthermore of interest to analyze the peptide PeB^{GF}. It had already shown binding to recombinant hemagglutinin as described in subsection 7.1.1 and was then investigated as ligand on the four arm DNA nanostructure ($ss3PeB^{GF}$). Christin Möser from Fraunhofer IZI, Leipzig, prepared the coupled DNA-PeB^{GF}- nanostructures. The PeB^{GF} sample used for the conjugation was not ordered freshly, but was a remainder from previous experiments. Although it was not possible to determine the exact age of the sample, it can be assumed that it had been stored for years. The sample was lyophilized and kept at -20 °C prior to use, but the age has to be mentioned. The epitope binding sequence of amino acids for PeB^{GF} is FYGYDVFF. The third and the last position of the sequence are different from the sequence of PeB (FYDYDVFY). Henry Memczak had determined that the binding affinity of PeB^{GF} was higher than that of PeB [57].

The DNA-peptide structure was immobilized as ligand on the sensor surface and subsequently X31 virus solution was injected at various concentrations. Exemplarily, the resulting graph for the injection of $c_{X31} = 40\,\mu g\ mL^{-1}$ is shown

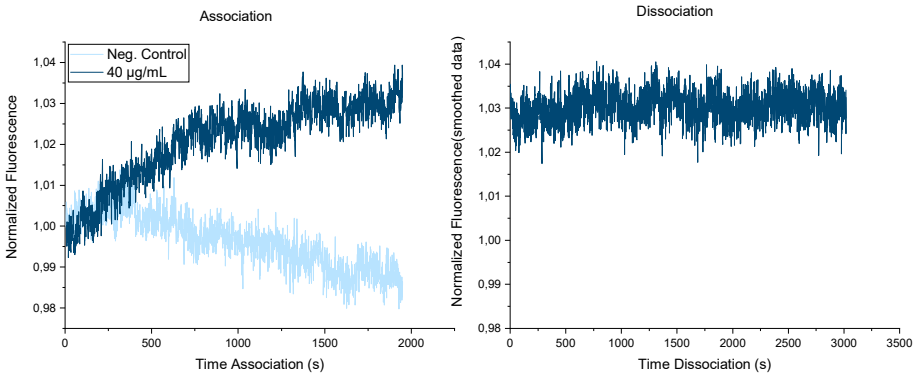

Figure 15: Peptide variation: ss3PeB^{GF} was immobilized on the sensor surface and X31 was injected at a concentration of $c_{X31} = 40\,\mu g\ mL^{-1}$. The injection led to a signal increase during the association, which was clearly discernable from the blank measurement (injection of running buffer).

in Figure 15.

The results showed a signal increase upon injection of virus material during the association. It could be distinguished from the injection of running buffer (negative control). The signal increase was weak but visible. The fact that the signal increased and did not decrease was surprising. It would have been expected that the signal would decrease, as it had been the case for ss3PeB.

Since the sample was old and only ss3PeB^{GF} was analyzed, the results have to be interpreted carefully. Additionally, while the result was reproducible, it was not as stable as the experiments with ss1/2/3PeB regarding reproducibility.

Generally though, the result showed that it is possible to vary the peptide on the sensor surface and observe binding to virus material.

7.1.7 Sandwich assay

As has been shown in subchapter 7.1.1, the virus material did not dissociate well from the sensor surface. It remained practically immobilized on the DNA-peptide structures for the measurement time of 750 s. The DRX^2 is equipped with two excitation light sources, two detectors and two fluorescence channels. The “2” in the name of the instrument indicates this. The immobilization of the virus particles and the two available fluorescence channels were combined into a “sandwich assay”. In this setup, DNA-peptide structures (ss2PeB in this case) were immobilized on the sensor surface and X31 virus material was injected into the channel as before and immobilized as ligand. A fluorescently labeled version of the DNA-peptide structure was injected as analyte after virus immobilization. While the anchor DNA (NL-B48) carried a red fluorophore, the analyte DNA-peptide nanostructure was labeled with a green fluorophore (G1).

In this setup, inter-hemagglutinin binding was excluded. This allowed the determination of the individual binding strengths of the DNA-peptide nanos-

tructures. A schematic overview of the experiment and the results of the binding interaction of ss2PeB-G1 to X31 can be seen in Figure 16.

As can be seen in Figure 16 B), the fluorescence signal increased strongly during the association and decreased during the dissociation. The increase of signal during the association can be attributed to the accumulation of green fluorescence on the viral surface. The reverse effect happened during the dissociation (accumulated green fluorophores on DNA-peptide structures dissociated from the viral surface). The graphs were fit by a mono-exponential function assuming again a "pseudo-monovalent" interaction, also for the bi- and trivalent peptide presenting DNA structures. The binding rates can be found in Table 4.

DNA-peptide nanostructure	K_D **[nM]**
ss1PeB	12 ± 9
ss2PeB	12 ± 7
ss3PeB	8 ± 7

Table 4: Dissociation constants for binding of DNA-nanostructures to X31 virus as determined by the sandwich assay.

All three DNA-peptide structures bound strongly to the immobilized viruses. The resulting values for the dissociation constants are in a similar order of magnitude. It was expected, that the oligovalent presentation of the peptides would have a larger influence on the K_D. However, there are factors that have to be considered.

When the fluorescently labelled DNA-peptide nanostructures were injected into the microchannel and the sample reached the area of detection, a stepwise increase of fluorescence signal in the green channel was visible. This is not surprising, as the solution contains the then excited green fluorophores. For the case of the dissociation, the step appeared as soon as the buffer solution that was injected reached the sensor surface. The step is not shown in the results presented in Figure 16. The step was problematic as it masked parts of the fast association and dissociation processes. Cutting the step from the graph and fitting the rest might have resulted in false binding rate constants. There are possibilities to minimize this effect (e.g. a systematic analysis of background effects and their influence on the signal). In the negative control shown here, no virus was immobilized and only the stepwise increase and decrease was measured for the injection of ss2PeB-G1. The resulting graphs could be subtracted from the measurement signal that were obtained for the DNA-peptide virus binding experiments and would then leave the binding signal without the influence of the step function. This was done as negative control, but the graph was not subtracted from the measurement results.

An additional negative control was performed using ss0PEB-G1 as analyte after virus immobilization. This showed that the DNA structures without peptides led to a slight signal increase. While the resulting signal was drastically lower for ss0PeB-G1 compared to ss1/2/3PeB-G1, the signal should be considered and subtracted.

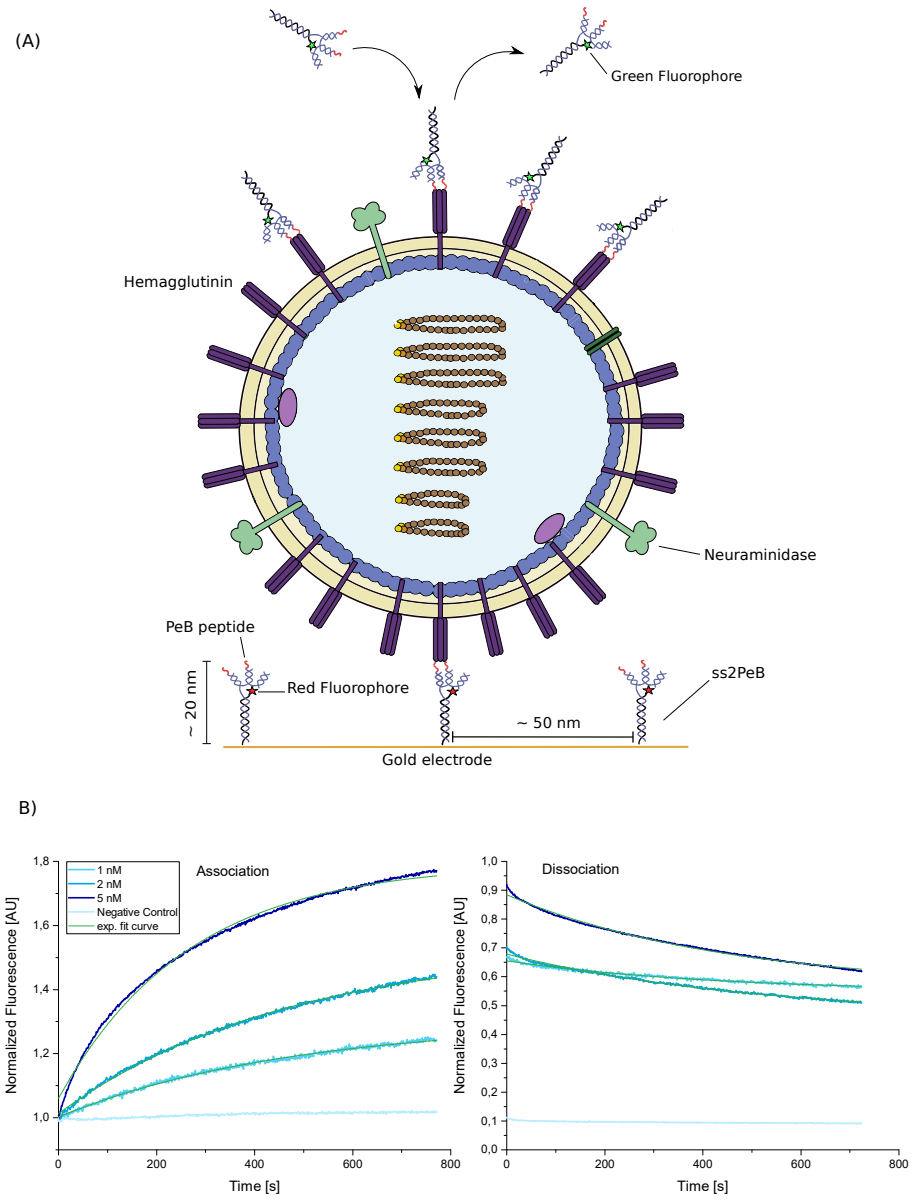

Figure 16: A) Schematic overview of experimental setup of the sandwich assay. B) Results of ss2PeB-G1 binding to immobilized X31 virus particle in the sandwich assay.

The sensitivity of the single photon counter was easily saturated. Higher fluorophore concentrations led to a shut down of the detector to avoid damage to the sensor. This meant that the concentration range used here for the ss1/2/3PeB-G1 was limited by the dynamic range of the sensor. Generally, it is advised (for SPR [87]) to use a concentration range between $c \in [0.1 \cdot K_D, 10 \cdot K_D]$ and to analyze around 10 concentrations for the optimal determination of binding rate constants. This was not possible here.

The order of magnitude of the binding strength of a K_D in the low nanomolar range can be discussed. It is in good agreement with the findings of Takemoto et al. [86], who described a nM dissociation constant for the interaction of X31 and sialic acid in SPR.

Henry Memczak et al. [61] found a lower binding strength ($K_D \sim$ µM). Their experiments were performed with uncoupled peptides and recombinant hemagglutinin. The influence of the DNA structure and electrostatic effects has to be considered.

As has been reported by Lauster et al. [15], who investigated the binding of PeB attached to polyglycerol-based nanoparticles to X31, larger particles ($\sim 20-30$ nm) that have a low functionalization density showed binding affinities in the nanomolar range. The DNA-peptide-nanostructures, which were used here, have a similar size of around $\sim$ 20 nm. The size could be beneficial for the binding interaction, as well as the negatively charged DNA backbone. Furthermore, the nanoparticles used by Lauster et al. also bound multivalently to the viral surface. Therefore, the order of magnitude found here for the binding interaction strength can be interpreted as reasonable.

The sandwich assay appears to be the method of choice towards a reliable measurement of the binding strengths of the individual DNA-peptide nanostructures to viral proteins as they appear in their "native" environment on viral surfaces. There are improvements that could be made though.

First, the fluorescent labelling of the DNA-peptide nanostructures needs optimization. The conjugate hybridization of a fluorescently labeled DNA appeared easy but had some drawbacks. The partly single- and partly double-stranded DNA overhang (NL-W48 and NL-B48-cNL-B48) might influence the binding process unnecessarily. While the additional negative charge might facilitate binding, this overhang is not strictly necessary. A DNA-peptide nanostructure that directly carries a fluorophore, similar to what was presented by Möser et al. [17], would be preferable.

Furthermore, the fluorophore could be chosen to fit the setup. A fluorophore could be selected, which emits the appropriate number of photons in order to avoid oversaturation of the sensor.

Additionally, the oversaturation problem could be addressed by reducing the excitation power of the LED. This could enable the use of higher concentrations of the labelled DNA-peptide construct to determine more reliable rate constants.

The challenges of the mathematical analysis of the results has been mentioned before. The stepwise increase has to be characterized systematically as well as the influence of background signals. Additionally, the graphs were all fit by a mono-exponential function. The development of a theoretical model or a

molecular simulation of the process could refine this mathematical interpretation.

Generally, the sandwich assay experiments were quite successful and seem to be a promising way to determine binding interaction rates for virus-peptide interactions. The additional fluorescence channel enabled the observation of binding to an immobilized virus. One could think of various experiments that could be performed using this setup, including the variation of the peptide, or analysis of labeled antibodies or other binders. The sandwich assay could be the way to go for exact quantification of binding rates of oligovalent interactions.

7.2 SARS CoV-2 spike protein - peptide interaction

The content of this subchapter has been published under the title of "Characterization of binding interactions of SARS-COV-2 spike protein and DNA-peptide nanostructures" by Kruse et al. in the journal Scientific Reports [75].

In the beginning of 2020 a pandemic of the severe acute respiratory coronavirus 2 (SARS-CoV-2) broke out. The spread of SARS-CoV-2, first detected in Wuhan, China, was characterized by rapid transmission between humans, severe courses of disease and high mortality rates [89].

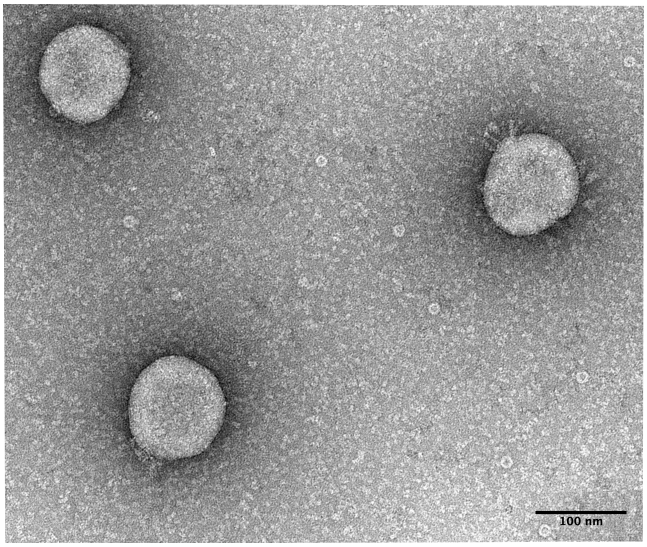

Figure 17: Transmission electron microscopy image of SARS-CoV-2 sample. Image taken by Elena Willner of TU München. (Shown with permission)

The effort that was put into the study of SARS-CoV-2 by the international scientific community however was immense [90]. Publishing companies of scientific journals made all publications on the subject openly accessible. Preprint publications were getting extremely important for sharing study results immediately with a broad scientific and public community. While this enabled fast publications of findings of international importance, the lack of an orderly peer review process also led to preprint publications of questionable reliance and a magnitude of publications that was easily overwhelming [90]. Some publications that were originally published on preprint servers never reached regular publication.

In the beginning of the year 2020, our research on the influenza A - peptide interactions using switchSENSE technology was at an advanced stage and a publication of the results was imminent. The outbreak of SARS-CoV-2 inspired the idea of applying switchSENSE technology to investigate binding of this new virus to a ligand. While the peptide PeB had been developed at the institute

and X31 had been studied for a long time in house and at the institutes of cooperation partners, the knowledge of SARS-CoV-2 and its ligands was limited at the time.

The project was based on the work on influenza A (see subsection 7.1) and the main idea was to investigate binding interactions between the spike protein of SARS-CoV-2 and a peptide coupled to the DNA nanostructures that had been used in the influenza research as well [73]. The spike protein of SARS-CoV-2, like hemagglutinin, has three receptor binding sites [91].

In order to start the project, a peptide had to be found. Research on preprint servers led to the publication of Zhang et al., in which a peptide called SBP1 was presented, which is 23 amino acids long and binds the receptor binding domain (RBD) of the spike protein of SARS-CoV-2. In the original version of the manuscript from March 2020 [80], the authors described a strong binding interaction of "low nanomolar affinity" of SBP1 to the receptor binding domain of the spike protein of SARS-CoV-2. The peptide is derived from the alpha 1 helix sequence of the N-terminal region of the human angiotensin converting enzyme 2 (hACE2), which is a known receptor of the spike protein [92]. In an updated version of the manuscript from June 2020, the binding strength of the peptide SBP1 to RBD of one supplier was in the µM-range. RBD samples from other suppliers did not show binding [93].

Based on the first preprint publication from March 2020, the descibed peptide was ordered and then coupled to the same four-arm DNA strands, which had been used for the influenza A-PeB interactions [73]. The coupling of SBP1 to DNA nanostructures was performed by the group of Dr. David M. Smith at Fraunhofer IZI, Leipzig, namely by Basma Altattan and Nico Grasse. Subsequently, it was decided to investigate the binding interaction of the SBP1 on the DNA nanostructures to subparts of the spike protein, as well as to the full-length spike proteins and to SARS-CoV-2 material. The influence of the trimeric peptide presentation was supposed to be determined and compared to the monovalent peptide presentation. The trimeric presentation of peptides mirrors the targeted binding sites. It was expected that a trivalent presentation would increase binding affinity.

The binding interactions were first measured by enzyme-linked immunosorbent assay (ELISA) and subsequently by switchSENSE. Basma Altattan and Nico Grasse performed the ELISAs. The assays were primarily used to investigate the binding qualitatively. It also showed that the DNA-nanostructures are easily integrated into the two techniques and can be transferred to other methods as well (e.g. SPR).

7.2.1 Spike proteins binding to DNA-Peptide nanostructures

The first experiments involved DNA-peptide nanostructures as ligands and spike protein and its subfragements as analyte. Virus samples containing inactivated whole virus particles (biosafety level S1) were not available at the beginning of the project in 2020.

The four-arm DNA structures were functionalized to carry three peptides.

After hybridization of the nanostructure, the analyte was injected into the flow channel (see Figure 18). All experiments were performed in static mode.

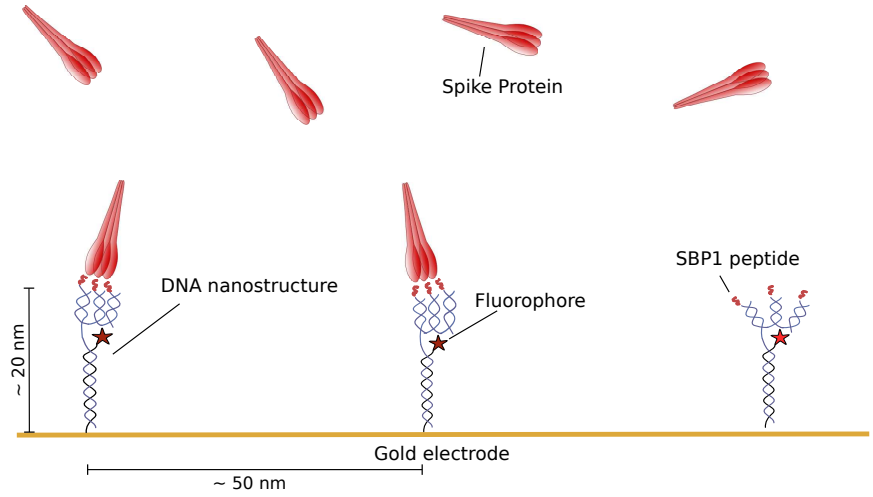

Figure 18: Experimental setup: The four arm DNA nanostructures that carry three peptides were immobilized on the gold electrode surface and spike protein was injected as analyte. Binding of a protein led to a decrease in detected fluorescence intensity.

The full-length spike protein (ectodomain) was used as analyte as well as two of its subfragments. The protein is divided into the subunit 1 (S1) and the subunit 2 (S2) [91]. The receptor binding domain (RBD) is a part of S1, which in turn is part of the full-length protein [91]. It was expected that the peptide would bind RBD, S1 and the full-length proteins, since RBD had been reported to bind to the hACE2 receptor [92, 94].

In the updated version of the preprint, Zhang et al. [93] showed that the peptide bound weakly to RBD ($K_D \sim \mu M$) from one manufacturer. For samples from other sources, binding could not be observed. Our experiments with ELISA and switchSENSE confirmed these findings. RBD from different suppliers did not bind to the DNA-peptide nanostructure, even at high protein concentrations ($c \sim$ mM). The same result was found for S1 binding to the DNA-peptide structure. However, a strong binding interaction was detected for some full-length spike proteins. An exemplary collection of the results can be found in Figure 19.

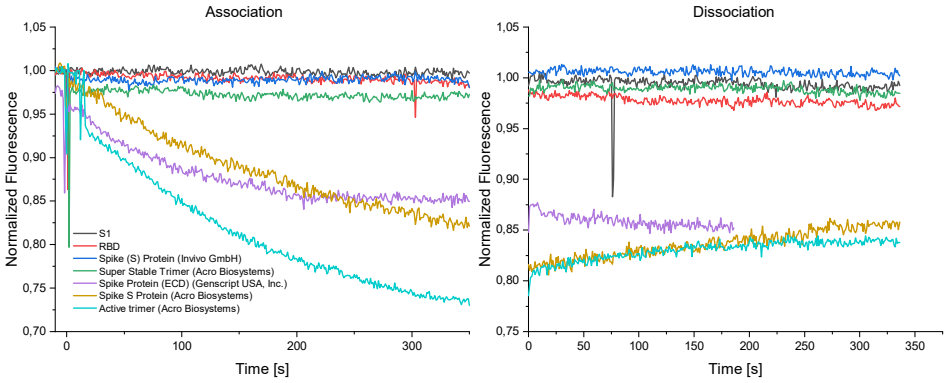

Figure 19: Binding of spike proteins and various subfragments to DNA-SBP1 nanostructures. Three full-length spike protein samples showed a strong binding interaction, while the subparts S1 and RBD as well as two full-length proteins showed no binding signal.

All measurement besides RBD and S1 were performed with full-length spike proteins. As can be seen in Figure 19, only three samples showed a binding signal, namely the "SARS-CoV-2 Spike Protein (ECD)" by Genscript USA, Inc. and the two proteins "SARS-CoV-2 S protein" and "SARS-CoV-2 S protein, Active Trimer" by Acro Biosystems. For these three samples, a significant signal change was visible. Curiously, the injection of two additional full-length spike proteins, namely the "Super Stable Trimer" by Acro Biosystems and "Spike (S) Protein" by Invivo BioTech Services GmbH did not induce a change in fluorescence (see Table 2 in section 5 for protein specifics).

A first theory on why some full-length proteins bound and some did not included the expression systems. However, since the proteins were produced in various expression systems and there was no correlation to binding and non-binding signals, this is most likely not the reason for the various behaviors.

The exact amino acid sequences of the full-length proteins varied. The "SARS-CoV-2 S protein, Active Trimer" was modified at the C-terminal with a so called "trimer motif" made up of 26 additional amino acids that support a stable trimeric structure. The "SARS-CoV-2 S protein" from the same company lacked this modification. The "Active Trimer" showed the strongest binding signal in the experiment.

The two proteins were analyzed by dynamic light scattering and sizing measurements in switchSENSE. It could be shown, that the hydrodynamic diameters of both proteins are of the same order on magnitude $d_{hyd} = (9 \pm 1)$ nm.

For "SARS-COV-2 Spike Protein (ECD)" by Genscript, no variations of the amino acid sequence were documented. This unmodified version bound well to the peptide.

Two samples of full-length proteins did not bind to the DNA-peptide nanostructure, namely "SARS-CoV-2 S protein, Super Stable Trimer" by Acro Biosystems and "Spike (S) protein" by Invivo BioTech Services GmbH. These two

proteins were varied at multiple sites in their amino acid sequences. Both had identical variations at the furin cleavage site (R683A and R685A) and two additional proline substitutions (K986P and V987P).

The furin cleavage site is the object of much research regarding SARS-CoV-2 (e.g.[95–99]) and has even been controversially discussed with regard to the origin of the virus (e.g. [100]). The site is responsible for increased transmissibility compared to other coronaviruses [97, 98]. A variation at this site, as had been done for the two proteins here, might be responsible for the loss of binding in this setup.

The variations at the positions 986 and 987 are furthermore relevant, as they are part of the Heptad-Repeat Domain 1 (HR-1) [101]. Hsieh et al. [102] described the replacement to proline and named the resulting protein "S-2P". The two prolines stabilize the prefusion state of the protein and prevent a conformational change to the postfusion state. Interestingly, the two mRNA vaccines by Biontech/Pfizer and Moderna code the S-2P spike protein [103].

The prefusion state can be stabilized further by adding four additional substitutions to proline (F817P, A892P, A899P and A942P), as was the case for the "Super Stable Trimer" by Acro Biosystems. Hsieh et al.[102] named the protein that carries all of these variations "HexaPro" (furin cleavage site: R683A and R685A, HR-1: K986P, V987P, F817P, A892P, A899P and A942P). While these variations stabilize the conformation of the spike protein, an influence on the binding behavior seems plausible.

While it was unclear, which variation was responsible for the loss of binding or if it was the combination, it could be shown that the variations influenced the binding of the proteins to the SBP1 peptide. Proteins that carry only one of the amino acid sequence variations should be tested for their binding behavior in order to determine the influence of each experimentally. It would also be interesting to compare the results to the binding ability of the peptide to spike proteins from other coronaviruses (e.g. SARS-CoV).

Furthermore, the peptide could be varied in order to determine its influence on the result. The SBP1 peptide was taken from the hACE2 receptor and with its alpha-helical conformation should be comparable to the binding domain of the hACE2 receptor [93, 104]. Still, it would be interesting to compare the results to measurements with different peptides and with the full-length hACE2 protein as ligand.

Another hypothesis might be that the region from which the peptide was taken is somehow involved in the process of fusion and of conformational change of the spike protein during binding.

There are also reports about the behavior of the spike protein in electric fields [105]. This effect might also be relevant in this case as the DNA and the sensor surface are negatively charged.

Altogether, the results show that small variations of the amino acid sequence strongly influence the binding behavior up to a complete loss of binding.

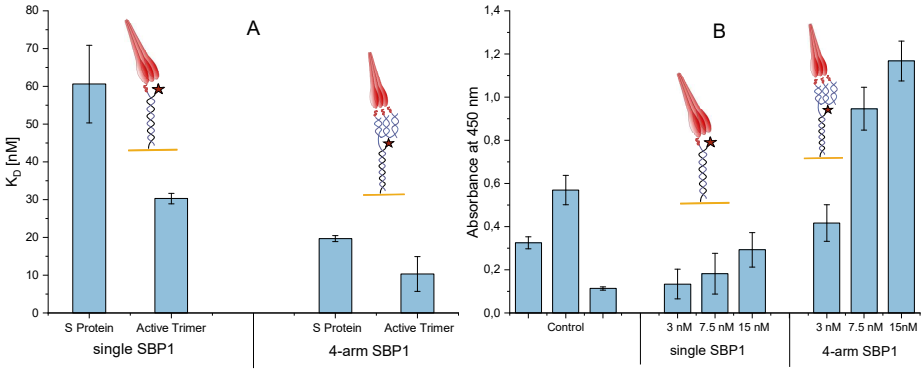

Figure 20: Mono- vs. trivalent peptide presentation and the binding strength towards spike protein. Either single peptide presenting DNA (single SBP1) or four-arm DNA structures (4-arm SBP1) were immobilized as ligands. Spike protein was injected as analyte. A) Dissociation constants calculated from switchSENSE measurements. The two proteins "SARS-CoV-2 S protein" and "SARS-CoV-2 S protein, active trimer" were used as analytes. B) Results from ELISAs. The graphs here represent the results for the binding of "SARS-CoV-2 S protein, active trimer" to the peptides coupled to the DNA nanostructures.

7.2.2 Quantification of oligovalent binding

The binding signal was strongest for the two full-length proteins "SARS-CoV-2 S protein" and "SARS-CoV-2 S protein, active trimer", both by Acro Biosystems. Therefore, they were chose for comparative measurements of their binding stregth to DNA nanostructures carrying one or three peptides. The experiments were done in ELISA and switchSENSE. The DNA structures in this case are either the trimeric ones that were used in subsection 7.2.1 or simple cNL-B48-SBP1 conjugates. Basma Altattan and Nico Grasse performed the ELISAs. For the switchSENSE experiments, measurement parameters were adjusted slightly (see subsection 4.2), including for example longer dissociation times. The resulting graphs were fit with a global exponential fit curve for the determination of binding rate constants.

The dissociation constants K_D for the interaction between the spike proteins "SARS-CoV-2 S protein" and "SARS-CoV-2 S protein, active trimer" to the monovalent peptide presentation (single SBP1) and the trivalent peptide presentation (4-arm SBP1) are presented in Figure 20 A). The exact results are given in Table 5.

The results show that the trivalent peptide presentation increased binding affinity significantly. The K_D for the monovalent peptide presentation was around three times larger than for the trivalent peptide presentation for both proteins. This behavior was expected as it has been previously reported [17, 106].

Figure 20 B) shows the results from ELISAs for the active trimer protein

	K_D [nM], single SBP1	K_D [nM], 4-arm SBP1
S Protein	60.1 ± 10.2	19.7 ± 0.8
S Protein, Active Trimer	30.3 ± 1.4	10.3 ± 4.6

Table 5: Calculated values from switchSENSE experiments of the dissociation constants K_D for the binding interaction between the two spike proteins to the monovalent and the trivalent peptide-DNA-nanostructures.

binding to the mono- and trivalent peptide-DNA-structures. They confirmed that the trimeric peptide presentation led to a tripled signal in the absorbance compared to the monovalent peptide presentation for the same protein concentrations. Furthermore, the signal was concentration dependent for both setups. The control showed no concentration dependency, although the signal strength was comparably high. Non-specific binding to the well plate was observable during ELISA experiments and was minimized by the application of blocking buffer.

The results were reproducible. Still, it was observed that the protein stability seemed to degrade over time. It had been planned originally to also investigate the binding of the proteins to the 4-arm DNA structure carrying one or two peptides. The experiments were done months after the one presented in this subchapter. The remaining protein samples had been kept at -80 °C in aliquots. Additionally, protein was reordered from Acro Biosystems. The company had stopped producing the two proteins “S-protein” and “active trimer” and had completely switched to the “Super stable trimer”. The only way to receive more of the two original variations was to order remaining stock. The results that were obtained with the samples that had been stored at the institute and the reordered samples were less reliable. The signal strength in both ELISA and switchSENSE assays decreased strongly. Differences between the two and one peptide per construct binding to the proteins were very weak.

Hsieh et al. have reported that the activity of the spike protein degrades over time [102] and this might have happened here. The measurements that are presented in Figure 20 and Table 5 come from measurements that were performed in the summer of 2020, shortly after ordering and probably shortly after the production of the proteins. Those measurements showed that the trimeric peptide presentation resulted in stronger affinities than the monovalent peptide presentation.

7.2.3 Inactivated SARS-CoV-2 viruses

The SBP1 peptide had shown strong binding to the unmodified full-length proteins. During the course of the pandemic, it became possible to acquire inactivated SARS-CoV-2 samples. Dr. Alexandra Rockstroh from Fraunhofer IZI, Leipzig, kindly provided the samples used here. The analysis of the sample with dynamic light scattering (DLS) that I performed, showed an average hydrodynamic diameter of $d = (82 \pm 25)$ nm. This is in good agreement with literature

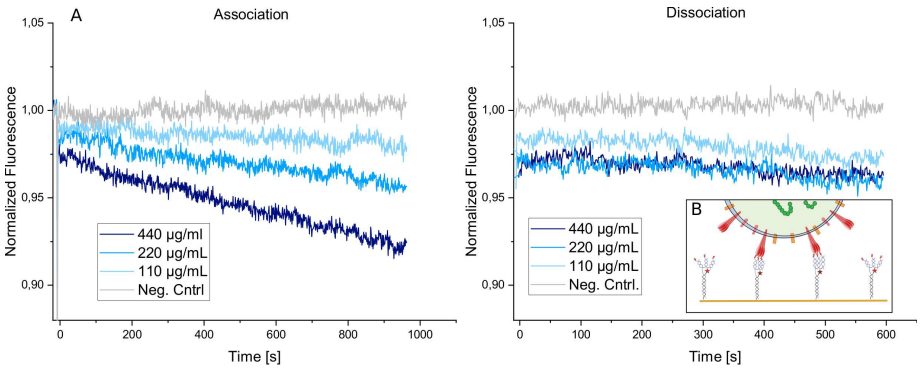

Figure 21: A) Fluorescence signal of inactivated SARS-CoV-2 binding to trimeric DNA-peptide-structures. The signal decreased linearly during the association measurement. The dissociation showed almost no signal change. B) Schematic presentation of the binding process of one virus particle binding to the peptide functionalized DNA nanostructures (not drawn to scale).

that predicts a diameter of around 90 nm [107]. Elena Marie Willner of the Technical University of Munich generously visualized the sample by transmission electron microscopy (TEM). The result can be seen in Figure 17 in the introduction to this subchapter. The results from DLS and TEM showed that the sample is of high purity and the virus particles do not agglomerate.

The four-arm DNA-structure that displayed the three peptides was utilized as ligand on the sensor surface of the DRX^2. The virus samples that were delivered in buffer were injected as analyte. The result of the binding interaction measurements can be seen in Figure 21.

The association of the inactivated virus material showed a concentration dependent signal decrease after sample injection. The signal change could be described as linear. This has been observed for influenza (see subsection 7.1.2) and has been described in literature [52]. A reason for this behavior could lie in multivalent binding interactions, as was the case for influenza as well. The size of one virus particle would suffice to bind more than one nanostructure on the surface.

The dissociation showed almost no signal change. This as well can be explained by multivalent binding. Additionally, the individual binding affinity of one spike protein to the trimeric peptide presenting DNA structure is high. If one virus particle then binds to more than one structure on the surface, rebinding effects etc. become so strong that dissociation cannot be observed during the used measurement times.

The negative control showed no signal change. Here, cNL-B48 without peptide was hybridized on the sensor surface and virus sample at a concentration of $c = 220\,\mu g\,mL^{-1}$ was injected.

7.2.4 Pseudo viruses

Besides inactivated viruses, pseudo viruses present another option for experiments with virus samples of biosafety level S1. In this case, they had a lentivirus basis and carried the spike protein of SARS-CoV-2 on their viral membrane. Lars Heinig of preclinics GmbH, Potsdam, prepared the pseudo virus samples [75].

Pseudo viruses have some advantages as well as disadvantages. Generally, the controllability of the conformation of the virus particles poses one significant advantage. The genetic material as well as the spike protein on the surface can be easily varied. A disadvantage lies in the difficult interpretation of the results. Pseudo viruses can behave differently than the "original" virus. Therefore, the transferability of the results can be limited. The results from pseudo virus experiments have to be interpreted cautiously [108].

The virus particles in this case carried genetic material that coded only for the green fluorescence protein. They were therefore unable to replicate. However, since they could infect cells once, the samples were additionally BPL inactivated to exclude any infectious ability and allow handling in an S1 laboratory environment [75].

It was to be determined, if pseudo virus binding to a ligand is measureable in switchSENSE and especially how the particles behave during interaction measurements with the DNA-peptide nanostructure. Therefore, the three SBP1-peptides carrying DNA structures were hybridized and the pseudo virus solution was injected. The result can be seen in Figure 22.

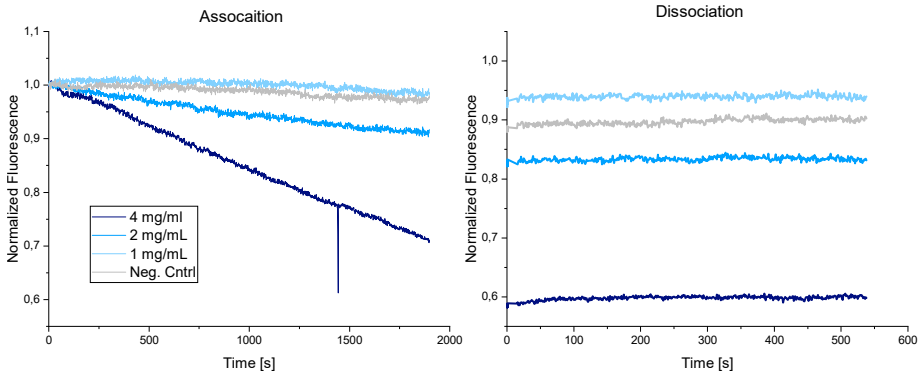

Figure 22: Pseudo virus sample binding to four-arm DNA-peptide nanostructures. Three concentrations of pseudo virus sample were injected and the binding to the SBP1 carrying DNA nanostructure was observed. For concentrations higher than 2 mg mL^{-1}, a linear signal change was measured that is distinguishable from the control. The dissociation showed no signal change.

In this experiment, it was once again plainly visible that the injection of the sample led to a linear signal change during the association. The dissociation

showed once again almost no signal change. The same arguments as for the inactivated original viruses apply here. The injection of 1 mg mL^{-1} virus solution showed a signal that was not distinguishable from the control.

For the negative control, cNL-B48 without peptide was immobilized and pseudo virus sample at a concentration of 2 mg mL^{-1} was injected. The signal showed a slight change.

Generally, the results showed that pseudo virus interactions were measureable.

The protein concentrations of the pseudo virus sample were chosen higher than for the original virus. This had various reasons. Primarily, the amount of available sample was larger than for the original virus. Especially for explorative binding interaction measurements, i.e. where no previous results regarding the measurability of the interaction are available, it is advantageous to use high concentrations.

Furthermore, the samples were prepared differently than the original viruses. The pseudo virus samples were delivered in buffer and although they were purified, it was expected that the purity of the original inactivated virus samples was higher. DLS measurement of the pseudo virus sample confirmed this. The samples contained more aggregates and also some smaller objects than expected.

Additionally, pseudo viruses have different structural characteristics than the original viruses. This includes for example the density of spike proteins on the viral membrane. Furthermore, there might be additional proteins available on the original virus. Also other properties like local charge densities etc. could vary and the production process is different from the original virus.

7.2.5 Pseudo virus variants

Pseudo viruses have the advantage that the spike proteins can be varied easily. During the pandemic, it was observed that the spike protein was a place of mutations [109, 110]. The pseudo viruses were adjusted to carry the spike protein with the existing mutations. The wild type virus was tested as well as two additional virus variants, namely the B1.1.7 or Alpha variant (first detected in the United Kingdom) and the B1.351 or Beta variant (first detected in South Africa) [111]. While the measurement parameters remained unchanged, the behavior of the variant pseudo viruses was qualitatively different from the behavior of the wild type pseudo virus. The result can be seen in Figure 23.

The association showed a strong signal change for all three samples. The shapes of the curves differed though. The graph corresponding to the wild type was linear, while the Alpha and Beta variants showed a binding interaction that followed an exponential behavior. The signal change for the Alpha variant was the strongest. This is especially remarkable since the protein concentration was lowest for the Alpha variant ($c \sim 3$ mg mL^{-1}), while for the wild type and the Beta variant the concentration was chosen at $c \sim 4$ mg mL^{-1}. The spikes in the signals of the Beta and Alpha variant can be attributed to air in the tubing system.

The two variants dissocitated differently from the ligand than the wild type.

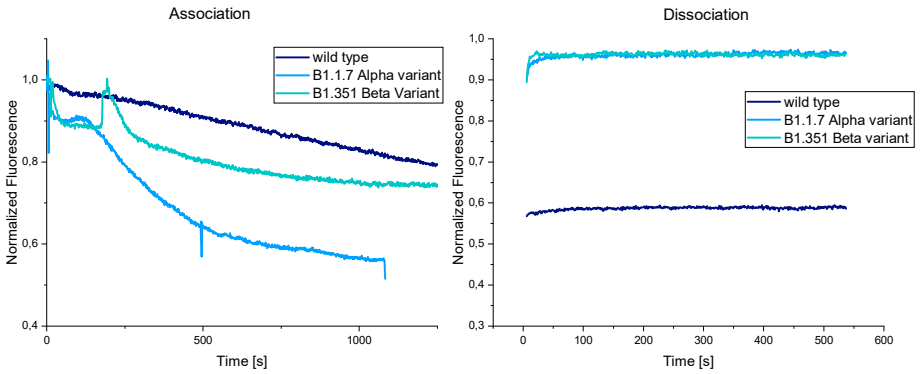

Figure 23: SARS-CoV-2 variants: The binding of the three pseudo virus samples with various spike protein variants to the DNA structure that carried three peptides was measured. The wild type showed a linear association, while the variants Alpha and Beta showed an exponential behavior during the association. The dissociation showed no signal change for any of the variants, although the signal returned to its original value for the Alpha and the Beta variant. This was not the case for the wild type.

The signal did not change during the measurement time, but it jumped back to almost the original value of the normalized fluorescence. This could be an indication for a fundamentally different behavior.

7.2.6 Conclusion

The measurements showed that the peptide SBP1 bound the spike protein of the SARS-CoV-2 virus. The subfragments of the receptor binding domain (RBD) and S1 did not bind the peptide-DNA structure, which was in accordance with the work of Zhang et al. [93]. The unmodified full-length proteins showed strong binding. Full-length spike proteins that had specific modifications to the amino acid sequence showed no binding to the peptide. Variations at the furin cleavage site and a stabilization of the prefusion state resulted in a loss of binding. A variation of the amino acid sequence at the C-terminal resulted in a strong binding signal. Altogether, it could be shown that already small variations of amino acids can have a strong influence on the binding behavior. While many publications focus on the RBD (e.g. [112–114]), our results show that also amino acid variations in other regions of the spike protein might be relevant for its binding behavior.

We compared the binding rate constants of two full-length spike proteins to the trimeric peptide presentation and to the monomeric peptide presentation. The trimeric peptide presentation resulted in higher affinities than the monomeric presentation both in ELISA and switchSENSE measurements. These findings are compatible with the work of Möser et al. [17]. The authors described a similar DNA-peptide nanostructure and showed that the trimeric

peptide presentation increased the binding affinity. This could be confirmed here with a different peptide and a different measurement technology. The findings further encourage the research on oligovalent peptide-DNA nanostructures for a possible application in therapy and diagnostics.

Inactivated SARS-CoV-2 samples were analyzed for their binding to the trimeric peptide-DNA structure and showed strong concentration dependent binding signals during the association. As was the case for the influenza A virus, the signal followed a linear behavior. This is most likely due to multivalent binding interactions and rebinding effects. Dissociations were not measureable.

The trimeric peptide-DNA nanostructures were used as ligands for binding interactions with pseudo viruses. The signal was strong for the wild type and showed the characteristic linear signal change during the association. The concentrations of the pseudo viruses were higher as compared to the original virus samples.

Two pseudo virus variants, namely Alpha and Beta, were tested for their binding to the peptide and showed a qualitatively different behavior. The injection of the variants resulted in exponential signal changes, while the original strain showed the linear behavior. The findings are purely qualitative and further investigations would be necessary to quantify the effect.

As can be found in Boehm et al. [115], the Alpha variant shows a mutation near the furin cleavage site (P681H) that is suspected to influence transmissability. The wild type and the Beta variant both do not show this variation. This could explain the especially strong signal change that was visible for in the Alpha variant.

Additionally, both the Alpha and Beta variant have amino acid variations at two positions that are associated with increased affinity towards the hACE2 receptor, namely N502Y and E484 [115]. Both variants induced a faster signal change that also had an increased intensity, which could be caused by this higher affinity. The results are a confirmation of the literature [115–117].

7.3 SARS CoV-2 nucleocapsid - antibody interaction

In this chapter, the switchSENSE technology was applied to rank the binding strengths of six antibodies against the nucleocapsid protein of SARS-CoV-2.

Jörg Schenk and Frank Sellrie of HybroTech GmbH produced six monoclonal antibodies that bind the nucleocapsid protein of SARS-CoV-2 [118–120]. They were developed for a rapid antigen test against SARS-CoV-2 (by ImmunoGnost GmbH [121]). Prior to switchSENSE measurements, Jörg Schenk and Frank Sellrie tested the six antibodies for binding to nucleocapsid protein in ELISAs. While the ELISAs revealed binding interactions reliably, the DRX^2 enabled the quantification of the individual binding affinities. A schematic overview of the experimental setup can be found in Figure 24.

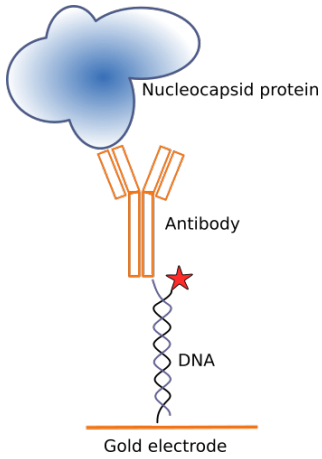

Figure 24: Schematic visualization of antibody - nucleocapsid protein binding interaction. The antibody is immobilized on the sensor surface and the protein is injected as analyte at various concentrations. The schema is not drawn to scale. Furthermore, it is unknown at which site the antibody binds to the cNL-B48 strand during coupling.

I coupled the six antibodies individually to cNLB-48, since antibody samples were available in large amounts. Conjugation of nucleocapsid protein to cNLB-48 was not pursued due to limited sample availability at the time.

The dissociation constants of the antibodies binding to recombinant nucleocapsid protein from *Escherichia coli (E.coli)* bacterial cells were quantified. Furthermore, the binding of one antibody to nucleocapsid protein from HEK293 cells as well as to heat-inactivated SARS-CoV-2 was analyzed.

7.3.1 Binding of six antibodies to nucleocapsid protein of SARS-CoV-2 from *E.coli*

The hybridization curves of the antibody-cNLB-48 conjugate showed correct functionalization. Subsequently, protein solution containing *E.coli*-expressed

recombinant nucleocapsid protein of SARS-CoV-2 was injected at various concentrations. The nucleocapsid protein has a molecular weight of 49.5 kDa [122]. The assay was optimized prior to measurements for determination of kinetic parameters. The finalized parameters were then applied to all antibody-protein measurements. To this end, the concentration of the nucleocapsid protein was set to 100 nM, 50 nM and 25 nM. One result is presented exemplarily for antibody G230GG4 in Figure 25.

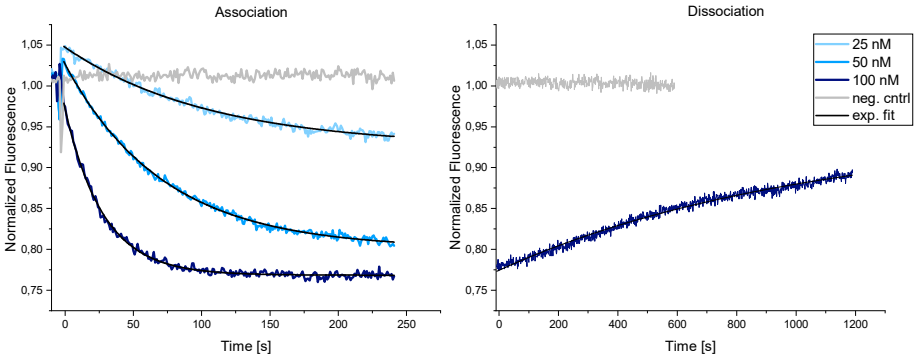

Figure 25: Antibody G230GG4 binding to nucleocapsid protein: the sensor surface was regenerated with fresh cNLB-antibody conjugate in between each injection. The concentration of nucleocapsid protein was varied between 25 nM and 100 nM. Injection of protein led to a decrease of fluorescence signal that could be fit by a mono-exponential curve. As negative control, cNL-B48-G230GG4 was immobilized and the protein S1 of SARS-CoV-2 was injected at a concentration of 400 nM. There was no binding observable for this combination.

For the association of nucleocapsid protein binding to G230GG4, a decrease in fluorescence intensity is observable over the measurement time of 250 s. For the injection of nucleocapsid protein at a concentration of 100 nM, the signal reaches an equilibrium at around $t \geq 100\,\mathrm{s}$. For the concentrations of 50 nM and 25 nM, the signal change is weaker and the time until an equilibrium state is reached is longer. Still, all three graphs follow a strictly mono-exponential behavior for the association, as expected.

The dissociation is only shown for the highest analyte concentration of 100 nM. The measurement time was set to $t = 20\,\mathrm{min}$. While the original signal level is not reached, the unbinding of the protein is clearly observable as the signal increases. There can be various reasons why the fluorescence signal does not reach the original level. Complete dissociation and a regeneration of the original value of fluorescence intensity after dissociation have rarely been observed during the years of experimental work with the DRX^2. Especially when strong binding signals were measured, as was the case here, the signal generally did not regain its original intensity. This could be due to degradation of the sensor surface by the strain of the binding. DNA strands might be removed from the sensor

Antibody	$\mathbf{k_{on}}\,10^5$ $[\mathbf{M^{-1}\ s^{-1}}]$	$\mathbf{k_{off}}\,10^{-3}$ $[\mathbf{s^{-1}}]$	$\mathbf{K_D}$ $[\mathbf{nM}]$
G229 FA10	2.02 ± 0.06	2.21 ± 0.09	11.0 ± 0.5
G230 JC3	2.96 ± 0.08	1.88 ± 0.07	6.3 ± 0.3
G230 AH2	2.54 ± 0.03	1.15 ± 0.09	4.5 ± 0.4
G230 DE6	7.16 ± 0.19	2.75 ± 0.04	3.9 ± 0.8
G230 GG4	3.07 ± 0.03	1.02 ± 0.02	3.3 ± 0.1
G230 HC9	3.49 ± 0.07	0.82 ± 0.01	2.3 ± 0.2

Table 6: Binding rate constants for six antibodies binding to nucleocapsid protein of SARS-CoV-2. The antibodies are ranked from weakest to strongest binding affinity. All six dissociation constants lie in the low nano-molar range.

surface during the measurement or fluorophores are damaged or bleached. Even if the protein dissociated completely, the intensity would not reach its original value. Furthermore, the measurement time could have been too short.

For the binding interaction of nucleocapsid protein and G230GG4, the association rate constant was $k_{\text{on}} = (3.07 \pm 0.03) \cdot 10^5\,\text{M}^{-1}\text{s}^{-1}$, the dissociation rate constant was $k_{\text{off}} = (1.02 \pm 0.02) \cdot 10^{-3}\,\text{s}^{-1}$, and hence the dissociation constant was $\text{K}_\text{D} = (3.32 \pm 0.08)\,\text{nM}$.

The specificity of the binding was verified by a negative control experiment, in which the S1 subdomain of the spike protein of SARS-CoV-2 was injected as analyte after a re-functionalization of the sensor surface with cNLB-G230GG4. There was no signal change visible for the association or the dissociation. It can be concluded that the antibody specifically binds the nucleocapsid protein and does not bind the S1 subdomain of the spike protein.

Binding rate constants of the additional five antibodies were determined on the same measurement chip, the same channel and the same electrodes. The summarized results for all six antibodies can be found in Table 6.

The binding affinities of all six antibodies were in the low nanomolar range as expected [4]. Antibody G229FA10 showed the highest value for K_D and therefore the lowest binding affinity. The strongest binder was antibody G230HC9 with a $\text{K}_\text{D} = (2.3 \pm 0.2)\,\text{nM}$.

The observation of the association and dissociation rate constants can be of interest. A visualization of the rate constants can be seen in Figure 26.

Especially antibody G230DE6 behaved differently than the other antibodies. It showed a higher association rate constant, which indicates a faster on-binding process, but it also showed a higher off-rate, indicating a faster dissociation from the antibody. While the rate constants differ for G230DE6, the resulting K_D is average as compared to the other antibodies. Depending on the application of a protein, the rate constants can be of great importance [26].

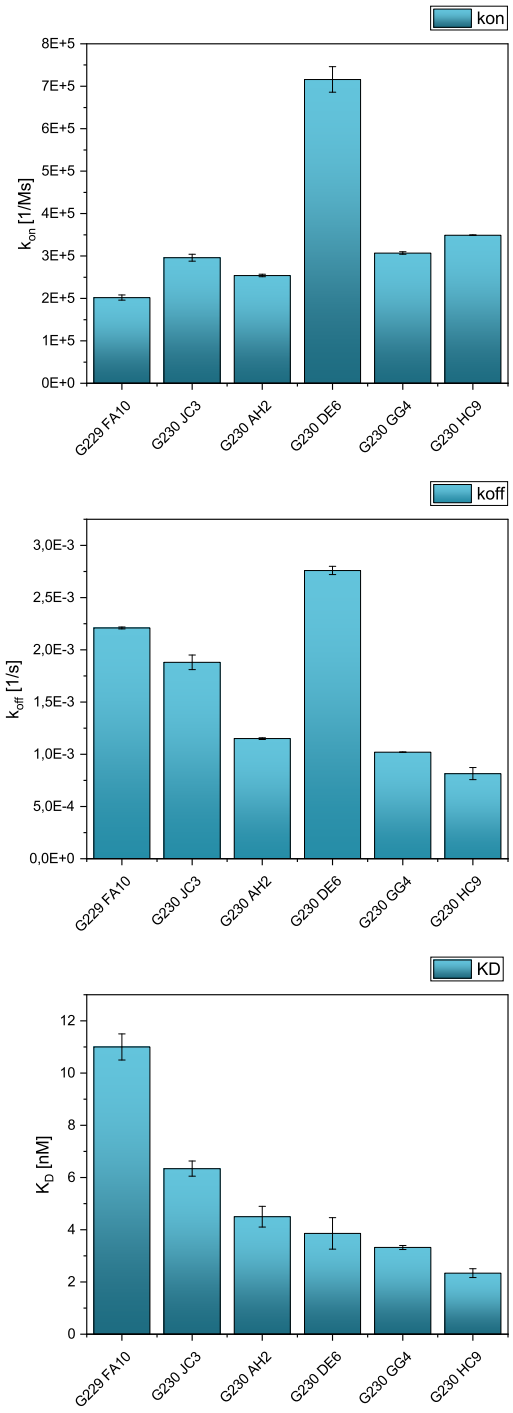

Figure 26: Rate constants and dissociation constant for six antibodies binding to nucleocapsid protein form *E.coli* cells. The association and dissociation rate constants reveal that antibody G230DE6 behaved differently than the other antibodies, although the resulting K_D was average.

7.3.2 Binding of G230AH2 to nucleocapsid protein of SARS-CoV-2 from HEK293 cells

In order to examine, if the expression system of the nucleocapsid protein influenced the binding affinity, nucleocapsid protein from human embryonic kidney 293 (HEK 293) cells was utilized as analyte. Exemplarily, the antibody G230AH2 was employed as ligand. The parameters of the measurement were largely identical to the ones chosen for nucleocapsid protein from *E.coli* cells (see subsections 7.3.1 and 4.3). The result can be seen in Figure 27.

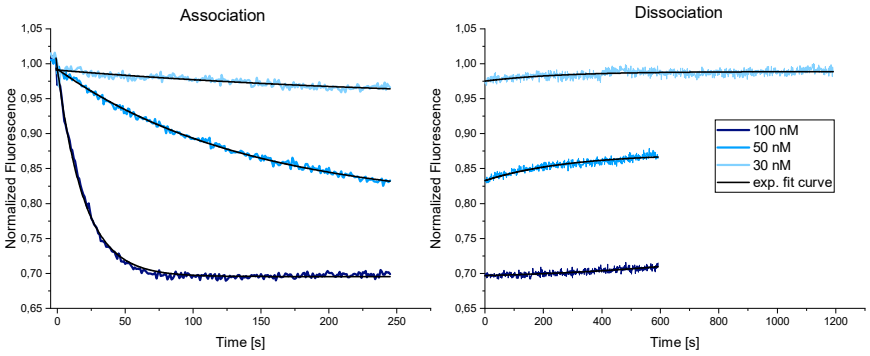

Figure 27: G230AH2 and its binding to nucleocapsid protein expressed in HEK293 cells. The signal change of the association happened fast while the dissociation signal increased only slowly. This indicated a strong binding interaction. Calculated rate constants were similar to the ones found for nucleocapsid protein from *E.coli* cells.

The injection of the nucleocapsid protein from HEK 293 cells led to a strong signal decrease during association that followed a mono-exponential behavior and was concentration dependent. For an analyte concentration of 100 nM, the signal reached an equilibrium at around $t \cong 75$ s.

The dissociation showed only a slight signal increase. For the analyte concentration of 30 nM, the dissociation was almost complete over the measurement time of 1200 s, but the signal strength was low overall. The dissociation remained incomplete for the analyte concentrations of 50 nM and 100 nM during the measurement time of 600 s. This indicates a strong binding behavior.

The mono-exponential fit curves returned binding rate constants of: $k_{\text{on}} = (1.9 \pm 1.2) \cdot 10^5\,\text{M}^{-1}\text{s}^{-1}$, and $k_{\text{off}} = (2.0 \pm 0.9) \cdot 10^{-3}\,\text{s}^{-1}$, and a dissociation constant of $\text{K}_\text{D} = (10.9 \pm 8.5)$nM. This is in agreement with the results for G230AH2 binding to nucleocapsid protein from *E.coli* cells ($\text{K}_\text{D} = (4.5 \pm 0.4)$ nM), considering the error and the slight differences in measurement parameters (e.g. different measurement chip).

Altogether the results showed that the antibody G230AH2 bound almost equally well to nucleocapsid protein from both expression systems.

7.3.3 Binding of G230HC9 to inactivated SARS-CoV-2

Finally, the binding of the antibodies to virus material was tested. Inactivated virus material replaced the recombinant nucleocapsid protein as analyte. As G230HC9 had shown the strongest binding affinity towards nucleocapsid protein (see Figure 26), it was selected as ligand. After immobilization of the antibody, undiluted heat-inactivated SARS-CoV-2 sample was injected.

The virus sample was dissolved in cell culture medium (RPMI-1640). The specific characteristics of this environment have to be considered. In previous experiments, it could be shown that the injection of cell culture medium induces a stepwise signal increase of the fluorescence signal during association and a corresponding stepwise decrease during dissociation (see also subsection 10.2). This is due to fluorescently excitable constituents in the cell culture medium [123] (e.g. amino acids [124]). The stepwise increase and decrease are not shown in result of the measurement in Figure 28.

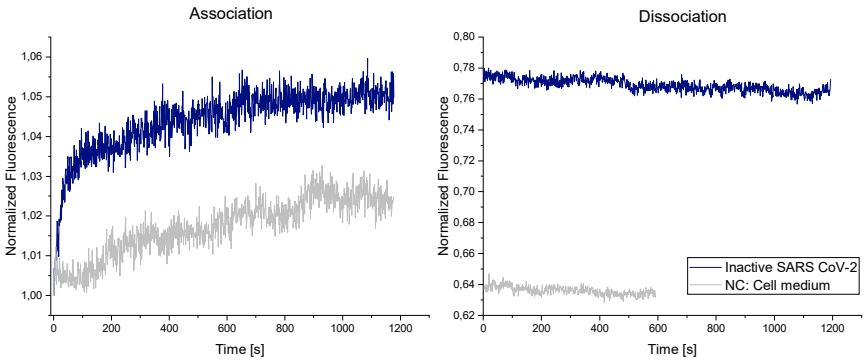

Figure 28: Heat inactivated SARS-CoV-2 binding to G23HC9. As negative control, pure cell culture medium was injected.

The graphs show, that there was a qualitatively different signal for the injection of pure cell culture medium as compared to the injection of cell culture medium that contained SARS-CoV-2 material. The injection of virus containing sample led to a steep rise of signal intensity in the first 200 s, which afterwards flattened and became a steady but slower signal increase for times $t > 400$ s. This could be interpreted as an approach towards an equilibrium state.

The signal of the negative control showed a different behavior. A steady and more linear as well as weaker signal increase of fluorescence intensity was observable during the association, which can be attributed to unspecific binding of components of the cell medium to the antibody, the DNA or the sensor surface.

The dissociation was observed for 20 min for virus containing sample and 10 min for cell medium. Here a slow signal decrease is observable for both samples.

The graphs were not fit by a mono exponential function, as the binding process is more complex due to multivalent binding and influences of the cell

culture medium. Binding affinity parameters were not quantified. Still, the results prove that the antibody G230HC9 bound inactivated virus sample.

7.3.4 Conclusion

The switchSENSE technology was primarily developed for the measurement of protein-protein interactions and the determination of binding rate constants of these interactions [16, 125]. This was done in this subchapter. The six antibodies were successively analyzed for their binding affinity towards the nucleocapsid protein of SARS-CoV-2. The ranking of the antibodies according to their dissociation constant showed that all of them bound strongly to nucleocapsid protein with a $K_D \sim$ nM, which is in good agreement with literature [4].

The determination of association and dissociation rate constants furthermore allowed for the comparison of specific binding behavior. Especially for application purposes, these parameters can be of great interest. The determination of rate constants was an intermediate step towards the development of a rapid antigen test. While the clinical performance of these tests is what actually counts in the end, it can be extremely important to determine the optimal antibodies during the development process. Literature shows that the clinical performance of rapid antigen tests against SARS-CoV-2 varies (e.g. [126–128]). While this can have various reasons, including for example the emergence of new variants [129] or difficulties in application, a thorough characterization of the utilized antibodies can be beneficial in order to exclude low affinity as a source of insufficient clinical performance.

As the antibodies were immobilized on the sensor surface, the analyte molecule could be easily varied. The antibodies bound to the nucleocapsid protein from *E.coli* cells, as well as to the nucleocapsid protein from HEK293 cells. The order of magnitude for the two dissociation constants was in good agreement.

Finally, the binding of one antibody to inactivated SARS-CoV-2 was investigated. While a qualitative difference was observable between negative control and sample, the effect was small.

Only few works on monoclonal antibodies against SARS-CoV-2 nucleocapsid proteins are published (known exceptions are the work of Terry et al. [130] and Yamaoka et al. [131]). It is suspected that the development of monoclonal antibodies for rapid antigen tests is often not published because of economic reasons. Still, they are also useful in other scientific contexts and it is therefore generally helpful to develop well charcterized monoclonal antibodies.

7.4 Virus variation

In this subchapter, the results of virus variations are presented in order to illustrate the broad applicability of switchSENSE technology to virus-receptor interactions. In the previously described experiments, influenza A and SARS-CoV-2 were used as analytes. Here, two additional kinds of viruses were used: inactivated adenovirus and norovirus-like particles. Both were analyzed for their binding to corresponding antibodies.

7.4.1 Adenovirus - antibody interaction

The adenovirus is a well-studied object, as it has been used as a vector in various therapies (e.g. [132–134]). The virus used here is adenovirus type 6, strain tonsil 99.

The virus was analyzed for its binding to an antibody called 8C4. The antibody was produced by the same company as the virus (HyTest Ltd, Finland) and was recommended as "capture" antibody for ELISA assays. Therefore, it was expected that the affinity between the binding partners would be high. The antibody binds the hexon protein on the viral surface.

The DNA-8C4 conjugate was immobilized and virus sample was injected at varying concentrations. The resulting kinetics can be seen in Figure 29.

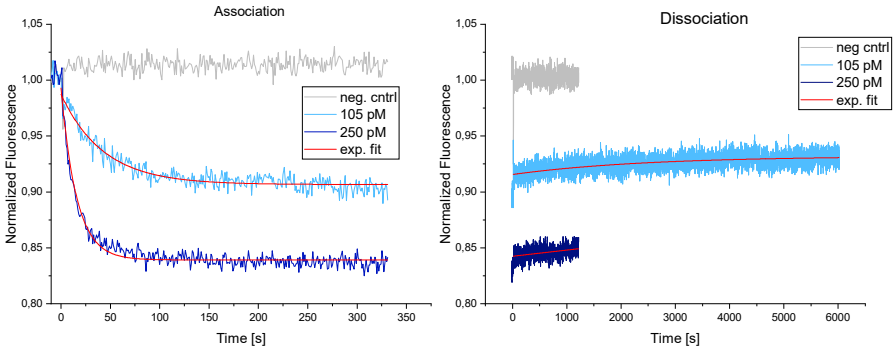

Figure 29: Binding kinetics of adenovirus to the immobilized antibody 8C4.

The association of the virus to the antibody can be fit by a mono-exponential function. The fluorescence signal for the higher concentration of 250 pM reached an equilibrium after $t \approx 80\,\mathrm{s}$. The signal for the lower concentration reached an equilibrium after around $t \approx 150\,\mathrm{s}$. The dissociation showed only weak signal changes for both injections and the calculated value for the dissociation constant lies at $K_D = (13.4 \pm 5.2)\,\mathrm{pM}$. This indicates strong binding. Bottermann et al. [135] reported dissociation constants in the low nM-range for Fab fragments of antibodies binding to the hexon protein. The K_D in the pM-range that was determined in the DRX[2] is lower. Reasons for the discrepancy might be, that the virus concentration was not sufficiently verified or the differences in antibody,

virus strain or the utilized measurement technique. The strong affinity of the antibody to the hexon protein however could be shown here as well.

Buffer solution without virus material was injected into the channel as a control (blank measurement). No signal change was visible in this case.

The experiment showed that adenovirus and antibody interaction can be measured using the DRX^2.

While the results of the kinetic experiments looked very convincing, a restriction to the informative value has to be mentioned. In the course of a quality control test of the purchased samples, a dynamic light scattering (DLS) experiment was performed. From literature one would expect a diameter of around 70-100 nm for adenoviruses [136]. The result of the dynamic light scattering resulted in a diameter of around $d = (7.6 \pm 1.4)$ nm (see Figure 30), although larger particles were visible as well.

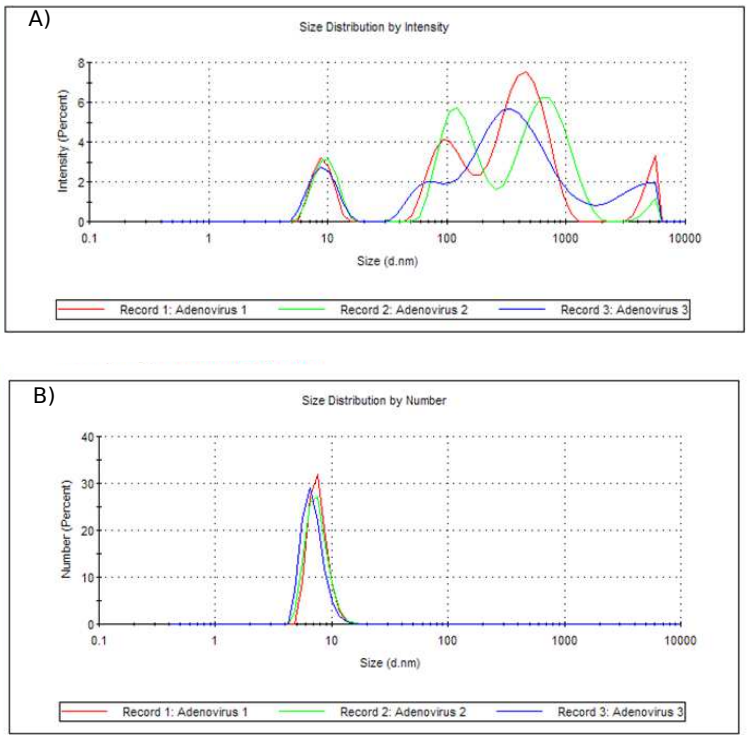

Figure 30: Dynamic light scattering measurement of adenovirus sample. A) Size distribution by intensity. Beside the peak at around 10 nm, the graph indicates the presence of larger particles or agglomerates. B) Size distribution by number.

A hydrodynamic diameter of around 10 nm is on the order of magnitude that is found for proteins [137]. The result from the DLS has to be considered

when the binding kinetics curve in Figure 29 is interpreted. It is possible that primarily viral proteins were present in the sample and bound strongly to the antibody, which resulted in the mono-exponential signal change, but no actual virus particle-antibody interaction was measured.

The supplier was contacted with regard to the matter, but no explanation for the results from the DLS could be found. For influenza A and SARS-CoV-2, DLS measurements resulted in the expected values for the hydrodynamic diameters of the particles in the samples.

Additionally, virus-receptor binding experiments normally resulted in linear fluorescence signal changes [73, 75]. Further characterization of the adenovirus samples would be necessary. This could include transmission electron microscopy in order to visualize the sample constituents.

7.4.2 Norovirus-like particle - antibody interaction

The human norovirus (previously called Norwalk virus) is a non-enveloped virus that has a spherical shape and a diameter of around 27 nm [138]. The sample, which was used here, was made up of the virus protein 1 (VP1) of the norovirus genogroup GII.4, which is one of the most common noroviruses responsible for outbreaks in humans [139]. The VP1 makes up the major capsid protein of the virions and builds the spherical capsid of the virions [139]. The sample contained only the VP1 and no other non-structural proteins or RNA. Samples like this are called virus-like particles (VLP). Virus-like particles like those used here can be handled in S1 biosafety environments and have been used in vaccines for example against the human papillomavirus [140].

The recombinant protein for the human norovirus-like particles used here was produced in HEK 293 cells. Since the sample contained no genetic material, inactivation of virus-like particles was not necessary. This is one advantage of virus-like particles in research. The mouse anti-norovirus GII monoclonal IgG antibody specifically binds norovirus of genotype GII. It was produced by the same company as the antigen (The Native Antigen Company, Oxfordshire, Great Britain).

The antibody was coupled via standard coupling. After immobilization of the DNA-antibody conjugate, norovirus VLP sample was injected into the channel. The resulting graph for the binding kinetic can be found in Figure 31.

It shows a slight signal increase upon association and a signal decrease upon dissociation. The signal change is weak compared to what was observed for the adenovirus. Still, especially the resulting dissociation might point towards a binding interaction. The graph could be fit by a mono-exponential fit curve. Since the concentration of the original sample was uncertain and only a single concentration is shown, the resulting numerical values for the rate constants are not very reliable and are therefore not presented. The negative control in this case was a blank measurement, where buffer solution was injected after immobilization of antibody-DNA conjugate. In this specific case, the sample was not analyzed by dynamic light scattering.

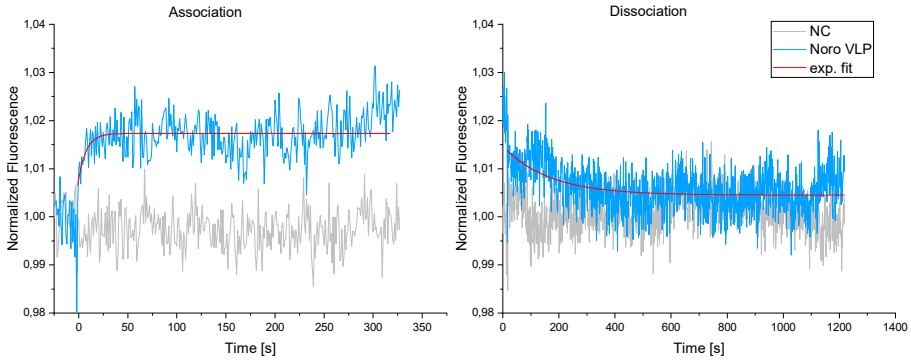

Figure 31: Norovirus-like particles binding to antibodies.

In principle the results show that also antibody-VLP binding kinetics can be observed in the DRX^2.

7.5 Discussion virus-receptor interactions

In this subchapter, some general aspects of measuring virus-receptor interactions with switchSENSE technology are discussed. While the technique is generally suitable for these measurements, there are some challenges and some advantages. Some of them are specific for the technology and virus-receptor interactions but some are generally important for measuring interactions of biological molecules.

7.5.1 Virus samples

Virus samples are complex. The production of virus material is a complicated procedure that underlies biological variations [141, 142]. All samples used in this thesis were acquired from outside and not produced in the institute. The quality control of the provided samples is difficult. Generally, the information about the samples includes the biological safety level, inactivation technique, buffer, concentration technique and concentration.

Most viruses were delivered in buffer (e.g. PBS) but some were also delivered in cell medium or distilled water. The buffer environment is important for binding interaction measurements [24]. It is generally advisable to use the same buffer for all samples and for the running buffer. Measurements in cell medium were possible but influenced the resulting fluorescence signal. Samples in distilled water were not used in this thesis.

The concentration of virus samples is another issue. While some manufacturers measured protein concentrations after inactivation (e.g. by BCA test), some provided values in "plaque forming units" (PFU) from before inactivation or for the case of the pseudo viruses the unit was "relative light units per milliliter" (RLU mL^{-1}). The units are difficult to compare. Furthermore, all units related to infectivity of the virus samples are hardly usable after inactivation. They merely give an idea about the original infectivity.

Protein concentrations are easier to handle and compare, but the questions remains, if all proteins in the sample are viral proteins and if the sample consists of broken up protein fragments. For quantitative evaluations of dissociation constants, it is essential to determine the concentrations of the binding partners [24]. Since the work here was mostly qualitative or semi-quantitative, this is less urgent. For further and quantitative results, reliable concentration determinations would be of great importance.

Generally, a quality control for virus samples is advisable. In an ideal world, one could start with a protein concentration determination, continue with dynamic light scattering to measure the hydrodynamic radius of the viral particles, run a gel electrophoresis and finally visualize the samples, for example by electron microscopy. These aspects should be considered when starting work on a new sample.

Additionally, one should consider biological stability. It was observed that the influenza A virus sample lost its binding activity over time, when stored at 4 °C.

7.5.2 Buffer

While the buffer of the samples can already influence the fluorescence signal, the choice of running buffer and the preparation of them can also be of great importance. It is known that for example the pH, the salt concentration or the concentration of cations (e.g. Mg^{++}) of the buffer can influence binding affinity [24].

Most of the time, PE140 at a pH of 7.4 was used as running buffer. This buffer was self-prepared. While the preparation in the lab saves money, there is a possibility for mistakes and variations between charges.

7.5.3 Binding signal

The switchSENSE technology is based on the collection of a fluorescence signal. For virus-receptor interactions, it has been observed that the binding signal can consist of an increase in fluorescence signal or more often a decrease in fluorescence. Since the signal can be small, it should be kept in mind that both is possible.

7.5.4 Interpretation of fits

The software that is delivered with the instrument is very valuable and reliable. However, when interpreting the measurement data it is advisable to question the resulting values. The software can fit signals with no or almost no change during association or dissociation by a monoexponential fit-curve and it calculates rate constants and a dissociation constant. These values should not be trusted blindly. As a first step, it is advisable to consider, whether a binding event has happened. There are different ways of determining this. A general procedure is briefly described in the following paragraphs.

First, onoe should make sure that there is a ligand coupled to the DNA. A good indication for this is a sizing measurement. The freshly conjugated DNA-ligand sample should be analyzed in a sizing measurement and compared to pure double-stranded DNA (e.g. cNL-B48). If the ligand is attached to the DNA, the dynamic response of the lever is normally different from the one for pure DNA. The sizing measurements have proven to be sensitive. If there is already no difference between the conjugated sample and pure DNA, chances are high that the coupling process failed and no ligand is attached. Therefore, further binding measurements to an analyte would be without any sense.

Secondly, a signal change should be visible during kinetic measurements. As mentioned above, the software also fits basically flat curves. This should be avoided. Although signal changes can be weak, it should be visible and it should be dependent on the injected concentration of the analyte. It is generally advisable to regenerate the surface in between different concentrations, especially when dissociations remain incomplete. If one already has an idea of the order of magnitude of the dissociation constant, the signal should be strong for concentrations higher than the K_D.

A good control of whether a binding event took place is also to look at dynamic mode measurements during a kinetic measurement. There is the option to apply an alternating voltage prior to and after the association, even when measuring the kinetics in static mode. If a binding took place, generally it should be visible as a reduction of switching speed. If there is no change in the dynamic response and there is no or almost no signal change in the kinetic data, it is very likely that no binding happened.

Thirdly, it is important to keep in mind, what one actually knows about the sample. As mentioned above for virus samples, it was often unclear what the actual concentration of the analyte was. The software only works on the available data and for an assay setup in switchBUILD, it is necessary to enter concrete numbers for the analyte concentrations. After a measurement and the subsequent visualization in switchANALYSIS, it can be tempting to accept the calculated rate constants plus error as the correct values. It is advisable to remember the starting point and interpret the calculated values accordingly.

As the functions utilized by switchANALYSIS are not disclosed, it is also advisable to export all data and analyze it in an external program. In that case, one is able to control fit functions and for example, what data points are included in the fit more easily. This was done in this thesis for all quantitative or semi-quantitative analyses.

7.5.5 Control experiments

This aspect is also related to the previous paragraph. Control experiments are extremely important and should always be performed! One control is generally advised for all binding measurements: pure complementary DNA should be hybridized (e.g. cNL-B48) and analyte solution at a high concentration (similarly high as during positive binding experiments to a ligand) should be injected. This excludes binding of the analyte to the pure DNA, the fluorophore or the sensor surface.

The blank measurement (i.e. injection of running buffer) can also be instructive. It can be an indication of the stability of the DNA-ligand conjugate in the experimental setup. It excludes signal changes that are not caused by the binding event, but by degradation of the chip surface, the conjugate or the fluorophore.

Control experiments with other fluorophores can also be necessary to exclude interactions between the analyte and the fluorescence molecule.

If they are available, it is also extremely helpful to have binding measurement results from other techniques (e.g. ELISA). If it is already known, whether a binding is to be expected and at what concentrations of analyte, a qualitative and quantitative verification of the results in switchSENSE can be of great value.

7.5.6 Comparison

In this last paragraph of the discussion, the switchSENSE technology applied to virus-receptor interactions is compared to existing literature and other tech-

niques.

A direct comparison is possible with the work of Memczak et al. [57, 61], as the same peptide and influenza virus was utilized. The switchSENSE technique enabled the quantification of the binding strength of one peptide to the virus (ss1PeB binding to X31 in the sandwich assay in subsection 7.1.7) and the general determination of oligovalent binding behavior. This had not been possible with SPR. Peptide, virus subtype and temperature variations were possible in both techniques.

The controllability of the receptor density as was shown in subsection 7.1.3 is an advantage of switchSENSE over SPR. After a controlled reduction of the receptor density, the dissociation of the virus particles was visible.

It was shown that switchSENSE technology enables the measurement of interactions of the unlabeled viruses with ligands in their native environment. In MST [143] or FCS measurements [144], one of the binding partners has to be labeled with a fluorophore (if the binding partners have no intrinsic fluorescence).

Compared to techniques that are based on the interaction of single particles as described by Cuellar-Camacho et al. [51] and Müller et al. [52], the switchSENSE technology produces results from an averaged signal. While this can be a disadvantage for the understanding of the individual interactions, the averaged signal can be closer to the natural behavior of virus material and its binding to a receptor functionalized surface. This could be beneficial for a future application of potential therapeutics.

Challenges remain that are similar for other techniques that require immobilization of one of the binding partners.

Altogether, swithSENSE can be an additional technique that can be used to quantify virus-receptor interactions.

8 Sizing of influenza A viruses

Sizing measurements can be performed in the switchSENSE technology in order to determine the hydrodynamic radius or diameter of objects. According to the manufacturer, the sizing measurements are limited to molecules that have a hydrodynamic diameter between 2 nm and 14 nm [71]. Here it is shown, that the range can be extended to larger objects, when the lever length is increased. While the existing theoretical model is not applicable in this setup, the results of the experiments still prove the feasibility of sizing larger objects.

8.1 Sizing measurements

As previously described, the DRX^2 can be applied for measurements of hydrodynamic radii. To determine absolute values for the hydrodynamic diameter, experimental parameters have to be adjusted to fit the theoretical model of Langer et al. [49]. These parameters include the 48 base pair long DNA nanolever on the gold surface as well as the specific ion concentration of the running buffer (PE40).

Both parameters cannot be used for measurements of influenza A viruses. The 48 base pair long DNA has a length of around 15 nm [4]. If the length of the DNA nanostructure ss3PeB is included, the length increases to around 20 nm. Compared to the diameter that is known for influenza A viruses ($\sim$ 120 nm [145]), this lever is too short to reasonably try switching of the viruses. The much larger virus particle would hinder any switching motion. Furthermore, as was shown before, one virus particle can attach to more than one DNA nanolever, which would further impede switching. Therefore, a longer lever was necessary.

The virus material is stable in salt concentrations of around 100 mM NaCl [146]. PE140, which has a salt concentration of 140 mM, was used for all experiments. The salt concentration of PE40 (40 mM NaCl) would not have been optimal.

Therefore, the sizing measurements performed here are limited to qualitative comparisons. They are foremost a proof of concept that larger objects with a hydrodynamic diameter of more than 14 nm can be switched using this technique.

8.2 Adapter chips

During a beta testing phase in 2019, we were able to try out the adapter chip design by Dynamic Biosensors that was new at the time. The basic chip layout stayed the same (four channels, 6 electrodes each etc.), but the DNA configuration on the gold electrodes was modified.

The hybridization scheme can be seen in Figure 32. On the novel chips a 48 base pair long anchor strand (cNL-W48) is immobilized, which, contrary to the standard chips, does not carry a fluorescent molecule at the 5'-end. The chips are therefore also called “dark chips”. The complementary or also called

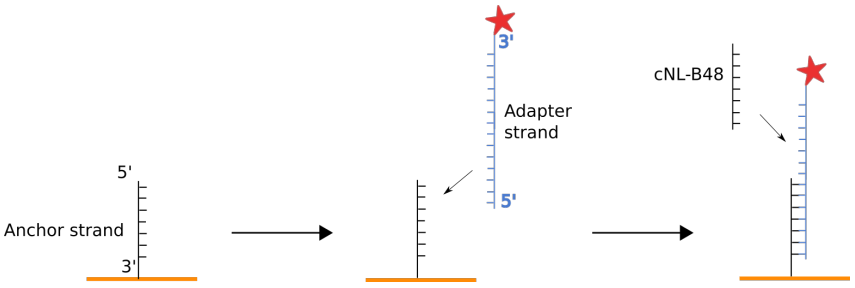

Figure 32: Adapterchip: A single strand of DNA is bound to the gold electrode surface. A longer single-stranded DNA, which has a partly complementary part and carries a fluorophore is hybridized. Then, cNL-B48 can be functionalized subsequently.

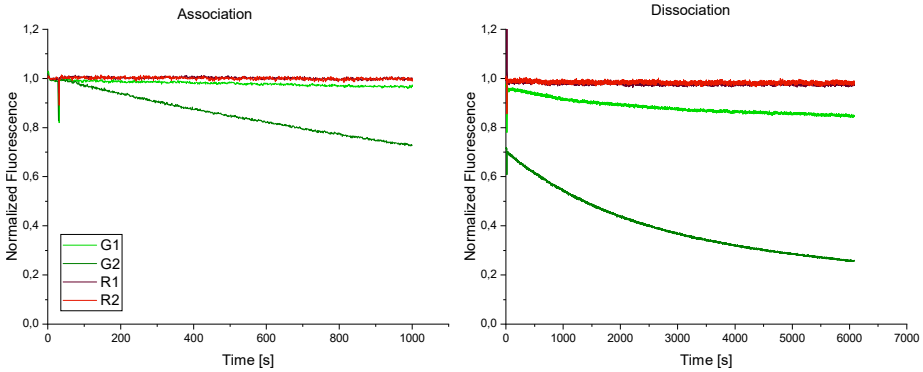

Figure 33: Bleaching test for four fluorophores: R1 and R2 emit light in the red wavelength range, G1 and G2 in the green range.

adapter strand (NL-W48-B48-XX) carries double the amount of bases and is complementary to the anchor strand in the lower 48 bases. This strand carries a fluorescent molecule (XX in the strand code) and can be easily varied. For specific experiments it can be desirable to use different fluorophores depending on the characteristics of the analyte proteins, the experimental setup or the fluorophores. The surplus 48 base pairs are made up of the B48 sequence. Therefore, as was the case for the standard multipurpose chips, the cNL-B48-ligand conjugates can be easily hybridized.

As part of the beta test, four fluorophores (R1, R2 G1 and G2), each attached to an adapter strand, were tested for their specific bleaching properties on the new adapter chips in the DRX^2 (see Figure 33).

The red fluorophores (R1 and R2) show almost no bleaching during the measurement time of almost two hours. The fluorescence signal from the green fluorophores decreases significantly over time. The G2 fluorophore's signal decreases to about 20% of the original value. The measurement times were comparable to

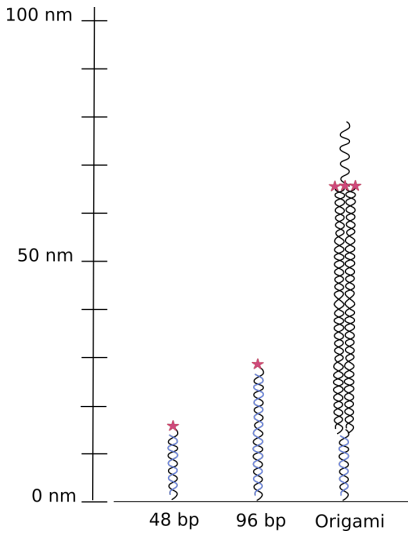

Figure 34: Size comparison between different lever lengths.

the ones used in the virus-receptor binding interactions. It is therefore preferable to use one of the red fluorophores (R1 or R2) for these measurements. On the standard multipurpose biochips, the NL-B48 DNA carries the R1 fluorophore.

8.3 DNA origami levers

The concept of the adapter chips also opened the possibility to attach longer DNA levers easily to the anchor strand. As the viruses have a diameter of around 120 nm [145], it was desirable to increase the lever length for switching experiments. During the beta testing phase of the adapter chips, DNA origami structures with a length of around 50 nm were used. The origamis were made up of the complementary strand to the anchor strand, of four DNA double strands, four fluorophores and the B48 overhang to which the normal cNL-B48-ligand conjugate can be attached. The entire lever has a length of around 83 nm. The core four double-stranded DNA strands carry a fluorescent molecule each. A schematic view of the origami levers compared to the standard 48 base pair lever and the 96 base pair lever can be seen in Figure 34.

8.4 Sizing of influenza A viruses

For the sizing experiments with influenza A viruses, the adapter chip and the DNA origami levers were used in combination. Prior to hybridization of the origamis, they were functionalized with ss3PeB. Origami solution was mixed with a solution of ss3PeB (100x excess) and incubated for 1 hour at room temperature in the dark. The dark environment was chosen to protect the fluorophores from bleaching. After functionalization, the solution was directly

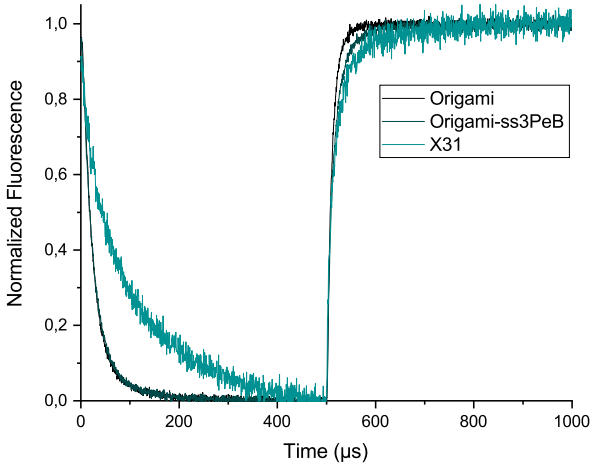

Figure 35: Results of the molecular dynamics measurement with the virus solution at a frequency of 1 kHz.

injected into the device for hybridization. Since there was no binding partner or complementary strand for the ss3PeB on the electrode surface, the excess amount was washed out, making further purification prior to hybridization unnecessary. After hybridization, a dynamic response measurement was performed. The frequency of the alternating current was reduced to $f = 1$ kHz during this measurement step as was advised for the longer DNA origami levers. Then the virus solution was injected and subsequently another dynamic response measurement at two different frequencies, namely $f_1 = 1$ kHz and $f_2 = 50$ Hz was performed. The data can be compared between the motion of the origami nanolever prior to binding of viruses and afterwards. The result shows, that the viruses bind to the peptides attached to the origamis and significantly slow down the motion of the origami lever. Especially the downward motion is decelerated. The result can be seen in Figure 35.

In the upward motion it is even possible to differentiate between the origami and the origami that was functionalized with ss3PeB. This indicates the sensitivity of the sizing measurements.

8.5 Discussion

The adapter chip and the origami levers open the possibility of switching larger objects with a hydrodynamic diameter of more than 14 nm. Here it was demonstrated that this is possible for influenza A virus material. After association of the viruses, a significant slowing of the motion of the around 80 nm long DNA origami levers was visible.

It is possible that not all origami levers were occupied by a virus particle. Since the signal is averaged over the entire electrode, the signal of unoccupied levers influences the signal. This has to be considered, when the analysis should be extended to a quantification of the hydrodynamic radius for example.

While the diameter of the viruses is said to lie around 120 nm, it is also known, that the influenza A virus particles show a heterogeneous size distribution [84]. Some virus particles have a larger and some a smaller diameter than 120 nm. It would therefore be interesting to test this system on objects with a homogeneous size distribution as for example nanobeads (e.g. with a diameter of 100 nm or 50 nm). These beads could be coupled via biotin-streptavidin capture. In order to extend the theoretical model, precisely defined objects would be of great advantage. First tests for the sizing of nanobeads using the adapter chip and the origami were run but need further experiments. The instability of the DNA origami posed an obstacle. After some weeks of storage at 4 °C, the origami levers could not be hybridized or switched any more.

The DNA origami levers and the adapter chip combined open new possibilities to expand the range of molecular sizing beyond the 14 nm limit.

A popular technique for sizing measurements is dynamic light scattering (DLS). As described by Hallett [147] there are challenges for working with DLS. They lie for example in the sample preparation and in possible misinterpretation of the resulting data. Aggregations or larger particles in the solution are problematic [148]. For DLS measurements, the scattered intensity is dependent on the particle radius to the sixth power [148]. When using the switchSENSE technology for sizing of objects it is as well necessary to have a sample that is as homogeneous as possible. Still, the influence of aggregates or dust etc. on the result is smaller. Foreign objects like dust would not bind to the ligands. Aggregates of analyte can bind to ligands and influence the result. The effect is smaller though. Extending the measurement range beyond the limit of 14 nm for switchSENSE can therefore be an important contribution to sizing measurements.

9 Protein binding interactions

In the following subchapter, two projects are presented that presumeably hold informative and instructive value for anyone working with this technology. They are not strictly related to virus - receptor interactions.

The first section starts with one of the first experiments that was performed on the DRX^2 during this thesis. It was in close cooperation with Jörg Schenk of HybroTech GmbH. The idea was to measure the binding of an antibody to the fluorophore on the DNA strand. The antibody was expected to inhibit the fluorescence quenching at the gold surface. HybroTech GmbH developed the antibody.

The second section includes the results of a work performed for Dr. Nenad Gajovic-Eichelmann of Fraunhofer IZI-BB, who was interested in binding rates of an antibody towards small molecules, namely ferrocene and its derivatives. While the experiments in themselves did not produce the desired binding rate constants, the issues that arose are presented here as they hold instructive value.

Both sections only include brief descriptions of the scientific background.

9.1 Tamra - antibody binding interaction

The antibody developed by HybroTech GmbH was supposed to inhibit fluorescence quenching of the fluorophore 5-Carboxytetramethylrhodamin, also called "5-Tamra" close to a gold surface. The effect of fluorescence quenching close to a gold surface creates the signal for measurements in the dynamic mode [41] (see also subsection 2.2). Quenching of the fluorescence signal in close proximity to the gold surface leads to a reduction of the light intensity that reaches the sensor according to the position of the fluorophore above the gold electrode. The antibody binds to the fluorescence molecule and inhibits, most likely through steric hindrance, an approach to the surface and therefore a reduction of the fluorescence signal. In order to examine this behavior and to show the effectiveness of the inhibited fluorescence quenching, the antibody was analyzed in the DRX^2 in the dynamic mode.

As the fluorophore is attached to the immobilized NL-B48 DNA strand, complementary DNA (cNL-B48) without any additional ligand was hybridized. Subsequently, the antibody with the name of G71-BE11 at eight different concentrations was injected. The results for the signal of “fluorescence down” can be seen in Figure 36. “Fluorescence down” is the minimal fluorescence signal during the phase, in which the DNA is in a position close to the surface.

The signal that was measured for the fluorescence down shows an increase for injections of higher concentrations ($c > 5$ µg mL^{-1}). The association showed a concentration dependent signal increase of the fluorescence down during the association and regained its original value during the dissociation. The dissociation showed an additional decrease for longer measurement times, that was the same for all concentrations. It is suspected that this was due to effects on the chip surface. It has been observed that the dynamic mode strains the surface more than the static mode. DNA strands can be damaged or detach

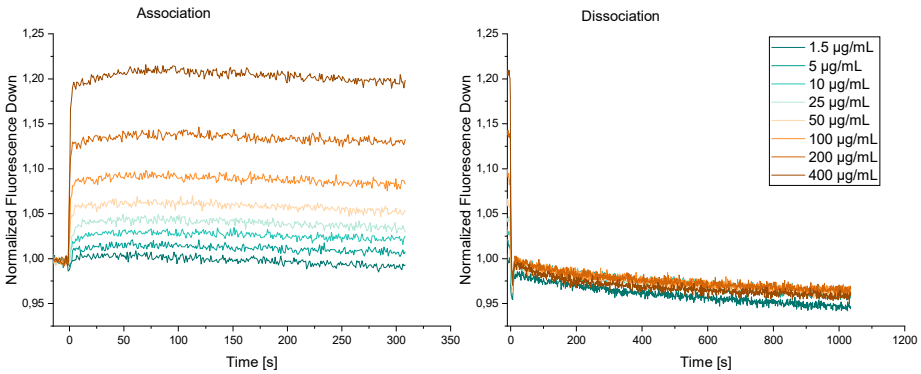

Figure 36: "Fluorescence down" signal for the various injections of G71-BE11. The signals are normalized. The effect is clearly visible as the fluorescence increases according to the concentration of injected antibody.

from the surface due to the mechanical stress of the constant switching motion. As can be seen in the resulting graph, the dissociation time could have been chosen shorter (around 100 s) as the dissociation occurs during the first 100 s of measurement time and the additional time only damages the sensor surface unnecessarily.

The interaction happened surprisingly fast. An exponential increase like for general binding interactions had been expected, but the results showed an almost stepwise signal increase for the association and the dissociation. The interaction could therefore be extremely fast, or there was some other effect taking place here.

A negative control with a different antibody in the same setup led to a decrease in "fluorescence up" and a decrease in "fluorescence down" upon antibody injection.

Generally, it was shown that the injection of the antibody led to an increase of the fluorescence, when the DNA is close to the chip surface. It remains unclear, what a useful application of this might be. Still, there is no publication known to the author that describes an antibody that has this effect.

9.2 Ferrocene - antibody binding interaction

During the work with Dr. Nenad Gajovic-Eichelmann from Fraunhofer IZI-BB, the binding strength of antibodies towards ferrocene (Fc) and its derivatives was supposed to be determined. Ferrocene is a small molecule ($Fe(C_5H_5)_2$). It is made up of two cyclopentadienyl rings and a central iron atom [149]. The antibody called BD10 developed by HybroTech GmbH, which is meant to bind ferrocene, was used as binding partner. The buffer chosen for the binding interaction measurement was AcP45Sal14. This was an acetate buffer at a pH of 4.5. The low pH value was chosen as it had been observed by Dr. Gajovic-Eichelmann that the binding of the antibody to ferrocene was only visible in

this acidic pH range. Additionally, the buffer included salt (salicylate) for stabilisation.

The buffer environment was originally thought to be problematic, since the DRX^2 is only recommended to be useable with buffers down to a pH value of 5 [150]. Originally, it was suspected that the buffer could be problematic for the chip surface and could lead to a loss of DNA strands on the gold surface. To exclude this, a "sizing" experiment of pure cNL-B48 DNA was performed with AcP45Sal14 as running buffer. If the buffer had an influence on the DNA strands on the sensor surface, this would have been visible in the multiple functionalizations of complementary DNA. This was not the case. Successive hybridizations of cNL-B48 on the sensor surface in AcP45Sal14 as running buffer were possible without an unusual decline in fluorescence amplitude or signal intensity. It was concluded that the AcP45Sal14 buffer was suitable for experiments in the DRX^2 even though its pH value was outside the recommended range.

The binding experiments included the immobilization of cNL-B48-BD10 and the subsequent observation of the interaction of Fc-PEG and Fc-BSA with the antibody. In both cases, the signal strength was weak and it was unclear, if a binding event had actually taken place. For Fc-BSA though, there might have been a weak binding signal.

It was suspected that a reversal of the assay might be beneficial for the signal strength and would reveal a binding. Therefore, Dr. Gajovic-Eichelmann coupled the small molecule (Fc) to cNL-B48. After immobilization of the conjugate, the antibody BD10 was injected as analyte. In this setup, the measured signal strength was extraordinarily strong upon association (see blue graph in Figure 37). Unfortunately, a negative control, in which pure cNL-B48 was immobilized, revealed that the effect was not a binding of the antibody to the ferrocene (graph not shown). The binding signal was similarly strong for cNL-B48 as ligand as for cNL-B48-Fc as ligand. The ferrocene did not influence the binding strength. It was suspected that the acetate buffer might be responsible. Apparently, the antibodies and/or proteins in general became positively charged in the AcP45 or AcP45Sal14 environment and "bound" to the negatively charged gold surface and the negatively charged double-stranded DNA. The binding was not visible at all in a PBS environment (grey graph Figure 37). The same curves were measured for various samples, which included three more monoclonal antibodies, from which two should not bind ferrocene at all as, well as for a bovine IgG sample and BSA. All samples showed strong "binding" in AcP45Sal14 or AcP45 and no binding in PBS.

Additionally, the interactions of the proteins with the chip could be reversed by injecting PBS buffer. After injection of PBS buffer, the signal strength was restored and the surface could be once again functionalized.

It is unclear, whether the coupling of ferrocene to cNL-B48 was successful. The coupling was not done by a standard coupling kit of DBS and no purification was performed. Therefore, it is also possible that the ligand molecule was not available for binding interaction during the experiments. The coupling of the ligand to the DNA is always a crucial step in the assay setup and can be problematic. Generally, it is advisable to validate correct coupling by some

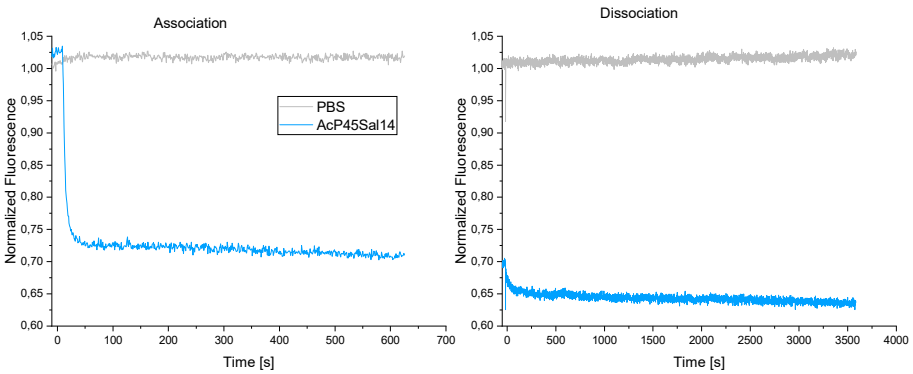

Figure 37: Injection of antibody BD10 in either AcP45Sal14 (blue curve) or PBS buffer (grey curve). cNL-B48 coupled to ferrocene was immobilized on the chip surface for both cases. It is clearly visible that the buffer influences the resulting signal strongly.

other method (e.g. check for binding in an ELISA after coupling).

Two lessons could be learned from the experiments. First, a pH of 4.5 is not per se harmful to the chip, the gold surface or the DNA. This AcP45Sal14 buffer and AcP45 (without Sal14, which was also tested) was usable multiple times without causing unusual reductions in fluorescence amplitudes.

Secondly, low pH environments can cause additional effects. Proteins can become positively charged. While this is not a new finding, it should be considered, when working with buffers of low pH value. This mistake can be avoided by checking for negative controls. The binding to pure DNA is a test that should always be performed as negative control for binding experiments with switchSENSE technology. Unspecific binding to the DNA or the sensor surface must always be excluded!

10 Reaction- vs. mass transport-limited kinetics

When performing binding interaction measurements, kinetics can be reaction-limited or mass transport-limited, depending on the experimental setup. Especially for the virus particles, which have a larger diameter ($\sim$ 120 nm for influenza A viruses [145]) compared to standard proteins ($\sim$ 10 nm [137]), this has to be taken into account. The theoretical considerations are therefore based on the experiments for X31 binding to DNA-PeB nanostructures. While exact calculations are complicated, there are possibilities to estimate, in which regime the measurements are taken. The theoretical calculations here are based on Squires et al. [151]. The results show that the parameters of the experiments enable the measurement of reaction-limited kinetics.

10.1 Calculations of reaction limited kinetics

The paper by Squires, Messinger and Manalis carries the title "Making it stick: convection, reaction and diffusion in surface-based biosensors" and was published in 2008 in the Journal "Nature Biotechnology" [151]. The described calculations can be applied to any kind of surface based biosensor that is used for the measurement of binding kinetics. The goal of the paper is to enable the scientists to develop a rough estimate of the regime, in which they are working. This includes the calculation of parameters like flux, collection rates and equilibration times. In this section, the calculations are described and directly applied to the measurements of X31 binding to DNA-PeB-nanostructures in the DRX^2 as described in subsections 4.1 and 7.1.

Many biosensors today, and the DRX^2 is no exception to this, use small amounts of sample at low concentrations. This is generally based on the intention to keep consumption of valuable samples at a minimum. The biosensors enable fast, sensitive and label-free analysis. Many utilize microfluidic geometries. The manuscript of Squires et al. helps to estimate, how long it takes molecules to reach the sensor surface, how many molecules actually bind to the ligands and how one can extract the parameters of a binding kinetic from the measured signals.

During the measurement process, different effects occur including diffusion and convection of molecules along with the solution in the microfluidic channel. The "random walk" describes the diffusion of the molecules. The displacement (s) from an origin grows with the square root of time (t): $s \sim \sqrt{t}$. The time it would take a molecule to diffuse across the length of a sensor surface therefore scales with the square of the distance.

Instead of describing single molecules, it is also possible to define a "concentration field" c, which represents the ensemble average of a collection of individual molecules stochastically.

10.1.1 General setup and parameters

In order to determine, if the parameters chosen for the X31-PeB binding measurements result in reaction limited kinetics, the Peclet number Pe_H, the shear Peclet number Pe_s and the Damköhler number Da are calculated.

The flux j_D is the number of molecules per area per time. The flux appears along a concentration gradient (∇c).

$$j_D = -D\nabla c \tag{5}$$

where D is the diffusion coefficient. Diffusion of analyte molecules towards the sensor surface and consequently a capture of these molecules by the ligands, lead to the formation of a depletion zone above the sensor surface.

Another important aspect is the flow of solution that is pumped along the microfluidic channel (convection). It can be described by the flow speed u, which depends on the flowrate Q, and the dimensions of the flow channel. Here we assume a rectangular channel geometry with a channel width W_c, a channel height H and then a variable height z in which the flow speed u is supposed to be calculated.

$$u(z) = \frac{6Q}{W_c H} z(H - z) \tag{6}$$

The flow speed u is dependent on the square of z. A sketch of the geometry of the biosensor can be seen in Figure 38. For further calculations, and to fit the theoretical model presented here, a rectangular sensor geometry is assumed. This is not strictly correct, as the gold electrodes of the DRX^2 are circular. However, it will be sufficient for this estimation. The side lengths of the supposed sensor are chosen to result in the same sensor surface area as the circular electrode with $L = W_s = 106.34\,\mu\mathrm{m}^2$. The height of the channel is $H = 60\,\mu\mathrm{m}$ and the width of the channel is $W_c = 1000\,\mu\mathrm{m}$.

Diffusion and convection are both present in the microfluidic channel, with diffusion generally dominating close to the sensor surface and convection generally dominating far away from the sensor. To account for both of them, the publication employs “matched and multiscale asymptotics”. The convection transports analyte molecules and counter balances the formation of the depletion zone.

10.1.2 Calculation of Peclet number

To estimate which regime, diffusion or convection, dominates for a specific case, the authors propose to calculate the Peclet number:

$$\frac{\text{diffusive time}}{\text{convective time}} \sim \frac{H^2/D}{H^2 W_c/Q} \sim \frac{Q}{DW_c} \equiv \mathrm{Pe}_H \tag{7}$$

If $\mathrm{Pe}_H \ll 1$, the diffusion regime dominates and the size of depletion zone is large compared to the channel. For the case in which $\mathrm{Pe}_H \gg 1$, the depletion zone is thinner than the channel. In order to determine the Peclet number

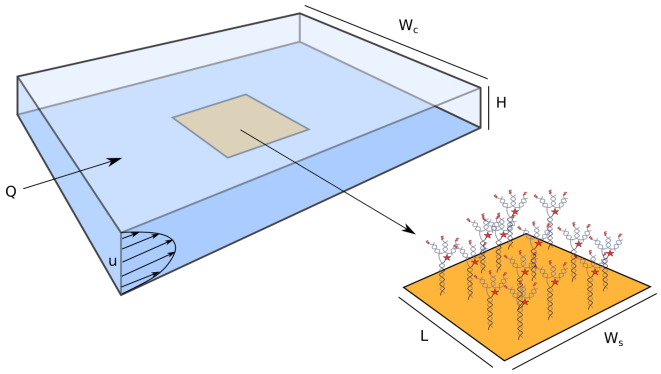

Figure 38: Schematic overview of the biosensor channel and the sensor surface. A square electrode is assumed in order to fit the theoretical model. The surface area of the gold electrode is the same for the chosen side length of the square and the actual circular electrode.

Pe_H for the X31 binding interaction measurements in the DRX^2, the individual values for Q, D and W_c are calculated.

For the diffusion coefficient D, the viscosity μ of the running buffer is required. PBS has a viscosity of $\mu = 0.000890\ \frac{Ns}{m^2}$ [152].

$$D = \frac{k_B T}{6\pi\mu R_0} \tag{8}$$

with k_B as the Boltzmann constant ($k_B = 1.38 \cdot 10^{-23}\ \frac{J}{K}$), T as the temperature ($T = 300\,\mathrm{K}$) and R_0 as the radius of the diffusing particles ($R_0(\mathrm{X31}) = 60\,\mathrm{nm}$). The value of R_0 is based on the average diameter $\emptyset = 2 \cdot R_0 = 120\,\mathrm{nm}$ of X31 virus particles [145]. Using these parameters, one can calculate a diffusion coefficient of:

$$D_{\mathrm{X31}} = 4.121\ \frac{\mu\mathrm{m}^2}{\mathrm{s}}$$

The flow rate generally chosen for association measurements was

$$Q = 1\ \frac{\mu\mathrm{L}}{\mathrm{min}} = 16.67 \cdot 10^6\ \frac{\mu\mathrm{m}^3}{\mathrm{s}}$$

Using these values, the Peclet number can be calculated.

$$\mathrm{Pe}_H = \frac{Q}{W_c D} = \frac{16.67 \cdot 10^6\ \frac{\mu\mathrm{m}^3}{s}}{1000\,\mu\mathrm{m} \cdot 4.121 \frac{\mu\mathrm{m}^2}{\mathrm{s}}} = 4.0 \cdot 10^3 \gg 1 \tag{9}$$

The resulting Peclet number is three orders of magnitude larger than 1. According to the manuscript, this indicates that the depletion zone is thinner than the channel and diffusion does not dominate. This is already the case for flow rates as low as $Q = 1\ \frac{\mu\mathrm{L}}{\mathrm{min}}$.

10.1.3 Calculation of the shear Peclet number

Furthermore, the so-called "shear Peclet number" Pe_s can be calculated. It indicates whether the depletion zone is large or small compared to the sensor surface.

$$\mathrm{Pe}_s = 6\lambda \mathrm{Pe}_H = 6\frac{L}{H}\mathrm{Pe}_H = 4.2 \cdot 10^4 \gg 1 \tag{10}$$

The shear Peclet number is much greater than 1. This indicates that the depletion zone is small as compared to the sensor. This is another indication that the diffusion regime does not dominate.

In a next step, the dimensionless flux $\mathscr{F}$ and the depletion zone δ are calculated.

$$\delta \sim L/Pe_s^{\frac{1}{3}} \sim \frac{106.34\,\mu\mathrm{m}}{(4.2 \cdot 10^4)^{\frac{1}{3}}} = 3.06\,\mu\mathrm{m} \tag{11}$$

$$\mathscr{F} \approx 0,81 \cdot (Pe_s)^{\frac{1}{3}} + 0,71 \cdot (Pe_s)^{-\frac{1}{6}} - 0,2 \cdot (Pe_s)^{-\frac{1}{3}} \approx 28.27 \tag{12}$$

From this the collection rate J_D is calculated

$$J_D = Dc_0 W_s \mathscr{F} \tag{13}$$

using

$$c_0 = 250\,\mathrm{pM} = 0,15\,\frac{\mathrm{molecules}}{\mu\mathrm{m}^3} \tag{14}$$

$$1\,mol = 6,023 \cdot 10^{23}\mathrm{molecules} \tag{15}$$

$$1\,pmol = 6,023 \cdot 10^{11}\,\mathrm{molecules} \tag{16}$$

$$1\,L = 10^{15}\,\mu\mathrm{m}^3 \tag{17}$$

We find a collection rate of:

$$J_D = 4.121\,\frac{\mu\mathrm{m}^2}{s} \cdot 0,15\,\frac{\mathrm{molecules}}{\mu\mathrm{m}^3} \cdot 106.34\,\mu\mathrm{m} \cdot 28.27 = 1858\,\frac{\mathrm{molecules}}{\mathrm{s}} \tag{18}$$

The manuscript shows how the reaction limit can be calculated. It is necessary to estimate the association and dissociation rate constants $\mathrm{k_{on}}$ and $\mathrm{k_{off}}$ and the dissociation constant $\mathrm{K_D}$. For this calculation, the value for $\mathrm{K_D} = 1\,\mu\mathrm{M}$ is estimated. This is most likely a underestimation of the binding affinity of X31 to ss3PeB. In view of the calculation for these specific experiments though, an underestimation is reasonable, as it can show whether the results were measured in the reaction-limited regime. The value for $\mathrm{k_{off}} = 1.5 \cdot 10^{-4}\,\frac{1}{\mathrm{s}}$ is taken from Memczak et al. [61]. From these two values, one finds a value for $\mathrm{k_{on}}$:

$$\mathrm{k_{on}} = \frac{\mathrm{k_{off}}}{\mathrm{K_D}} = 150\,\frac{1}{\mathrm{Ms}} \tag{19}$$

With the values of the binding rate constants, it is possible to determine the critical concentration c^*. At the critical concetration, one molecule binds to the sensor surface in equilibrium on average. The concentration for the binding affinity measurements should lie above this value.

$$c^* = K_D/N_R \tag{20}$$

where N_R is the number of binding sites on the sensor. In the case of the DRX^2, this value is given at around $N_R = 1{\cdot}10^6$ DNA nanolevers on one gold electrode. For the critical concentration, this results in:

$$c^* = 1\,\mu\mathrm{M}\,/1 \cdot 10^6 = 1\,\mathrm{pM}$$

The lowest concentration used in the experiments was around $c_0 = 250\,\mathrm{pM}$, which is 250 times larger than the critical concentration. From this, it is possible to calculate the number of molecules that bind to the sensor surface in equilibrium on average.

$$N_R^B = N_R c_0/K_D = \frac{1 \cdot 10^6 \cdot 250 \cdot 10^{-12}\mathrm{M}}{1 \cdot 10^{-6}\mathrm{M}} = 250 \tag{21}$$

Therefore, it is expected that 250 virus particles bind to one electrode in equilibrium on average. This is independent of how the system reaches the equilibrium.

10.1.4 Calculation of the Damköhler number

Furthermore, the Damköhler number is calculated. It is an indication of how the system reaches the equilibrium and whether this happens in the diffusion or the reaction-limited regime. For this calculation, $\mathrm{k_{on}} = 150\ \frac{1}{\mathrm{Ms}} = 2.49 \cdot 10^{-7} \frac{\mu\mathrm{m}^3}{\mathrm{molecules{\cdot}s}}$ is used again. Another necessary parameter is the density of binding sites:

$$b_m = \frac{N_R}{L \cdot W_s} = \frac{1 \cdot 10^6}{106.34\,\mu\mathrm{m} \cdot 106.34\,\mu\mathrm{m}} = 88.43\,\frac{\mathrm{molecules}}{\mu\mathrm{m}^2} \tag{22}$$

Using these values, the Damköhler number Da is calculated as follows:

$$\mathrm{Da} = \frac{\mathrm{k_{on}} b_m \delta}{D} = \frac{2.49 \cdot 10^{-7} \frac{\mu\mathrm{m}^3}{\mathrm{molecules{\cdot}s}} \cdot 88.43 \frac{\mathrm{molecules}}{\mu\mathrm{m}^2} \cdot 3.06\mu\mathrm{m}}{4.121 \frac{\mu\mathrm{m}^2}{s}} = 1.63{\cdot}10^{-5} \ll 1 \tag{23}$$

The Damköhler number is much smaller than 1. This is an indication for a reaction-limited kinetic.

10.1.5 Discussion

All calculations indicate that the measurements were in fact performed in the reaction-limited regime. The Peclet number Pe_H is much greater than 1, which

shows that the depletion zone is thinner than the channel. The shear Peclet number is much greater than 1, which indicates that the depletion zone is smaller than the sensor. Both of these results prove that the zone in which diffusion dominates is small as compared to the channel and the sensor.

The lowest concentration chosen for the experiments (250 pM $\cong$10 µg mL^{-1}) is still 250 times larger than the critical concentration c^*. The calculation of the Damköhler number proves that during the process of reaching equilibrium, the system is operating in the reaction-limited regime. Since it is unclear, whether the system actually reaches equilibrium during the association measurements of X31 binding to PeB, this finding might be the most relevant. The approximated values used for the calculations like for K_D are conservative estimates.

Part IV
Conclusion and outlook

The results of this thesis include primarily the investigation of viruses interacting with receptor proteins. Influenza A virus material was investigated with regard to its binding behavior towards peptides using the electrically controllable DNA nanolevers of the switchSENSE technology. Binding was measureable and distinguishable from negative controls. The association of virus material to the peptides on the sensor surface led to signal changes in the fluorescence intensity. Dissociation signals were weak and difficult to observe due to the strong multivalent binding of virus particles to multiple peptide-DNA structures. This binding behavior was in accordance with expectations and literature. The technology allowed for reversible variations of surface densities of ligands, which enabled the investigation of dissociation rate constants. While this process was promising, it would require further experiments in order to optimize the ratio of sufficient signal strength to the least possible amount of ligands on the surface. Furthermore, additional effects like the reduction of available DNA strands on the sensor surface due to degeneration of the chip surface must be taken into account. A quantitative analysis of the signal strength with regard to the amount of DNA on the surface would be desirable. Furthermore, the model system of influenza A was used for variations of viral subtypes, measurement temperature and peptide sequence. In order to quantify the influence of the trimeric peptide presentation on DNA nanostructures, a sandwich assay was developed, in which the viruses were first immobilized and then binding of fluorescently labeled DNA-peptide structures was quantified. It was possible to distinguish between the number of peptides per nanostructure, although experiment specific effects have to be considered. This approach, when optimized, could be the way to quantify the oligovalent interaction between the homotrimeric surface protein hemagglutinin on the viral surface and the peptide PeB on the DNA nanostructure. It could be a way to investigate not only various peptides, but also to actually quantify the influence of the scaffold on the binding strength of this oligovalent binding interaction. One could for instance vary the distance between the peptides, which could be easily increased or decreased with the arm length of the DNA structure. The flexibility of the scaffold could be altered by including additional segments of single-stranded DNA in the structure design. Additionally, the influence of the chemical linker between the DNA scaffold and the peptide still remains to be quantified.

The work on SARS-CoV-2 was primarily started due to the outbreak of the pandemic. The experience with influenza had proven that the switchSENSE technology is suitable for the measurement of virus-receptor interactions. Firstly, the interaction between recombinant spike proteins and a peptide on a DNA structure was investigated. The results showed that some full-length proteins bind strongly to the peptide, while sub fragments and full-length proteins that were altered in their amino acid sequence showed no binding. Triva-

lent and monovalent peptide presentations on DNA structures were compared with regard to their binding affinity to recombinant protein. The effect of multivalent binding became quantifiable. Additionally, the binding of the peptide on the DNA scaffold to inactivated SARS-CoV-2 as well as SARS-CoV-2 pseudo viruses could be shown. In the case of pseudo virus particles, signal variations were observable for SARS-CoV-2 variants. These results were purely qualitative and they should be treated carefully, as many aspects have to be considered while interpreting the results.

Six antibodies against the nucleocapsid protein of SARS-CoV-2 were characterized using the switchSENSE technology. Individual affinities were quantified. The characterization was part of the development process of an antigen rapid test point-of-care device, which now utilizes two of the antibodies. In this work, the antibodies were immobilized on the sensor surface and binding to proteins as well as binding to inactivated virus material was measured.

Furthermore, varying virus types showed the broad applicability of the switchSENSE technology to virus-receptor interactions. Adenoviruses and norovirus-like particles were investigated for their binding to antibodies, showing that also interactions of non-enveloped virus particles can be measured.

Additionally, the characteristic ability of the technology to oscillate electrically charged DNA levers and attached particles in order to determine hydrodynamic radii was applied to virus particles. According to the handbook, the technique was limited to sizing particles with a diameter of less than 14 nm. The results of the experiments with longer DNA nanolevers and X31 virus particles show that also larger particles are “switchable”. While the heterogeneous size distribution of influenza A virus particles and the application range of the underlying theoretical model did not allow for quantification of hydrodynamic radii of the attached virus particles, the results proved the general possibility of sizing particles larger than 14 nm.

As the technique was originally designed for protein - protein or protein - nucleotide interactions, the results of two additional small projects are presented. The first one involved an antibody that binds to the fluorophore attached to the double-stranded DNA on the sensor surface. The antibody was shown to inhibit the quenching effect of the gold surface that is normally used for the detection of the DNA’s position relative to the gold surface in the dynamic measurement mode. The second project involved the detection of a small molecule. While the detection was not possible, the measurements were very instructive. As the interaction required running buffer with a low pH value, it was detected that the measurement chips remained unharmed by the acetate buffer. Furthermore, the results showed that in this low pH environment unspecific binding of proteins to the sensor surface and the negatively charged DNA was extreme.

The final chapter includes a theoretical evaluation of the regime in which the virus-receptor kinetics were measured. It could be shown that the measurements were in fact reaction-limited and not mass transport-limited. All values calculated from the model of Squires et al. support this statement.

The applicability of switchSENSE technology to characterize virus-receptor interactions was demonstrated. The analyte as well as the receptor structures

were varied to prove the broad spectrum of measureable interactions. Enveloped and non-enveloped viruses, virus-like particles, pseudo viruses and viral proteins were used as analyte. As ligands, peptides coupled to specifically designed DNA nanostructures, antibodies or proteins were utilized. Affinities for different peptides could be distinguished as well as variations of subtypes of viruses binding to one peptide. The DNA nanostructure allowed for the presentation of various numbers of peptides and the quantification of oligovalent binding interactions. Further refinements of these experiments including variations to the DNA structure could enable deeper understanding of this complex binding process. The reproducibility of the results as well as data analysis and interpretation can be optimized, but are a common problem for any experimental binding affinity measurement technology on biological samples.

The challenges that remain in the investigation of binding interactions of biological molecules in general and multivalent binding in particular require all three natural sciences. Preparation of reliable and stable biological samples is critical and requires deep biological understanding. The question which coupling strategy of a protein to the DNA structure is optimal and the execution of these coupling processes requires chemical expertise. The experimental procedures performed using the instrument and the subsequent data analysis and interpretation pose mathematical and physical questions.

Overall, it could be shown that the electrically controllable DNA nanolevers as used in this technology are well suited for interaction measurements of viruses and receptors. While challenges remain that have to be addressed further, the general applicability has been shown. The inherent characteristics of the technology enable the investigation of oligovalent binding interactions, as could be shown for example in the sandwich experiments for influenza A and the binding of the trivalent and monovalent peptide-DNA structure to SARS-CoV-2 spike protein. These experiments prove the possibilities that are inherent in this technology and in its combination with DNA origami structures for experimental investigation of oligovalent binding interactions.

Part V
Appendix

10.2 Cell culture medium injection and signal change

During multiple projects, samples were delivered in cell culture medium. According to the handbook of the DRX^2, it is possible to utilize cell lysate, but it advises to keep the concentration as low as possible [150]. Some virus samples were delivered in cell culture medium. A transfer to buffer would have been possible, but would have included the risk of losing precious virus sample. Therefore, it was favorable to test the influence of the cell culture medium on the chip and the device. For these experiments, cNL-B48 was immobilized on the sensor surface and cell medium was injected as "analyte" at various concentrations. Gibco Roswell Park Memorial Institute (RPMI) 1640 Medium (Thermo Fisher Scientific) was diluted in PE140 buffer. The results can be seen in Figure 39.

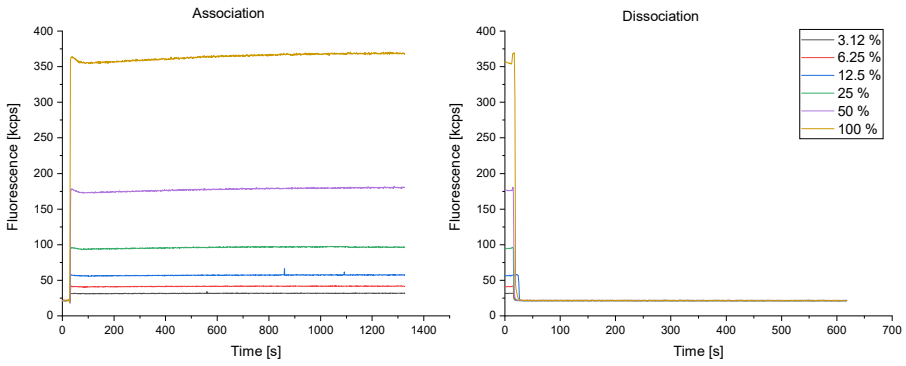

Figure 39: Fluorescence signal for the injection of RPMI cell medium at various concentrations. The cell medium was diluted in PE140 buffer, which was also used as running buffer.

As can be seen in the results, the injection of the cell culture medium led to an increase in fluorescence intensity during the association. The increase is dependent on the concentration. A high concentration of RPMI led to a strong signal change upon injection. The effect is reversed for the dissociation. As soon as the running buffer replaces the cell culture medium, the signal is restored to its original value. It does not seem to impair the chip as the signal does not decrease as compared to the original value. With the exception of 100% cell culture medium, all association graphs seem to be stable over the measurement time of around 1300 s. This means that any potential binding curve might be visible even in cell culture medium, when the background is subtracted. For the case of 100% cell culture medium, a slight signal increase is visible for the time $t > 100$ s. A small dip in signal is visible for the three highest concentrations

(25%, 50% and 100%) right after the stepwise increase ($30\,\mathrm{s} \leq t < 70\,\mathrm{s}$). These characteristics would have to be considered in the case of an analyte binding to a ligand in cell culture medium.

Generally, it seems like the use of cell culture medium is possible. The effect on the fluorescence signal is strong but stable especially for concentrations of less than 25% medium.

One could avoid the step-wise signal change that is shown here, if cell culture medium at the needed concentration was used as running buffer. This was not performed here.

10.3 Cell-free protein production

During the work on binding interactions between SARS-CoV-2 spike protein and the SBP1 peptide, a couple of experiments were performed with spike proteins from so-called "cell-free protein production". The proteins were produced by Franziska Ramm from Fraunhofer IZI-BB. The protein fragments that were investigated were RBD, S1 and the full-length protein. Cell free protein production can be performed on the basis of various cell types (e.g. CHO or human cell lines) [153, 154].

The original idea was to determine, whether proteins from the cell free production were suitable for binding interaction measurements in the DRX^2. Therefore, various cell lysates and spike proteins were tested. The result might also be valuable for any future work with cell free proteins and switchSENSE technology.

It was found that many of the samples attacked the chip surface strongly and led to a loss of DNA levers on the surface. This was visible by a significant decrease up to complete loss of fluorescence amplitude during status tests.

The DNA degeneration is visible during kinetics measurements as a decrease in fluorescence signal that can be easily misinterpreted as a binding signal.

However, binding might have happened nontheless. This was revealed by a sizing measurement that showed that the switching speed of the DNA nanolever was reduced after association of spike protein (see Batch MF in Figure 40).

The difference between the DNA nanostructure prior to and after association of the spike protein was an indication for a binding event.

The fact that the cell lysate damaged the DNA strands on the chip surface could be explained by residual enzymes that digest DNA (e.g. nucleases). It is possible that not all of them were removed during the purification processes of the sample. Residues of these enzymes are extremely problematic for the switchSENSE technology, as they result in a signal decrease during association that can be falsely interpreted as a binding event. Additionally, the utilized sensor surfaces quickly become unusable. In order to utilize proteins from the cell-free protein production, this obstacle of chip surface degeneration would have to be overcome. Other than that, the sizing measurement shown in Figure 40 indicate that a binding event can be measured also between a ligand and a protein that was produced cell-free.

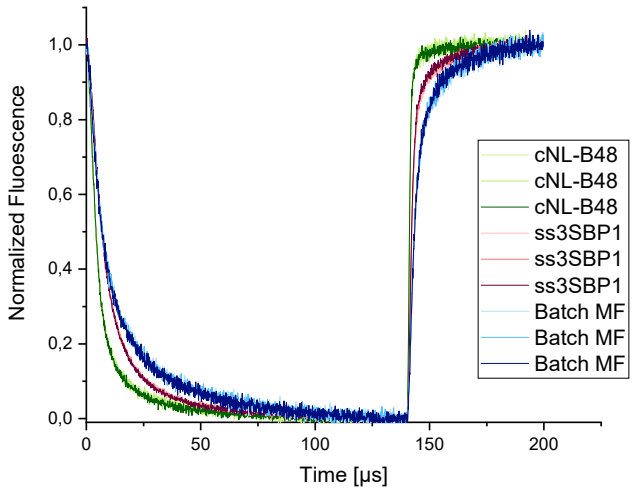

Figure 40: Sizing measurement of pure DNA (cNL-B48, green graphs), after functionalization with the DNA nanostructure carrying three peptides (ss3SBP1, red graphs) and after the association of spike protein form cell free protein production (Batch MF, blue graphs). The slowing of the DNA motion after association of spike protein indicated that a binding had actually taken place. All sizing measurements were performed on three electrodes.

References

[1] Werner Müller-Esterl. *Biochemie*. Springer Berlin Heidelberg, 2018.

[2] Jane Flint, Anna Marie Skalka, Glenn F. Rall, and Vincent R. Racaniello. *Principles of Virology, Volume I: Molecular Biology*. American Society of Microbiology, jan 2015.

[3] Markus Linnemann. *Biochemie fur Mediziner ein Lern- und Arbeitsbuch mit klinischem Bezug mit 186 Tabellen*. Springer, Berlin Heidelberg, 2005.

[4] Jeremy M. Berg, John L. Tymoczko, Gregory J. Gatto, and Lubert Stryer. *Stryer Biochemie*. Springer Berlin Heidelberg, 2018.

[5] Daniel Zuckerman. *Statistical physics of biomolecules an introduction*. CRC Press Taylor and Francis, Boca Raton, FL, 2010.

[6] Weina Ma, Liu Yang, and Langchong He. Overview of the detection methods for equilibrium dissociation constant KD of drug-receptor interaction. *Journal of Pharmaceutical Analysis*, 8(3):147–152, jun 2018.

[7] Thomas D. Pollard. A guide to simple and informative binding assays. *Molecular Biology of the Cell*, 21(23):4061–4067, dec 2010.

[8] Haidong Wang, Katherine R Paulson, Spencer A Pease, Stefanie Watson, Haley Comfort, Peng Zheng, Aleksandr Y Aravkin, Catherine Bisignano, Ryan M Barber, Tahiya Alam, John E Fuller, Erin A May, Darwin Phan Jones, Meghan E Frisch, Cristiana Abbafati, Christopher Adolph, Adrien Allorant, Joanne O Amlag, Bree Bang-Jensen, Gregory J Bertolacci, Sabina S Bloom, Austin Carter, Emma Castro, Suman Chakrabarti, Jhilik Chattopadhyay, Rebecca M Cogen, James K Collins, Kimberly Cooperrider, Xiaochen Dai, William James Dangel, Farah Daoud, Carolyn Dapper, Amanda Deen, Bruce B Duncan, Megan Erickson, Samuel B Ewald, Tatiana Fedosseeva, Alize J Ferrari, Joseph Jon Frostad, Nancy Fullman, John Gallagher, Amiran Gamkrelidze, Gaorui Guo, Jiawei He, Monika Helak, Nathaniel J Henry, Erin N Hulland, Bethany M Huntley, Maia Kereselidze, Alice Lazzar-Atwood, Kate E LeGrand, Akiaja Lindstrom, Emily Linebarger, Paulo A Lotufo, Rafael Lozano, Beatrice Magistro, Deborah Carvalho Malta, Johan Månsson, Ana M Mantilla Herrera, Fatima Marinho, Alemnesh H Mirkuzie, Awoke Temesgen Misganaw, Lorenzo Monasta, Paulami Naik, Shuhei Nomura, Edward G O'Brien, James Kevin O'Halloran, Latera Tesfaye Olana, Samuel M Ostroff, Louise Penberthy, Robert C Reiner Jr, Grace Reinke, Antonio Luiz P Ribeiro, Damian Francesco Santomauro, Maria Inês Schmidt, David H Shaw, Brittney S Sheena, Aleksei Sholokhov, Natia Skhvitaridze, Reed J D Sorensen, Emma Elizabeth Spurlock, Ruri Syailendrawati, Roman Topor-Madry, Christopher E Troeger, Rebecca Walcott, Ally Walker, Charles Shey Wiysonge, Nahom Alemseged Worku, Bethany Zigler, David M Pigott,

Mohsen Naghavi, Ali H Mokdad, Stephen S Lim, Simon I Hay, Emmanuela Gakidou, and Christopher J L Murray. Estimating excess mortality due to the COVID-19 pandemic: a systematic analysis of COVID-19-related mortality, 2020 to 21. *The Lancet*, mar 2022.

[9] Arnold S. Monto and Robert G. Webster. *Influenza pandemics: history and lessons learned*, chapter 2, pages 20–33. John Wiley and Sons, second edition, 2013.

[10] Daniel B. Jernigan and Nancy J. Cox. *Human influenza: one health, one world*, chapter 1, pages 3–19. John Wiley and Sons, second edition, 2013.

[11] Susanne Modrow. *Molekulare Virologie*. Spektrum Akademischer Verlag, Heidelberg, 2010.

[12] Rebecca L. Rich and David G. Myszka. Survey of the year 2007 commercial optical biosensor literature. *Journal of Molecular Recognition*, 21(6):355–400, nov 2008.

[13] Jurriaan Huskens, Alart Mulder, Tommaso Auletta, Christian A. Nijhuis, Manon J. W. Ludden, and David N. Reinhoudt. A model for describing the thermodynamics of multivalent host-guest interactions at interfaces. *Journal of the American Chemical Society*, 126(21):6784–6797, may 2004.

[14] Susanne Liese and Roland R. Netz. Quantitative prediction of multivalent ligand–receptor binding affinities for influenza, cholera, and anthrax inhibition. *ACS Nano*, 12(5):4140–4147, feb 2018.

[15] Daniel Lauster, Maria Glanz, Markus Bardua, Kai Ludwig, Markus Hellmund, Ute Hoffmann, Alf Hamann, Christoph Böttcher, Rainer Haag, Christian P. R. Hackenberger, and Andreas Herrmann. Multivalent peptide-nanoparticle conjugates for influenza-virus inhibition. *Angewandte Chemie International Edition*, 56(21):5931–5936, apr 2017.

[16] Andreas Langer, Paul A. Hampel, Wolfgang Kaiser, Jelena Knezevic, Thomas Welte, Valentina Villa, Makiko Maruyama, Matej Svejda, Simone Jähner, Frank Fischer, Ralf Strasser, and Ulrich Rant. Protein analysis by time-resolved measurements with an electro-switchable DNA chip. *Nature Communications*, 4(1), jul 2013.

[17] Christin Möser, Jessica Lorenz, Martin Sajfutdinow, and David Smith. Pinpointed stimulation of EphA2 receptors via DNA-templated oligovalence. *International Journal of Molecular Sciences*, 19(11):3482, nov 2018.

[18] David M. Smith, Jessica S. Lorenz, Christin Möser, Jasmin Fertey, Walter Stöcklein, Andreas Herrmann, and Daniel Lauster. Nanostructure with a nucleic acid scaffold and virus-binding peptide moieties, 2018.

[19] David M. Smith, Christin Möser, Thomas Grunwald, Leila Mail, Christian Jäger, Martin Kleinschmidt, Daniel Ramsbeck, and Mirko Buchholz. Biological and synthetic molecules inhibiting respiratory syncytial virus infection, 2020.

[20] Chun-Wa Chung and Peter N. Lowe. *Biophysical Methods Mechanism of Action studies*, chapter 7, pages 155–199. Springer, 2007.

[21] Horst Bannwarth, Bruno P. Kremer, and Andreas Schulz. *Basiswissen Physik, Chemie und Biochemie*. Springer Berlin Heidelberg, 2013.

[22] Wolfgang Demtröder. *Experimentalphysik 2*. Springer Berlin Heidelberg, Berlin, 2009.

[23] Hanna Müller-Landau and Paloma Fernández Varela. Standard operation procedure for switchSENSE DRX systems. *European Biophysics Journal*, 50(3-4):389–400, mar 2021.

[24] James A. Goodrich and Jennifer F. Kugel. *Binding and Kinetics for Molecular Biologists*. John Inglis, Cold Spring Harbor, N.Y, 2006.

[25] Noelia Ferruz and Gianni De Fabritiis. Binding kinetics in drug discovery. *Molecular Informatics*, 35(6-7):216–226, may 2016.

[26] Albert C. Pan, David W. Borhani, Ron O. Dror, and David E. Shaw. Molecular determinants of drug–receptor binding kinetics. *Drug Discovery Today*, 18(13-14):667–673, jul 2013.

[27] Jurriaan Huskens. *Models and Methods in Multivalent Systems*, chapter 2, pages 23–75. John Wiley and Sons, 2017.

[28] Vijay M. Krishnamurthy, Lara A. Estroff, and George M. Whitesides. *Multivalency in Ligand Design*, chapter Chapter 2, pages 11–45. Wiley-VCH, Weinheim, 2006.

[29] Sumati Bhatia, Benjamin Ziem, and Rainer Haag. *Blocking Pathogens by Multivalent Inhibitors*, chapter 9, pages 207–224. Wiley and Sons Ltd, 2018.

[30] Susanne Liese and Roland R Netz. Influence of length and flexibility of spacers on the binding affinity of divalent ligands. *Beilstein Journal of Organic Chemistry*, 11:804–816, may 2015.

[31] Miguel A. Soler and Sara Fortuna. Influence of linker flexibility on the binding affinity of bidentate binders. *The Journal of Physical Chemistry B*, 121(16):3918–3924, apr 2017.

[32] Nicholas B. Tito, Stefano Angioletti-Uberti, and Daan Frenkel. Communication: Simple approach for calculating the binding free energy of a multivalent particle. *The Journal of Chemical Physics*, 144(16):161101, apr 2016.

[33] Marcus Weber, Alexander Bujotzek, and Rainer Haag. Quantifying the rebinding effect in multivalent chemical ligand-receptor systems. *The Journal of Chemical Physics*, 137(5):054111, aug 2012.

[34] Franziska Erlekam, Sinaida Igde, Susanna Röblitz, Laura Hartmann, and Marcus Weber. Modeling of multivalent ligand-receptor binding measured by kinITC. *Computation*, 7(3):46, aug 2019.

[35] D. J. Diestler and E. W. Knapp. Statistical thermodynamics of the stability of multivalent ligand-receptor complexes. *Physical Review Letters*, 100(17):178101, apr 2008.

[36] Pallavi Kiran, Sumati Bhatia, Daniel Lauster, Stevan Aleksić, Carsten Fleck, Natalija Peric, Wolfgang Maison, Susanne Liese, Bettina G. Keller, Andreas Herrmann, and Rainer Haag. Exploring rigid and flexible core trivalent sialosides for influenza virus inhibition. *Chemistry – A European Journal*, 24(72):19373–19385, nov 2018.

[37] Jason E. Gestwicki, Christopher W. Cairo, Laura E. Strong, Karolyn A. Oetjen, and Laura L. Kiessling. Influencing receptor-ligand binding mechanisms with multivalent ligand architecture. *Journal of the American Chemical Society*, 124(50):14922–14933, nov 2002.

[38] Victor Bandlow, Susanne Liese, Daniel Lauster, Kai Ludwig, Roland R. Netz, Andreas Herrmann, and Oliver Seitz. Spatial screening of hemagglutinin on influenza a virus particles: Sialyl-LacNAc displays on DNA and PEG scaffolds reveal the requirements for bivalency enhanced interactions with weak monovalent binders. *Journal of the American Chemical Society*, 139(45):16389–16397, nov 2017.

[39] Ulrich Rant, Kenji Arinaga, Shozo Fujita, Naoki Yokoyama, Gerhard Abstreiter, and Marc Tornow. Dynamic electrical switching of DNA layers on a metal surface. *Nano Letters*, 4(12):2441–2445, nov 2004.

[40] Ulrich Rant, Kenji Arinaga, Shozo Fujita, Naoki Yokoyama, Gerhard Abstreiter, and Marc Tornow. Structural properties of oligonucleotide monolayers on gold surfaces probed by fluorescence investigations. *Langmuir*, 20(23):10086–10092, oct 2004.

[41] Ulrich Rant, Kenji Arinaga, Shozo Fujita, Naoki Yokoyama, Gerhard Abstreiter, and Marc Tornow. Electrical manipulation of oligonucleotides grafted to charged surfaces. *Organic & Biomolecular Chemistry*, 4(18):3448, 2006.

[42] Ulrich Rant, Kenji Arinaga, Marc Tornow, Yong Woon Kim, Roland R. Netz, Shozo Fujita, Naoki Yokoyama, and Gerhard Abstreiter. Dissimilar kinetic behavior of electrically manipulated single- and double-stranded DNA tethered to a gold surface. *Biophysical Journal*, 90(10):3666–3671, may 2006.

[43] Wolfgang Kaiser and Ulrich Rant. Conformations of end-tethered DNA molecules on gold surfaces: Influences of applied electric potential, electrolyte screening, and temperature. *Journal of the American Chemical Society*, 132(23):7935–7945, may 2010.

[44] Ulrich Rant, Kenji Arinaga, Simon Scherer, Erika Pringsheim, Shozo Fujita, Naoki Yokoyama, Marc Tornow, and Gerhard Abstreiter. Switchable DNA interfaces for the highly sensitive detection of label-free DNA targets. *Proceedings of the National Academy of Sciences*, 104(44):17364–17369, oct 2007.

[45] *The Immunoassay Handbook: Theory and Applications of Ligand Binding, Elisa and Related Techniques*. Elsevier Science & Technology, 2013.

[46] Jens Kurreck, Joachim W. Engels, and Friedrich Lottspeich, editors. *Bioanalytik*. Springer Berlin Heidelberg, December 2021.

[47] Xiaowei Guo. Surface plasmon resonance based biosensor technique: A review. *Journal of Biophotonics*, 5(7):483–501, mar 2012.

[48] Eric Helmerhorst, David J. Chandler, Matt Nussio, and Cyril D. Mamotte. Real-time and label-free bio-sensing of molecular interactions by surface plasmon resonance: A laboratory medicine perspective. *The Clinical Biochemist Reviews*, 33:161–173, November 2012.

[49] A. Langer, W. Kaiser, M. Svejda, P. Schwertler, and U. Rant. Molecular dynamics of DNA–protein conjugates on electrified surfaces: Solutions to the drift-diffusion equation. *The Journal of Physical Chemistry B*, 118(2):597–607, jan 2014.

[50] Eric Ennifar. Multi-approach benchmarking of macromolecular interactions. Conference Talk, 2021.

[51] Jose Luis Cuellar-Camacho, Sumati Bhatia, Valentin Reiter-Scherer, Daniel Lauster, Susanne Liese, Jürgen P. Rabe, Andreas Herrmann, and Rainer Haag. Quantification of multivalent interactions between sialic acid and influenza a virus spike proteins by single-molecule force spectroscopy. *Journal of the American Chemical Society*, 142(28):12181–12192, jun 2020.

[52] Matthias Müller, Daniel Lauster, Helen H. K. Wildenauer, Andreas Herrmann, and Stephan Block. Mobility-based quantification of multivalent virus-receptor interactions: New insights into influenza a virus binding mode. *Nano Letters*, 19(3):1875–1882, feb 2019.

[53] Christian Sigl, Elena M. Willner, Wouter Engelen, Jessica A. Kretzmann, Ken Sachenbacher, Anna Liedl, Fenna Kolbe, Florian Wilsch, S. Ali Aghvami, Ulrike Protzer, Michael F. Hagan, Seth Fraden, and Hendrik Dietz. Programmable icosahedral shell system for virus trapping. *Nature Materials*, 20(9):1281–1289, jun 2021.

[54] Clemens Schulte, Alice Solda, Sebastian Spänig, Nathan Adams, Ivana Bekic, Werner Streicher, Dominik Heider, Ralf Strasser, and Hans Maric. Multivalent binding kinetics resolved by fluorescence proximity sensing. apr 2022.

[55] Silvia Pavan and Federico Berti. Short peptides as biosensor transducers. *Analytical and Bioanalytical Chemistry*, 402(10):3055–3070, dec 2011.

[56] Burcu Ucar, Tayfun Acar, Pelin Pelit Arayici, Melis Sen, Serap Dermanand, and Zeynep Mustafaeva. *Peptide Synthesis*, chapter 2, pages 5–30. IntechOpen, dec 2019.

[57] Henry Memczak. *Entwicklung influenzabindender Peptide für die Biosensorik*. PhD thesis, University of Potsdam, 2014.

[58] Mathai Mammen, Seol-Ki Choi, and George M. Whitesides. Polyvalent interactions in biological systems: Implications for design and use of multivalent ligands and inhibitors. *Angewandte Chemie International Edition*, 37:2754–2794, 1998.

[59] Carlo Fasting, Christoph A. Schalley, Marcus Weber, Oliver Seitz, Stefan Hecht, Beate Koksch, Jens Dernedde, Christina Graf, Ernst-Walter Knapp, and Rainer Haag. Multivalenz als chemisches organisations- und wirkprinzip. *Angewandte Chemie*, 124(42):10622–10650, sep 2012.

[60] Jürgen Neumann. *Immunbiologie*. Springer Berlin Heidelberg, 2008.

[61] Henry Memczak, Daniel Lauster, Parimal Kar, Santiago Di Lella, Rudolf Volkmer, Volker Knecht, Andreas Herrmann, Eva Ehrentreich-Förster, Frank F. Bier, and Walter F. M. Stöcklein. Anti-hemagglutinin antibody derived lead peptides for inhibitors of influenza virus binding. *PLOS ONE*, 11(7):e0159074, jul 2016.

[62] Fuminori Sakurai, Masashi Tachibana, and Hiroyuki Mizuguchi. Adenovirus vector-based vaccine for infectious diseases. *Drug Metabolism and Pharmacokinetics*, 42:100432, feb 2022.

[63] WHO. Who coronavirus (covid-19) dashboard, August 2022. https://covid19.who.int/.

[64] https://www.bundestag.de/dokumente/textarchiv/2020/kw27-de-nachtragshaushaltsgesetz 701728. Nachtragshaushaltsgesetz.

[65] John J. Skehel and Don C. Wiley. Receptor binding and membrane fusion in virus entry: The influenza hemagglutinin. *Annual Review of Biochemistry*, 69(1):531–569, jun 2000.

[66] Debiprosad Nayak, Sakar Shivakoti, Rilwan A. Balogun, Gwendolyn Lee, and Hong Zhou. *Structure, disassembly, assembly and budding of influenza viruses*, chapter 3, pages 37–57. John Wiley & Sons, Ltd, 2013.

[67] Ilona Papp, Christian Sieben, Kai Ludwig, Meike Roskamp, Christoph Böttcher, Sabine Schlecht, Andreas Herrmann, and Rainer Haag. Inhibition of influenza virus infection by multivalent sialic-acid-functionalized gold nanoparticles. *Small*, 6(24):2900–2906, nov 2010.

[68] Dynamic Biosensors. *CK-NH2-1-B48 Amine Coupling Kit 1 for Proteins (> 5 kDa) Functionalization of 48mer nanolevers via amines (-NH2).* CK-NH2-1-B48.

[69] Greg T.Hermanson. Bioconjugate techniques. 2008.

[70] Dynamic Biosensors. https://www.dynamic-biosensors.com/reagents/.

[71] Dynamic Biosensors. *Technology Information DRX and DRX2 switchSENSE Analyzer*, 2017.

[72] Kenji Arinaga, Ulrich Rant, Jelena Knežević, Erika Pringsheim, Marc Tornow, Shozo Fujita, Gerhard Abstreiter, and Naoki Yokoyama. Controlling the surface density of DNA on gold by electrically induced desorption. *Biosensors and Bioelectronics*, 23(3):326–331, oct 2007.

[73] Marlen Kruse, Christin Möser, David M. Smith, Hanna Müller-Landau, Ulrich Rant, Ralph Hölzel, and Frank F. Bier. Measuring influenza a virus and peptide interaction using electrically controllable DNA nanolevers. *Advanced Materials Technologies*, page 2101141, oct 2021.

[74] Jessica S. Lorenz, Jörg Schnauß, Martin Glaser, Martin Sajfutdinow, Carsten Schuldt, Josef A. Käs, and David M. Smith. Synthetic transient crosslinks program the mechanics of soft, biopolymer-based materials. *Advanced Materials*, 30(13):1706092, feb 2018.

[75] Marlen Kruse, Basma Altattan, Eva-Maria Laux, Nico Grasse, Lars Heinig, Christin Möser, David M. Smith, and Ralph Hölzel. Characterization of binding interactions of SARS-CoV-2 spike protein and DNA-peptide nanostructures. *Scientific Reports*, 12(1), jul 2022.

[76] Julius Wiener, Daniel Kokotek, Simon Rosowski, Heiko Lickert, and Matthias Meier. Preparation of single- and double-oligonucleotide antibody conjugates and their application for protein analytics. *Scientific Reports*, 10(1), jan 2020.

[77] E Budowsky, E Friedman, N Zheleznova, and F Noskov. Principles of selective inactivation of viral genome. VI. inactivation of the infectivity of the influenza virus by the action of ß-propiolactone. *Vaccine*, 9(6):398–402, jun 1991.

[78] E.I. Budowsky, Yu.A. Smirnov, and S.F. Shenderovich. Principles of selective inactivation of viral genome. VIII. the influence of ß-propiolactone on immunogenic and protective activities of influenza virus. *Vaccine*, 11(3):343–348, jan 1993.

[79] Pierre Bonnafous, Marie-Claire Nicolaï, Jean-Christophe Taveau, Michel Chevalier, Fabienne Barrière, Julie Medina, Olivier Le Bihan, Olivier Adam, Frédéric Ronzon, and Olivier Lambert. Treatment of influenza virus with beta-propiolactone alters viral membrane fusion. *Biochimica et Biophysica Acta (BBA) - Biomembranes*, 1838(1):355–363, jan 2014.

[80] G. Zhang, S. Pomplun, A. R. Loftis, X. Tan, A. Loas, and B. L. Pentelute. The first-in-class peptide binder to the sars-cov-2 spike protein. *bioRxiv preprint*, mar 2020.

[81] Vincent C. C. Cheng, Kelvin K. W. To, Herman Tse, Ivan F. N. Hung, and Kwok-Yung Yuen. Two years after pandemic influenza a/2009/h1n1: What have we learned? *Clinical Microbiology Reviews*, 25(2):223–263, apr 2012.

[82] Natalie Pica and Peter Palese. Toward a universal influenza virus vaccine: prospects and challenges. *Annual Review of Medicine*, 64(1):189–202, jan 2013.

[83] Carole Henry, Anna-Karin E. Palm, Florian Krammer, and Patrick C. Wilson. From original antigenic sin to the universal influenza virus vaccine. *Trends in Immunology*, 39(1):70–79, jan 2018.

[84] Nicole M. Bouvier and Peter Palese. The biology of influenza viruses. *Vaccine*, 26:D49–D53, sep 2008.

[85] Chadi M. Saad-Roy, Nimalan Arinaminpathy, Ned S. Wingreen, Simon A. Levin, Joshua M. Akey, and Bryan T. Grenfell. Implications of localized charge for human influenza a h1n1 hemagglutinin evolution: Insights from deep mutational scans. *PLOS Computational Biology*, 16(6):e1007892, jun 2020.

[86] Darin K. Takemoto, John J. Skehel, and Don. C. Wiley. A surface plasmon resonance assay for the binding of influenza virus hemagglutinin to its sialic acid receptor. *Virology*, 217(2):452–458, mar 1996.

[87] Peter Schuck and Huaying Zhao. The role of mass transport limitation and surface heterogeneity in the biophysical characterization of macromolecular binding processes by SPR biosensing. pages 15–54, 2010.

[88] Chin Leong Lim, Chris Byrne, and Jason KW Lee. Human thermoregulation and measurement of body temperature in exercise and clinical settings. *Annals Academy of Medicine*, 37(4), April 2008.

[89] Shaylika Chauhan. Comprehensive review of coronavirus disease 2019 (COVID-19). *Biomedical Journal*, 43(4):334–340, aug 2020.

[90] Milad Haghani and Pegah Varamini. Temporal evolution, most influential studies and sleeping beauties of the coronavirus literature. *Scientometrics*, 126(8):7005–7050, jun 2021.

[91] Jun Lan, Jiwan Ge, Jinfang Yu, Sisi Shan, Huan Zhou, Shilong Fan, Qi Zhang, Xuanling Shi, Qisheng Wang, Linqi Zhang, and Xinquan Wang. Structure of the SARS-CoV-2 spike receptor-binding domain bound to the ACE2 receptor. *Nature*, 581(7807):215–220, mar 2020.

[92] Markus Hoffmann, Hannah Kleine-Weber, Simon Schroeder, Nadine Krüger, Tanja Herrler, Sandra Erichsen, Tobias S. Schiergens, Georg Herrler, Nai-Huei Wu, Andreas Nitsche, Marcel A. Müller, Christian Drosten, and Stefan Pöhlmann. SARS-CoV-2 cell entry depends on ACE2 and TMPRSS2 and is blocked by a clinically proven protease inhibitor. *Cell*, 181(2):271–280.e8, apr 2020.

[93] G. Zhang, S. Pomplun, A. R. Loftis, X. Tan, A. Loas, and B. L. Pentelute. Investigation of ACE2 n-terminal fragments binding to SARS-CoV-2 spike RBD. *bioRxiv preprint*, June 2020.

[94] Alexandra C. Walls, Young-Jun Park, M. Alejandra Tortorici, Abigail Wall, Andrew T. McGuire, and David Veesler. Structure, function, and antigenicity of the SARS-CoV-2 spike glycoprotein. *Cell*, 181(2):281–292.e6, apr 2020.

[95] Bryan A. Johnson, Xuping Xie, Adam L. Bailey, Birte Kalveram, Kumari G. Lokugamage, Antonio Muruato, Jing Zou, Xianwen Zhang, Terry Juelich, Jennifer K. Smith, Lihong Zhang, Nathen Bopp, Craig Schindewolf, Michelle Vu, Abigail Vanderheiden, Emma S. Winkler, Daniele Swetnam, Jessica A. Plante, Patricia Aguilar, Kenneth S. Plante, Vsevolod Popov, Benhur Lee, Scott C. Weaver, Mehul S. Suthar, Andrew L. Routh, Ping Ren, Zhiqiang Ku, Zhiqiang An, Kari Debbink, Michael S. Diamond, Pei-Yong Shi, Alexander N. Freiberg, and Vineet D. Menachery. Loss of furin cleavage site attenuates SARS-CoV-2 pathogenesis. *Nature*, 591(7849):293–299, jan 2021.

[96] Gary R Whittaker. SARS-CoV-2 spike and its adaptable furin cleavage site. *The Lancet Microbe*, 2(10):e488–e489, oct 2021.

[97] Thomas P. Peacock, Daniel H. Goldhill, Jie Zhou, Laury Baillon, Rebecca Frise, Olivia C. Swann, Ruthiran Kugathasan, Rebecca Penn, Jonathan C. Brown, Raul Y. Sanchez-David, Luca Braga, Maia Kavanagh Williamson, Jack A. Hassard, Ecco Staller, Brian Hanley, Michael Osborn, Mauro Giacca, Andrew D. Davidson, David A. Matthews, and Wendy S. Barclay. The furin cleavage site in the SARS-CoV-2 spike protein is required for transmission in ferrets. *Nature Microbiology*, 6(7):899–909, apr 2021.

[98] Michael Letko, Andrea Marzi, and Vincent Munster. Functional assessment of cell entry and receptor usage for SARS-CoV-2 and other lineage b betacoronaviruses. *Nature Microbiology*, 5(4):562–569, feb 2020.

[99] Antoni G. Wrobel, Donald J. Benton, Pengqi Xu, Chloë Roustan, Stephen R. Martin, Peter B. Rosenthal, John J. Skehel, and Steven J.

Gamblin. SARS-CoV-2 and bat RaTG13 spike glycoprotein structures inform on virus evolution and furin-cleavage effects. *Nature Structural & Molecular Biology*, 27(8):763–767, jul 2020.

[100] Yujia Alina Chan and Shing Hei Zhan. The emergence of the spike furin cleavage site in SARS-CoV-2. *Molecular Biology and Evolution*, 39(1), nov 2021.

[101] Xuhua Xia. Domains and functions of spike protein in SARS-cov-2 in the context of vaccine design. *Viruses*, 13(1):109, jan 2021.

[102] Ching-Lin Hsieh, Jory A. Goldsmith, Jeffrey M. Schaub, Andrea M. DiVenere, Hung-Che Kuo, Kamyab Javanmardi, Kevin C. Le, Daniel Wrapp, Alison G. Lee, Yutong Liu, Chia-Wei Chou, Patrick O. Byrne, Christy K. Hjorth, Nicole V. Johnson, John Ludes-Meyers, Annalee W. Nguyen, Juyeon Park, Nianshuang Wang, Dzifa Amengor, Jason J. Lavinder, Gregory C. Ippolito, Jennifer A. Maynard, Ilya J. Finkelstein, and Jason S. McLellan. Structure-based design of prefusion-stabilized SARS-CoV-2 spikes. *Science*, 369(6510):1501–1505, sep 2020.

[103] Jung Woo Park, Philip N.P. Lagniton, Yu Liu, and Ren-He Xu. mRNA vaccines for COVID-19: what, why and how. *International Journal of Biological Sciences*, 17(6):1446–1460, 2021.

[104] Mirza S. Baig, Manikandan Alagumuthu, Sajjan Rajpoot, and Uzma Saqib. Identification of a potential peptide inhibitor of SARS-CoV-2 targeting its entry into the host cells. *Drugs in R&D*, 20(3):161–169, jun 2020.

[105] Claudia R. Arbeitman, Pablo Rojas, Pedro Ojeda-May, and Martin E. Garcia. The SARS-CoV-2 spike protein is vulnerable to moderate electric fields. *Nature Communications*, 12(1), sep 2021.

[106] Victor Bandlow, Daniel Lauster, Kai Ludwig, Malte Hilsch, Valentin Reiter-Scherer, Christoph Böttcher, Jürgen Rabe, Andreas Herrmann, and Oliver Seitz. Sialyl-LacNAc-PNA-DNA concatamers by rolling circle amplification as multivalent inhibitors for influenza a virus particles. *ChemBioChem*, dec 2018.

[107] Steffen Klein, Mirko Cortese, Sophie L. Winter, Moritz Wachsmuth-Melm, Christopher J. Neufeldt, Berati Cerikan, Megan L. Stanifer, Steeve Boulant, Ralf Bartenschlager, and Petr Chlanda. SARS-CoV-2 structure and replication characterized by in situ cryo-electron tomography. *Nature Communications*, 11(1), nov 2020.

[108] Qi Xiang, Linhao Li, Jie Wu, Miao Tian, and Yang Fu. Application of pseudovirus system in the development of vaccine, antiviral-drugs, and neutralizing antibodies. *Microbiological Research*, 258:126993, may 2022.

[109] William T. Harvey, Alessandro M. Carabelli, Ben Jackson, Ravindra K. Gupta, Emma C. Thomson, Ewan M. Harrison, Catherine Ludden, Richard Reeve, Andrew Rambaut, Sharon J. Peacock, and David L. Robertson and. SARS-CoV-2 variants, spike mutations and immune escape. *Nature Reviews Microbiology*, 19(7):409–424, jun 2021.

[110] Chloe Rees-Spear, Luke Muir, Sarah A. Griffith, Judith Heaney, Yoann Aldon, Jonne L. Snitselaar, Peter Thomas, Carl Graham, Jeffrey Seow, Nayung Lee, Annachiara Rosa, Chloe Roustan, Catherine F. Houlihan, Rogier W. Sanders, Ravindra K. Gupta, Peter Cherepanov, Hans J. Stauss, Eleni Nastouli, Katie J. Doores, Marit J. van Gils, and Laura E. McCoy. The effect of spike mutations on SARS-CoV-2 neutralization. *Cell Reports*, 34(12):108890, mar 2021.

[111] Kaiming Tao, Philip L. Tzou, Janin Nouhin, Ravindra K. Gupta, Tulio de Oliveira, Sergei L. Kosakovsky Pond, Daniela Fera, and Robert W. Shafer. The biological and clinical significance of emerging SARS-CoV-2 variants. *Nature Reviews Genetics*, 22(12):757–773, sep 2021.

[112] Michael I Barton, Stuart A MacGowan, Mikhail A Kutuzov, Omer Dushek, Geoffrey John Barton, and P Anton van der Merwe. Effects of common mutations in the SARS-CoV-2 spike RBD and its ligand, the human ACE2 receptor on binding affinity and kinetics. *eLife*, 10, aug 2021.

[113] Muthukumar Ramanathan, Ian D Ferguson, Weili Miao, and Paul A Khavari. SARS-CoV-2 b.1.1.7 and b.1.351 spike variants bind human ACE2 with increased affinity. *The Lancet Infectious Diseases*, 21(8):1070, aug 2021.

[114] Shaolei Teng, Adebiyi Sobitan, Raina Rhoades, Dongxiao Liu, and Qiyi Tang. Systemic effects of missense mutations on SARS-CoV-2 spike glycoprotein stability and receptor-binding affinity. *Briefings in Bioinformatics*, 22(2):1239–1253, oct 2020.

[115] Erik Boehm, Ilona Kronig, Richard A. Neher, Isabella Eckerle, Pauline Vetter, and Laurent Kaiser. Novel SARS-CoV-2 variants: the pandemics within the pandemic. *Clinical Microbiology and Infection*, 27(8):1109–1117, aug 2021.

[116] Vipul Kumar, Jasdeep Singh, Seyed E. Hasnain, and Durai Sundar. Possible link between higher transmissibility of alpha, kappa and delta variants of SARS-CoV-2 and increased structural stability of its spike protein and hACE2 affinity. *International Journal of Molecular Sciences*, 22(17):9131, aug 2021.

[117] Hin Hark Gan, Alan Twaddle, Benoit Marchand, and Kristin C. Gunsalus. Structural modeling of the SARS-CoV-2 spike/human ACE2 complex interface can identify high-affinity variants associated with increased transmissibility. *Journal of Molecular Biology*, 433(15):167051, jul 2021.

[118] Jörg Schenk, Franziska Matyssek, and Burkhard Micheel. Interleukin 4 increases the antibody response against rubisco in mice. *in vivo*, 18:649–652, 2004.

[119] Jörg A. Schenk, Frank Sellrie, Volker Böttger, Astrid Menning, Walter F.M. Stöcklein, and Burkhard Micheel. Generation and application of a fluorescein-specific single chain antibody. *Biochimie*, 89(11):1304–1311, nov 2007.

[120] Barbara Kubickova, Jörg A. Schenk, Franziska Ramm, Kornelija Markuškienė, Jochen Reetz, Paul Dremsek, Paulius Lukas Tamosiunas, Laima Cepulyte, Hoai Anh Trinh, Johannes Scholz, Henry Memczak, Marc Hovestädt, René Ryll, Rasa Petraityte-Burneikiene, Victor M. Corman, Anika Andersson, Dietmar Becher, Martin H. Groschup, Stefan Kubick, Frank Sellrie, Reimar Johne, and Rainer G. Ulrich. A broadly cross-reactive monoclonal antibody against hepatitis e virus capsid antigen. *Applied Microbiology and Biotechnology*, 105(12):4957–4973, jun 2021.

[121] ImmunoGnost GmbH. *Immunognost SARS-CoV-2 Antigen Schnelltest (ImmunoGnost GmbH)*, November 2021. GI-IM-10101-25-05.

[122] Weihong Zeng, Guangfeng Liu, Huan Ma, Dan Zhao, Yunru Yang, Muziying Liu, Ahmed Mohammed, Changcheng Zhao, Yun Yang, Jiajia Xie, Chengchao Ding, Xiaoling Ma, Jianping Weng, Yong Gao, Hongliang He, and Tengchuan Jin. Biochemical characterization of SARS-CoV-2 nucleocapsid protein. *Biochemical and Biophysical Research Communications*, 527(3):618–623, jun 2020.

[123] Tatsuma Yao and Yuta Asayama. Animal-cell culture media: History, characteristics, and current issues. *Reproductive Medicine and Biology*, 16(2):99–117, mar 2017.

[124] Zhiming Cheng, Erkin Kuru, Amit Sachdeva, and Marc Vendrell. Fluorescent amino acids as versatile building blocks for chemical biology. *Nature Reviews Chemistry*, 4(6):275–290, may 2020.

[125] Ralf Strasser, Dirk Scholl, Paul Hampel, Andreas Langer, and Ulrich Rant. Messung molekularer interaktion mit dynamischen oberflächensensoren. *BIOspektrum*, 18(7):724–726, nov 2012.

[126] Jimin Kim, Heungsup Sung, Hyukmin Lee, Jae-Seok Kim, Sue Shin, Seri Jeong, Miyoung Choi, and Hyeon-Jeong Lee and. Clinical performance of rapid and point-of-care antigen tests for SARS-CoV-2 variants of concern: A living systematic review and meta-analysis. *Viruses*, 14(7):1479, jul 2022.

[127] Tuna Toptan, Lisa Eckermann, Annika E. Pfeiffer, Sebastian Hoehl, Sandra Ciesek, Christian Drosten, and Victor M. Corman. Evaluation of a SARS-CoV-2 rapid antigen test: Potential to help reduce community spread? *Journal of Clinical Virology*, 135:104713, feb 2021.

[128] Victor M Corman, Verena Claudia Haage, Tobias Bleicker, Marie Luisa Schmidt, Barbara Mühlemann, Marta Zuchowski, Wendy K Jo, Patricia Tscheak, Elisabeth Möncke-Buchner, Marcel A Müller, Andi Krumbholz, Jan Felix Drexler, and Christian Drosten. Comparison of seven commercial SARS-CoV-2 rapid point-of-care antigen tests: a single-centre laboratory evaluation study. *The Lancet Microbe*, apr 2021.

[129] Andreas Osterman, Irina Badell, Elif Basara, Marcel Stern, Fabian Kriesel, Marwa Eletreby, Gamze Naz Öztan, Melanie Huber, Hanna Autenrieth, Ricarda Knabe, Patricia M. Späth, Maximilian Muenchhoff, Alexander Graf, Stefan Krebs, Helmut Blum, Jürgen Durner, Ludwig Czibere, Christopher Dächert, Lars Kaderali, Hanna-Mari Baldauf, and Oliver T. Keppler. Impaired detection of omicron by SARS-CoV-2 rapid antigen tests. *Medical Microbiology and Immunology*, 211(2-3):105–117, feb 2022.

[130] James S. Terry, Loran BR. Anderson, Michael S. Scherman, Carley E. McAlister, Rushika Perera, Tony Schountz, and Brian J. Geiss. Development of a SARS-CoV-2 nucleocapsid specific monoclonal antibody. *Virology*, 558:28–37, jun 2021.

[131] Yutaro Yamaoka, Kei Miyakawa, Sundararaj Stanleyraj Jeremiah, Rikako Funabashi, Koji Okudela, Sayaka Kikuchi, Junichi Katada, Atsuhiko Wada, Toshiki Takei, Mayuko Nishi, Kohei Shimizu, Hiroki Ozawa, Shuzo Usuku, Chiharu Kawakami, Nobuko Tanaka, Takeshi Morita, Hiroyuki Hayashi, Hideaki Mitsui, Keita Suzuki, Daisuke Aizawa, Yukihiro Yoshimura, Tomoyuki Miyazaki, Etsuko Yamazaki, Tadaki Suzuki, Hirokazu Kimura, Hideaki Shimizu, Nobuhiko Okabe, Hideki Hasegawa, and Akihide Ryo. Highly specific monoclonal antibodies and epitope identification against SARS-CoV-2 nucleocapsid protein for antigen detection tests. *Cell Reports Medicine*, 2(6):100311, jun 2021.

[132] Samir Andrade Mendonça, Reka Lorincz, Paul Boucher, and David T. Curiel. Adenoviral vector vaccine platforms in the SARS-CoV-2 pandemic. *npj Vaccines*, 6(1), aug 2021.

[133] Frank L. Graham and Ludvik Prevec. Methods for construction of adenovirus vectors. In *Molecular Biotechnology*. Humana Press Inc., 1995.

[134] X Danthinne and M J Imperiale. Production of first generation adenovirus vectors: a review. *Gene Therapy*, 7(20):1707–1714, oct 2000.

[135] Maria Bottermann, Heidrun Elisabeth Lode, Ruth E. Watkinson, Stian Foss, Inger Sandlie, Jan Terje Andersen, and Leo C. James. Antibody-antigen kinetics constrain intracellular humoral immunity. *Scientific Reports*, 6(1), nov 2016.

[136] Walter Doerfler. *Medical Microbiology*. The University of Texas Medical Branch at Galveston, 1996. Chapter 65 Norwalk and other Caliciviruses.

[137] Jörg Stetefeld, Sean A. McKenna, and Trushar R. Patel. Dynamic light scattering: a practical guide and applications in biomedical sciences. *Biophysical Reviews*, 8(4):409–427, oct 2016.

[138] Neil R. Blacklow. *Medical Microbiology*. The University of Texas Medical Branch at Galveston, 1996. Chapter 67.

[139] Elizabeth Robilotti, Stan Deresinski, and Benjamin A. Pinsky. Norovirus. *Clinical Microbiology Reviews*, 28(1):134–164, jan 2015.

[140] Christopher B. Buck, Patricia M. Day, and Benes L. Trus. The papillomavirus major capsid protein l1. *Virology*, 445(1-2):169–174, oct 2013.

[141] Christine M Thompson, Emma Petiot, Alaka Mullick, Marc G Aucoin, Olivier Henry, and Amine A Kamen. Critical assessment of influenza VLP production in sf9 and HEK293 expression systems. *BMC Biotechnology*, 15(1), may 2015.

[142] Ailar Sabbaghi, Seyed Mohammad Miri, Mohsen Keshavarz, Mohsen Zargar, and Amir Ghaemi. Inactivation methods for whole influenza vaccine production. *Reviews in Medical Virology*, 29(6), jul 2019.

[143] Moran Jerabek-Willemsen, Chistoph J. Wienken, Dieter Braun, Philipp Baaske, and Stefan Duhr. Molecular interaction studies using microscale thermophoresis. *ASSAY and Drug Development Technologies*, 9(4):342–353, aug 2011.

[144] Elliot L. Elson. Fluorescence correlation spectroscopy: Past, present, future. *Biophysical Journal*, 101(12):2855–2870, dec 2011.

[145] Audray Harris, Giovanni Cardone, Dennis C. Winkler, J. Bernard Heymann, Matthew Brecher, Judith M. White, and Alasdair C. Steven. Influenza virus pleiomorphy characterized by cryoelectron tomography. *Proceedings of the National Academy of Sciences*, 103(50):19123–19127, dec 2006.

[146] C.A. Knight. The stability of influenza virus in the presence of salts. *Journal of Experimental Medicine*, 79(3):285–290, mar 1944.

[147] F. Ross Hallett. Particle size analysis by dynamic light scattering. *Food Research International*, (27):195–198, 1994.

[148] Alexander V. Malm and Jason C. W. Corbett. Improved dynamic light scattering using an adaptive and statistically driven time resolved treatment of correlation data. *Scientific Reports*, 9(1), sep 2019.

[149] https://en.wikipedia.org/wiki/Ferrocene. Ferrocene, June 2022.

[150] Dynamic Biosensors. *DRX and DRX2 Technical Handbook*, 2017.

[151] Todd M Squires, Robert J Messinger, and Scott R Manalis. Making it stick: convection, reaction and diffusion in surface-based biosensors. *Nature Biotechnology*, 26(4):417–426, apr 2008.

[152] David R. Lide. *CRC Handbook of Chemistry and Physics*. CRC Press, Boca Raton, FL, 85 edition, 2005.

[153] Anne Zemella, Solveig Grossmann, Rita Sachse, Andrei Sonnabend, Michael Schaefer, and Stefan Kubick. Qualifying a eukaryotic cell-free system for fluorescence based GPCR analyses. *Scientific Reports*, 7(1), jun 2017.

[154] Franziska Ramm, Srujan Kumar Dondapati, Lena Thoring, Anne Zemella, Doreen Anja Wüstenhagen, Hendrik Frentzel, Marlitt Stech, and Stefan Kubick. Mammalian cell-free protein expression promotes the functional characterization of the tripartite non-hemolytic enterotoxin from bacillus cereus. *Scientific Reports*, 10(1), feb 2020.

Publications and presentations

Peer-reviewed journals

Marlen Kruse, Christin Möser, David M. Smith, Hanna Müller-Landau, Ulrich Rant, Ralph Hölzel, and Frank F. Bier. Measuring Influenza A Virus and Peptide Interaction Using Electrically Controllable DNA Nanolevers. *Advanced Materials Technologies*, October 2021.

Marlen Kruse, Basma Altattan, Eva-Maria Laux, Nico Grasse, Lars Heinig, Christin Möser, David M. Smith and Ralph Hölzel. Characterization of Binding Interactions of SARS-CoV-2 Spike Protein and DNA-peptide Nanostructures. *Scientific Reports*, July 2022.

Presentations

- Poster: **Marlen Kruse**, Sandra Stanke, Christian Warmt, Hanna Müller-Landau, Ralph Hölzel, Ulrich Rant and Frank F. Bier. Measuring Multivalent Interaction of Influenza A and Peptides Using Electronically Switchable DNA Nanolevers *European Biosensor Symposium*, Florence, Feb. 2019
- Talk: **Marlen Kruse**, Christin Möser, David M. Smith, Ralph Hölzel and Frank F. Bier. Applying switchSENSE technology to virus detection - an approach to probe multivalent binding interaction, *Dynamic Biosensors User Meeting*, Munich, June 2019
- Poster: **Marlen Kruse**, Christin Möser, Frank F. Bier, David M. Smith and Ralph Hölzel. Measuring Multivalent Interaction of Influenza A and Peptides Using Electronically Switchable DNA Nanolevers, *5th International Symposium of the Collaborative Reseach Centre SFB 765 "Multivalency in Chemistry and Biology"*, Berlin, Sept. 2019 (Best Poster Award)
- Poster: **Marlen Kruse**, Christin Möser, David M. Smith, Ralph Hölzel and Frank F. Bier. Towards Measuring Multivalent Binding Interactions: Binding of Viruses and Peptides on DNA-nanoconstructs *European Biosensor Symposium 2021*, online event, March 2021
- Talk: **Marlen Kruse**, Christin Möser, David M. Smith, Ralph Hölzel and Frank F. Bier. Chances and Challenges of SwitchSENSE Technology Applied to Virus – Receptor Interactions. *Dynamic Biosensors User Meeting*, Munich, Sept. 2021

Acknowledgement

I thank Professor Carsten Beta of the University of Potsdam for supervising this dissertation.

The content of this dissertation was produced at Fraunhofer Institute for Cell Therapy and Immunology, Branch Bioanalytics and Bioprocesses in Potsdam in the group of Dr. Ralph Hölzel.

I thank Dr. Ralph Hölzel for giving me the opportunity to work on this topic and for the supervision. The combination of free and unhindered scientific work, reliable counsel, collective support and an atmosphere that also allowed for contradiction, sets a positive example of how science can be conducted. The scientific discussions and observations have helped broaden my horizon in a professional and personal way.

I furthermore thank Professor Frank F. Bier for developing the idea and finding the financial support for the multivalent Influenza A virus- peptide interaction study and the support for the project. The idea, the friendly discussions and his connections to Dynamic Biosensors and the Fraunhofer IZI in Leipzig formed the basis of this thesis.

I furthermore thank my group at IZI-BB, including Dr. Eva-Maria Laux, Dr. Xenia Knigge, Sandra Stanke, Mareike Prüfer and Victor Daisuke Kietzmann. The atmosphere in the group was welcoming from the beginning and always friendly. The high standard of discussions amazed me during all my time at the institute. I'd like to especially thank Sandra Stanke for her support. Her knowledge of fantastic viruses and where to find them was extremely helpful. Additionally, Mareike Prüfer has supported my work with her extensive chemical and biotechnological expertise. I thank Dr. Eva-Maria Laux for her continuous support and her contributions to the project on SARS-CoV-2.

Furthermore, I'd like to thank Dr. David Smith and Dr. Christin Möser from the Fraunhofer IZI in Leipzig, who have provided DNA-peptide nanostructures for all published projects. They have cooperated with us without hesitation and I hope the outcome was fruitful for everyone involved. I also would like to thank Basma Altattan for the extraordinarily wonderful teamwork during the loneliest days of COVID-19 and the results we were able to produce together. I also thank Nico Grasse from Fraunhofer IZI and Lars Heinig from preclinics GmbH for their important contributions and the good cooperation.

From Dynamic Biosensors GmbH, I thank Hanna Müller-Landau, who first introduced me to "my device" and was always an extremely helpful and always readily available source of knowledge regarding assay setups, conjugation strategies, error messages and the interpretation of results. The cooperation on the AmbiSENSE project was superb. From Dynamic Biosensors I'd also like to thank Ulrich Rant, Katharina Lang, Wolfgang Kaiser, Nena Matscheko and Piotr Stefanski for their support and assistance with AmbiSENSE and beyond.

Special thanks goes to Jörg Schenk and Frank Sellrie of HybroTech GmbH for the cooperation on many projects and for everything I learned from you on antibodies, ELISAs, etc.

I furthermore thank Jörg Henkel and Christian Warmt for operating the HPLC and Dr. Nenad Gajovich-Eichelmann for the cooperation.

I thank my friends for their support, their interest in my work and their ability to distract my attention away from work and towards the amazing things that exist in life outside of the lab.

I'd also like to thank my brother and his family as well as my grandmother for their support and interest.

I'd especially like to thank my parents Dr. Angela Weinowski and Henning Kruse. They have always been interested in the scientific details and the progress of this work. Their willingness to make things happen and to actively support any of my projects is phenomenal.

Finally, I'd like to thank Dr. Michael Broer. Thank you for all your encouragement and for being there during all the highs and lows of this dissertation and the last years.

Statutory declaration

I hereby formally declare that I have written the submitted dissertation independently. I did not use any outside support except for the quoted literature and other sources mentioned. The thesis has not been submitted at any other university for the conferral of a doctorate.

Berlin, December 20, 2022

(Marlen Kruse)